

12-1-2015

R-ketorolac targets Cdc42 and Rac1 and alters ovarian cancer behaviors critical for invasion and metastasis

Yuna Guo

Follow this and additional works at: https://digitalrepository.unm.edu/biom_etds



Part of the [Medicine and Health Sciences Commons](#)

Recommended Citation

Guo, Yuna. "R-ketorolac targets Cdc42 and Rac1 and alters ovarian cancer behaviors critical for invasion and metastasis." (2015).
https://digitalrepository.unm.edu/biom_etds/127

This Dissertation is brought to you for free and open access by the Electronic Theses and Dissertations at UNM Digital Repository. It has been accepted for inclusion in Biomedical Sciences ETDs by an authorized administrator of UNM Digital Repository. For more information, please contact disc@unm.edu.

Yuna Guo

Candidate

Department of Pathology

Department

This dissertation is approved, and it is acceptable in quality and form for publication:

Approved by the Dissertation Committee:

Angela Wandinger-Ness, Ph.D. , Chairperson

Laurie G. Hudson, Ph.D.

Larry A. Sklar, Ph.D.

Tione Buranda, Ph.D.

**R-ketorolac Targets Cdc42 and Rac1 and Alters Ovarian Cancer
Behaviors Critical for Invasion and Metastasis**

By

YUNA GUO

B.S., Biotechnology, China Pharmaceutical University, 2008

DISSERTATION

Submitted in Partial Fulfillment of the
Requirements for the Degree of

Doctor of Philosophy

Biomedical Sciences

The University of New Mexico

Albuquerque, New Mexico

December, 2015

DEDICATION

I dedicate my dissertation work to my family and friends.

I owe a special gratitude to my loving parents, Enhe Guo and Chongwei Yu and my boyfriend Lei Xiao for their moral support and precious love. They always encouraged and stood by me during the hard times of graduate school.

ACKNOWLEDGEMENT

I would like to express my sincere gratitude to my advisor and dissertation chair, **Dr. Angela Wandinger-Ness**, who has been an invaluable friend and mentor. I thank her for her continuous support of my Ph.D study, for her patience, encouragement and immense knowledge, for her great support and references on my job search, for the preparation and revisions on my dissertation. Without her guidance and persistent help this dissertation would not have been possible.

I would like to thank my committee members, Dr. Laurie G. Hudson, Dr. Larry A. Sklar and Dr. Tione Buranda for their valuable advice on my Ph.D project, for the revisions on this dissertation, and for the great support on my job search.

I thank the Wandinger-Ness research group for their kind help in my work and life: Ms Elsa Romero, Dr. Tess Shideler, Dr. Jacob Agola, Dr. Soumik Basuray, Dr. Stephanie Jerman. I acknowledge Dr. Jennifer E. Golden and Dr. Jeffrey B. Arterburn for their valuable advice on my dissertation.

I also thank to the UNM Center for Molecular Discovery, UNM Microscopy Facility, UNM Flow Cytometry Facility, the Clinical Trial Team (Dr. Carolyn Muller, Dr. Sarah Adams, Dr. Teresa Rutledge), the Ward group and all our collaborators.

R-ketorolac Targets Cdc42 and Rac1 and Alters Ovarian Cancer Behaviors Critical for Invasion and Metastasis

By

YUNA GUO

Ph.D., Biomedical Sciences, University of New Mexico, 2015

B.S., Biotechnology, China Pharmaceutical University, 2008

Abstract

Cdc42 (cell division control protein 42) and Rac1 (Ras-related C3 botulinum) are attractive therapeutic targets in ovarian cancer based on their established importance in tumor cell migration, adhesion and invasion. Despite a predicted benefit, targeting GTPases has not yet been translated to clinical practice. Based on lead identification through high-throughput screening and computational shape homology approaches, R-ketorolac is identified as a Cdc42 and Rac1 regulator, an activity that is distinct from the anti-inflammatory, cyclooxygenase inhibitory activity of S-ketorolac. In this dissertation, R-ketorolac is established as an allosteric inhibitor of Cdc42 and Rac1. Studies on immortalized human ovarian adenocarcinoma cells (SKOV3ip), and primary, patient-derived ovarian cancer cells show R-ketorolac is a robust inhibitor of growth factor or serum dependent Cdc42 and Rac1 and their downstream effector p21-activated kinases activation. Multiple assays of cell behavior show

that R-ketorolac significantly inhibits cell adhesion, migration and invasion. A clinical trial on ovarian cancer patients shows that ketorolac is enriched in the R-enantiomer in peritoneal fluids and GTPase activity is inhibited in ascites-derived tumor cells. A retrospective study suggests that a single dose of ketorolac in the perioperative period benefits patient outcomes. In sum, R-ketorolac inhibits Cdc42 and Rac1 activities and subsequent physiological consequences which are critical to tumor metastasis and likely contributes to the observed survival benefit in ovarian patients.

TABLE OF CONTENTS

LIST OF FIGURES	xi
LIST OF TABLES	xiv
LIST OF KEY ABBREVIATIONS.....	xv
CHAPTER 1: INTRODUCTION	1
Ovarian Cancer	1
Ovarian Cancer Metastasis and Microenvironment	2
Overview of Ovarian Cancer Treatment	6
Rho GTPases.....	7
Rho GTPase Signaling Pathways and Their Functions	10
Rho GTPase Inhibitors	15
NSAIDs and Their Roles in Cancer Therapy.....	16
Rationale of the Study	17
Hypothesis	18
Significance and Innovation	19
CHAPTER 2: R-KETOROLAC INHIBITION OF CDC42 AND RAC1 NUCLEOTIDE BINDING	20
Abstract.....	20
Introduction	22
Materials and Methods	26
Results	31
Conclusion and Discussion	62

CHAPTER 3: R-KETOROLAC TARGETS CDC42 AND RAC1 AND ALTERS OVARIAN CANCER BEHAVIORS CRITICAL FOR INVASION AND METASTASIS	65
Abstract.....	65
Introduction.	67
Materials and Methods.....	72
Results	80
Conclusion and Discussion	107
CHAPTER 4: A NOVEL PHARMACOLOGIC ACTIVITY OF KETOROLAC FOR THERAPEUTIC BENEFIT IN OVARIAN CANCER PATIENTS.....	111
Abstract.....	111
Introduction	112
Materials and Methods.....	115
Results	124
Conclusions and Discussion	146
CHAPTER 5: FUTURE PERSPECTIVES	150
APPENDICES	156
Appendix A. Time lapse imaging of HPY (490) labeled fluorescent compound RS-II-79 penetration into MCA	156
Appendix B. Patient Characteristics for IHC Microarrays OV1005 and OV8010.	157
Appendix C. Patient Characteristics for cDNA Microarray..	158
Appendix D. Survival estimates based on Cox-regression for Stage I (AJCC) with completion of chemotherapy.....	159
Appendix E. Survival estimates based on Cox-regression for Stage II (AJCC) with completion of chemotherapy.....	160

Appendix F. Survival estimates based on Cox-regression for Stage III (AJCC) with completion of chemotherapy.	160
Appendix G. Survival estimates based on Cox-regression for Stage IV (AJCC) with completion of chemotherapy.	161
REFERENCES	163

LIST OF FIGURES

Figure 1. Model of ovarian cancer metastasis.	5
Figure 2. Rho GTPase activation cycle and roles in signaling pathways.	9
Figure 3. Cdc42 and Rac1 GTPases regulate multiple downstream signaling pathways.	14
Figure 4. Structure of Rho GTPases.	24
Figure 5. DOCK9 mediates conformational change of Cdc42 to facilitate nucleotide exchange.	25
Figure 6. R-ketorolac acts as an allosteric inhibitor to selectively inhibit BODIPY-GTP binding to Cdc42 and Rac1 GTPases.	33
Figure 7. R-naproxen selectively inhibits BODIPY-GTP binding by Rac1 and Cdc42 in vitro.	36
Figure 8. Compound docking to Cdc42 based on a magnesium exclusion model.	39
Figure 9. The impact of ketorolac analogs on Cdc42 and Rac1 nucleotide binding.	43
Figure 10. Ketorolac derivatives exhibit different inhibitory effects on Cdc42 activation in SKOV3ip cells.	49
Figure 11. CID2950007 analogs inhibit BODIPY-linked nucleotide binding to Cdc42.	55
Figure 12. Fluorescent CID2950007 analog-RS-II-79 inhibits BODIPY-linked nucleotide binding to Cdc42.	58
Figure 13. Distribution of fluorescent RS-II-79 in living cells in a time-dependent manner.	61
Figure 14. A model for PAK1 activation.	68
Figure 15. Cell migration model.	71
Figure 16. Time course of maximal Cdc42 and Rac1 activation in SKOV3ip cells upon growth factor stimulation.	81

Figure 17. R-ketorolac preferentially inhibits Cdc42 and Rac1 activities in SKOV3ip cells.....	82
Figure 18. Characterization of primary ovarian cancer cell marker expression by immunofluorescence.	84
Figure 19. R-ketorolac preferentially inhibits Cdc42 and Rac1 activities in ascites derived primary human ovarian cancer cells.	85
Figure 20. R-ketorolac decreases the phosphorylation of PAK1(Ser144) / PAK2(Ser141) without affecting total PAK levels.....	87
Figure 21. Ketorolac inhibition of p-PAK1(Thr423) / PAK2(Thr402) and p-PAK1(Ser199) / PAK2(Ser192).	90
Figure 22. R-ketorolac decreases Cdc42 dependent filopodia formation in SKOV3ip cells following EGF stimulation.	92
Figure 23. R-ketorolac decreases Cdc42 dependent filopodia formation in primary human ovarian cancer cells following EGF stimulation.....	94
Figure 24. R-ketorolac inhibits cell-substrate adhesion in SKOV3ip cells and primary human ovarian cancer cells.	97
Figure 25. R-ketorolac selectively inhibits cell migration in a dose-dependent manner.	100
Figure 26. R-ketorolac inhibits invadopodia formation and gelatin degradation in SKOV3ip.....	103
Figure 27. R-ketorolac inhibits invadopodia formation and gelatin degradation in primary human ovarian cancer cells.	105
Figure 28. Purified ovarian tumor cells express EpCAM and MUC16/CA125..	120
Figure 29. Overexpression of Rac1 and Cdc42 protein in ovarian cancer specimens.	125
Figure 30. Expression of constitutively active Rac1b mRNA is elevated in ovarian cancer specimens.....	127
Figure 31. Overexpression of Rac1, Rac1b, Cdc42 and RhoA mRNA is dependent on ovarian cancer grade.	129

Figure 32. Ketorolac distributes to peritoneal fluids and is enriched in the R-enantiomer.	133
Figure 33. Enantiomer analyses of clinical drug.	136
Figure 34. GTPases are activated in patient ascites and inhibited by ketorolac administration in vivo.	139
Figure 35. RhoA activity is insensitive to ketorolac treatment.....	141
Figure 36. Retrospective survival analyses among ovarian cancer patients with and without peri-operative ketorolac.....	145

LIST OF TABELS

Table 1. Biochemical properties of Cdc42 and Rac1 nucleotide binding (BODIPY-GTP) with R- or S-ketorolac treatment.	35
Table 2. Impact of ketorolac analogs on in vitro Cdc42 nucleotide binding.	46
Table 3. Impact of ketorolac analogs on Cdc42 activation in cell-based assay. .	52
Table 4. Patient information of the ex vivo study.	74
Table 5. Ketorolac enantiomer concentration in serum or peritoneal fluids.	138
Table 6. Hazard ratios for ovarian cancer specific mortality for each characteristic adjusted for the other characteristics in the table.	144

LIST OF KEY ABBREVIATIONS

Abbreviation	Definition
ANOVA	Analysis of Variance
ARP	Actin related protein
BODIPY-GTP	BODIPY [®] (4,4-difluoro-4-bora-3a,4a-diaza-s-indacene or dipyrromethene boron difluoride) nucleotide analogue BODIPY [®] -GTP; 2'-(or 3')-O-[N-(2-aminoethyl)urethane]
CA125	cancer antigen 125
CD45	lymphocyte common antigen 45
Cdc42	cell division control protein 42
COX	cyclooxygenase
Cy3 / Cy5	Cyanines 3 / Cyanines 5
DAPI	4',6-diamidino-2-phenylindole
DBL	Oncogene identified in DNA from B-cell lymphoma, later known as homology domain found in Rho GEFs
DMSO	dimethyl sulfoxide
DOCK	dedicator of cytokinesis
EC ₅₀	half-maximal effective concentration
ECM	extracellular matrix
EGF	epidermal growth factor
EGFR/ErbB1	epidermal growth factor receptor
EMT	epithelial–mesenchymal transition
EpCAM	epithelial cell adhesion molecule
FAK	focal adhesion kinase
FDA	Food and Drug Administration
FITC	fluorescein isothiocyanate
GAP	GTPase-activating protein
GEF	guanine nucleotide exchange factor
GDI	guanosine nucleotide dissociation inhibitors
GSH	glutathione
GST	glutathione S-transferase
HMG-CoA	3-hydroxy-3-methylglutaryl-coenzyme A
IGF	insulin-like growth factor
IL	Interleukin
Ikk	IκB kinase
IP	Intraperitoneal

IQGAP	Ras GTPase-activating-like protein
IV	Intravenous
IP	Intraperitoneal
LIMK	LIM domain kinase
LPA	Lysophosphatidic acid
LSM	laser scanning microscope
mAb	monoclonal antibody
MAPK	mitogen-activated protein kinase
MCA	Multi-Cellular Aggregate
MCF	mean channel fluorescence
MLC	Myosin light chain
MLCK	myosin light-chain kinase
MMP	matrix metalloproteinase
NF- κ B	nuclear factor kappa-light-chain-enhancer of activated B cells
NP-40	nonyl phenoxypolyethoxylethanol
NSAID	nonsteroidal anti-inflammatory drug
PAK	p-21 activated kinase
PBD	p21 binding domain
PDGF	platelet-derived growth factor
PE	Phycoerythrin
PKG	Protein Kinase G
PMSF	phenylmethylsulfonyl fluoride
PI3K	phosphatidylinositol-4,5-bisphosphate 3-kinase
pRb	retinoblastoma protein
Rac1	Ras-related C3 botulinum toxin substrate 1
Ras	Rat sarcoma
Rho	Ras homolog
RIPA	high stringency cell lysis buffer
SAR	Structure Activity Relationship
Src	Proto-oncogene tyrosine-protein kinase Src
Tks5	Src tyrosine kinase substrate 5
TKR	Tyrosine kinase receptor
TNF	Tumor necrosis factor
VEGF	Vascular endothelial growth factor
WASP	Wiskott–Aldrich Syndrome protein
WAVE	WASP-family verprolin-homologous protein

CHAPTER 1

INTRODUCTION

Ovarian Cancer

Ovarian cancer is the fifth leading cause of gynecological cancer deaths in the United States with a 45% 5-year survival rate (1). A majority of malignant ovarian cancer in adult women is epithelial ovarian cancer, which is classified into distinct morphologic categories, including serous, mucinous, endometrioid, clear cell, transitional cell, or any combination of these (2, 3). Recent understanding of the etiology of “ovarian cancer” suggests that it is a general term for a series of molecularly and etiologically distinct diseases that simply share an anatomical location. New evidence shows that a majority of serous ovarian cancers originate from the distal end of dysplastic fallopian tubes, mostly presenting at an advanced stage disease; whereas early stage carcinomas, including clear-cell carcinoma, endometrioid, and low-grade serous carcinoma usually derive from endometriosis or borderline serous tumors (4-7).

Serous ovarian carcinoma is the most common (~70%) and aggressive epithelial ovarian tumor that is usually diagnosed at advanced stages with a high relapse rate (8). Due to lack of symptoms and effective early predictive markers, most patients are diagnosed at late stages with tumor dissemination on multiple abdominal organs at laparotomy (9, 10). A majority of patients relapse although tumor cannot be detected after first-line surgery and chemotherapy. Another

difficulty for ovarian cancer treatment is tumor heterogeneity. Many ovarian cancers are derived from non-ovarian tissues and share few molecular similarities among different histotypes (4-7). This leads to failure of most molecularly targeted therapies that are only effective at some tumor sites, and explains the high recurrence rate of a tumor that responds to initial treatment but soon develops chemoresistance (11-13). Thus, in comparison to other epithelial malignancies, the survival rate of epithelial ovarian cancer has shown little improvement since precise surgery and target chemotherapy were introduced over the past 30 years (14-16).

Ovarian Cancer Metastasis and Microenvironment

Often associated with malignant ascites, which facilitates metastasis, most patients are diagnosed at advanced stages with dissemination throughout the intraperitoneal cavity (17). Unlike many other epithelial cancers, at early stages, epithelial ovarian tumors grow and extend to the proximal sites adjacent to the primary tumors by cell proliferation, migration and colonization (16, 18). Metastatic spread of ovarian cancer beyond the ovary or fallopian tube is mediated by disruption of the ovarian tumor capsules and surface shedding of malignant cells from primary tumors into the peritoneum, where tumor cells survive as free-floating multicellular aggregates (MCA) in the ascites fluid, commonly known as spheroids. Subsequently, MCA anchor and attach on mesothelial extracellular matrix (ECM) and invade into the submesothelial matrix,

which leads to secondary lesions on peritoneal organs and surfaces at later stages (19, 20) (Figure 1).

Recent studies have shown that the tumor microenvironment contributes to the late diagnosis, intraperitoneal dissemination, chemoresistance and frequent recurrence (21, 22). The tumor microenvironment has a multicellular composition that includes tumor cells, tumor-infiltrating immune cells and stromal cells with the peritoneal cavity being considered as a highly receptive environment for carcinomatosis (22, 23). Mesothelial cells form a protective monolayer that maintains normal serosal membrane integrity and function. Peritoneal mesothelial cells play pivotal roles in protecting organs from tumor dissemination (24, 25). However, malignant tumor cells anchor on the mesothelium by overexpressing CA125 which facilitates cell implantation via the interaction with mesothelin expressed on mesothelial cells, and further invade into the submesothelial ECM of organs by secreting surface matrix metalloproteases (MMP) (26). The CD44/hyaluronan/versican macromolecular complex promotes tumor cell adhesion on mesothelium and invasion into the ECM (27). Integrins are involved in cell-ECM and cell-cell interaction, and ascites-associated MCA formation that are important for tumor migration and invasion (28, 29). Endothelial cells are critical during tumor progression for tumor growth because of their functions in neovasculature formation regulated by pro- and anti-angiogenic factors (30). Adipocytes have been reported to promote homing and proliferation of ovarian cancer to the omentum by secreting specific cytokines (e.g. IL-6, IL-8), chemokines and lipids (31, 32). Immune cells (e.g. macrophages,

T cells, dendritic cells and B cells) are another key component of tumor microenvironment because the quality of endogenous immune responses can have a significant impact on patient outcomes and are usually suppressed in the tumor microenvironment (33, 34). Cancer associated fibroblasts are a major component of tumor stroma that facilitate tumor cell growth and metastasis by expressing mitogenic factors. Moreover, the tumor stromal fibroblasts are speculated to be derived from ovarian surface epithelium that undergo epithelia-to-mesenchymal transition (EMT) (19, 35). In sum, all these components and the communication between them characterize the unique microenvironment that regulates ovarian tumor growth, angiogenesis and dissemination.

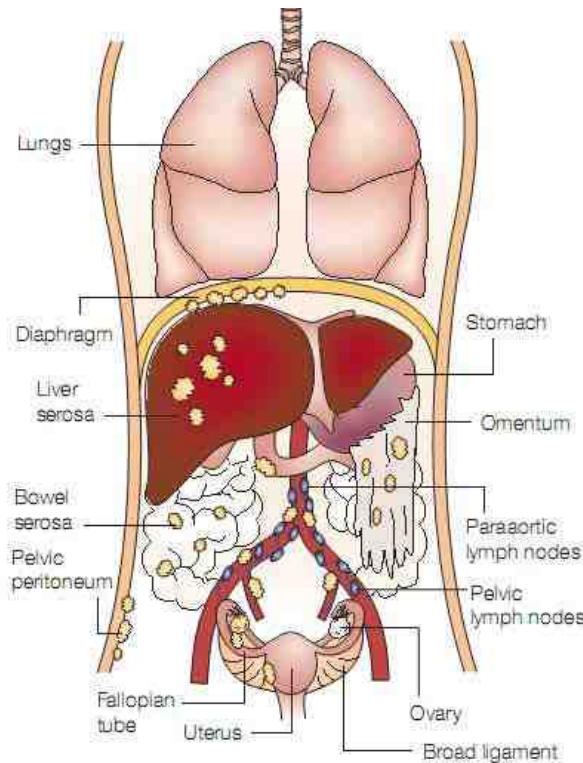


Figure 1. Model of ovarian cancer metastasis. At the earliest stage, the tumor is limited to one or two ovaries; no tumor is present on the ovarian surface or in ascites. Once the tumor progresses to later stages - when most patients are diagnosed – it spreads beyond the confines of the ovaries, extends and invades to adjacent tissues, such as the uterus, fallopian tubes, and mesothelial lining of peritoneum. Metastatic spread of the ovarian cancer beyond the ovary or fallopian tube is mediated by surface shedding of tumor cells and formation of free-floating multicellular aggregates in the ascites fluid. Subsequent mesothelial anchoring and invasion of the submesothelial matrix lead to secondary lesions on peritoneal organs and surfaces. (H. Naora, D. Montell, Nature Reviews Cancer, 2005;5:355-66)

Overview of Ovarian Cancer Treatment

The first line treatment for epithelial ovarian cancer is major debulking surgery to remove as much tumor burden as possible, most often followed by intraperitoneal chemotherapeutic treatment in optimally debulked patients after recovery from surgery (36). Cytoreductive surgery is initially conducted on patients with suspected epithelial ovarian cancer to determine a pathological diagnosis, precisely evaluate disease stage, and optimally excise tumors when feasible (37-39). After a perioperative period that allows patients to recover from primary surgery, patients are standardly treated with platinum/taxane based cytotoxic chemotherapy (40). The chemotherapeutic drugs are given systemically by intravenous (IV) injection, intraperitoneal (IP) injection or mouth, which allows the drugs to reach all areas of the body through the circulatory system. Because ovarian cancer mostly disseminates within the peritoneal cavity, IP chemotherapy is widely used and involves injecting drugs through a catheter directly into the abdominal cavity (41). Compared to IV chemotherapy, IP chemotherapy results in higher local concentrations of drugs in the peritoneal cavity and results in two-fold higher drug penetration into tumors (42). Although nearly 75% of patients initially respond favorably to chemotherapy, a majority of patients subsequently become chemoresistant, develop largely incurable recurrent disease, and die within five years (16).

The perioperative period, which is a days-to-weeks period between cytoreductive surgery and the first chemotherapy, has been reported to be crucial

for tumor recurrence and metastasis (43). Although the primary tumor is removed by surgery along with all tumors > 1 mm, due to wide dissemination and microscopic implants throughout the peritoneum, residual malignant tumor cells may be present in the circulatory system, distal organs or bone marrow which leads to disease recurrence (44, 45). During this period, surgery-induced perturbations (e.g. stress, nutritional status, inflammation and anesthesia) and consequent paracrine, neuroendocrine and immune responses, including increased prostaglandins, growth factors and cytokines (e.g. Tumor necrosis factors (TNF), interleukin factor (IL) 6, IL8) and decreased antiangiogenic factors (e.g. endostatin), create a pro-metastatic microenvironment, facilitating residual malignant tumor cell growth, proliferation, and survival (46-50). The malignant tumor cells are either cancer stem cells or metastatic tumor cells, which are frequently chemoresistant and represent the major cause of ovarian cancer relapse and mortality (51, 52). Therefore, targeting tumor cell adhesion, migration and invasion in the perioperative period presents an important potential window of opportunity for treatment that has not yet been extensively explored (43, 53).

Rho GTPases

Ras homology guanosine triphosphatases (Rho GTPases) (~21 kDa) are a family of small signaling G proteins, which were began to be discovered from 1985 as Ras-related proteins (54, 55). To date, there are twenty-two mammalian genes encoding Rho proteins that have been identified. Cdc42, Rac1 and Ras homolog gene family, member A (Rho A) are three well characterized members

of the Rho family GTPases (54, 56). Similar to other regulatory GTPases, Rho GTPases act as molecular switches by interconverting between an active GTP-bound form and an inactive GDP-bound form. Because GDP is tightly bound and GTP is hydrolyzed very slowly, the cycling between an active and an inactive conformational state is regulated by three classes of GTPase regulatory proteins: a) guanine nucleotide exchange factors (GEFs), which facilitate GDP dissociation; b) GTPase-activating proteins (GAPs), which stimulate GTP hydrolysis; c) guanine nucleotide exchange inhibitors (GDIs), which sequester GTPases from nucleotide exchange by shielding the lipids that are critical for membrane recruitment (54, 56-58) (Figure 2).

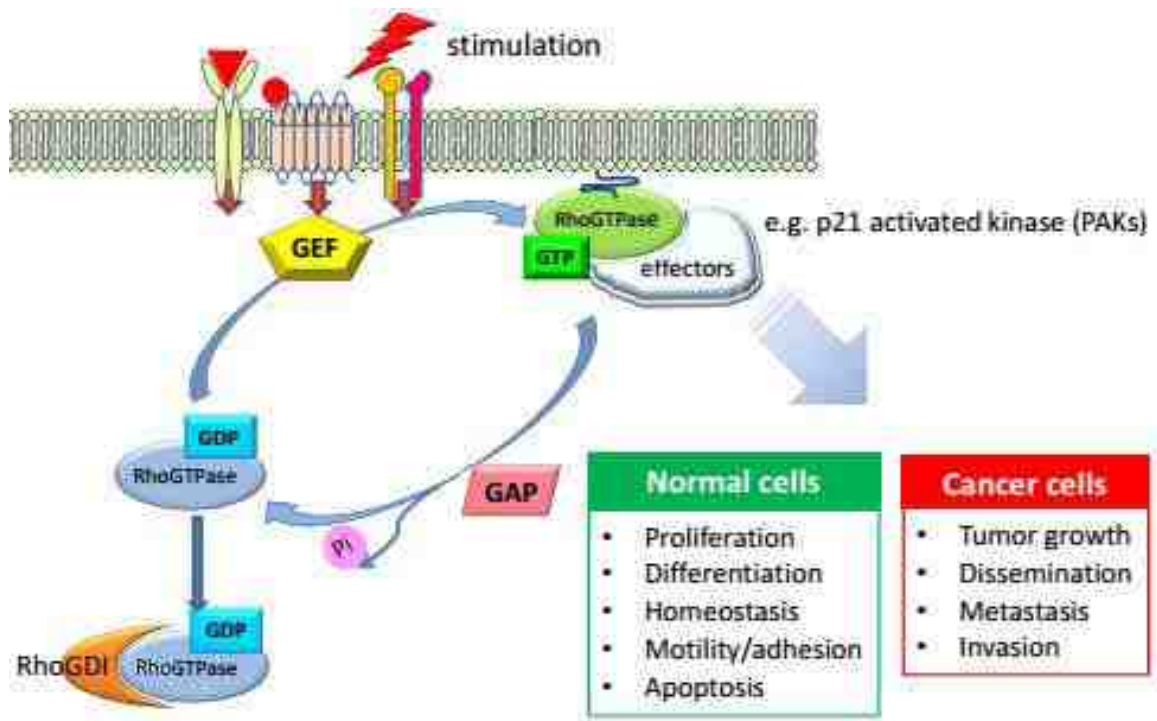


Figure 2. Rho GTPase activation cycle and roles in signaling pathways. In response to stimulatory signals, activated GEFs catalyze the exchange of GDP to GTP on Rho family GTPases. Active GTP-bound Rho GTPases interact with effector molecules (e.g. PAKs), leading to the activation of signaling cascades regulating a variety of cellular processes. GAP proteins promote GTP hydrolysis and inactivation of Rho GTPases. Rho GTPase activity is further inhibited by GDIs, which sequester the GTPase in the cytosol away from cell membranes.

Rho GTPase Signaling Pathways and Their Functions

Various extracellular stimuli trigger the activation of Rho GTPases at different points (Figure 3), such as G protein-coupled receptors, tyrosine kinase receptors and integrin. The seven-transmembrane-domain heterotrimeric G protein-coupled receptor family (e.g. bradykinin, Lysophosphatidic acid (LPA) and bombesin receptors) activate select Rho GTPases by the activation of heterotrimeric G proteins, which subsequently stimulates the RhoGEFs (59). Epidermal growth factor (EGF), platelet-derived growth factor (PDGF) and insulin-like growth factor (IGF) stimulate the activation of Rho GTPase by increasing GEF activity in a phosphatidylinositol-4,5-bisphosphate 3-kinase (PI3K) dependent manner. In addition, Rho GTPases are activated by cell-ECM adhesion which is mediated by integrins. The cytoplasmic tail of integrin ($\beta 1$, $\beta 3$, $\beta 5$) activates focal adhesion kinase (FAK), leading to the phosphorylation of downstream protein p130cas that activates DOCK180 (a Rac GEF) and inhibits RhoA. Overall, the activation of cell receptors and other molecules influence intracellular signaling by regulating Rho GTPase activity (60, 61).

Cdc42 and Rac1 activate multiple downstream effectors and initiate the sequential events which modulate various cell behaviors (Figure 3) (62). For example, p21-activated kinases (PAKs) interact with Cdc42 and Rac1 through a p21 binding domain (PBD), which causes auto-phosphorylation and conformational changes and initiates multiple cellular processes, including F-actin polymerization, Mitogen-activated protein kinases (MAPK) signaling, and

apoptosis signaling (63, 64). Other effectors of Cdc42 and Rac1 include the Wiskott-Aldrich syndrome protein (WASP)/WASP-family verprolin-homologous protein (WAVE) family and Ras GTPase-activating-like protein (IQGAP), which regulate actin nucleation through the actin related protein (Arp) 2/3 complex for actin polymerization (65, 66). In addition, Cdc42 promotes cell division and cell transformation by inducing the accumulation of EGFR, and facilitating the nuclear translocation of EGFR which induces EMT and angiogenesis (67). All these processes are critical for the regulation of cell growth, proliferation, motility and apoptosis.

Since Cdc42 and Rac1 GTPases play important roles in actin reorganization, their regulators and effectors have been suggested to control tumor progression and metastasis (68). The direct effectors of Cdc42 and Rac1 – PAK1 and PAK4 – are up-regulated in breast cancer and required for actin cytoskeleton remodeling and tumor cell motility (69). In colorectal cancer cells, active Cdc42 greatly promotes cells to spread, migrate, and invade via the PAK1-myosin light-chain kinase (MLCK) pathway important for tumor metastasis (70). In breast cancer cells, Rac1 is up-regulated as a consequence of enhanced upstream signals from multiple pathways (e.g. phosphoinositide-3-kinase (PI3K) and tyrosine kinase receptors (TKR) such as ErbB1/ epidermal growth factor receptor (EGFR) in response to EGF or transforming growth factor (TGF) ligands), which promotes tumor cell growth and proliferation (71, 72). Activated Cdc42 and Rac1 decrease p53 protein levels leading to increased vascular endothelial growth factor (VEGF) expression and tumor angiogenesis (73). $\alpha\beta4$

integrin-dependent Rac-PAK1 signaling enhances apoptosis-resistance by overexpressing nuclear factor kappa-light-chain-enhancer of activated B cells (NF- κ B) protein in mammary acini (74). Rho GTPases stimulate cell cycle progression by inhibiting retinoblastoma protein (pRb) checkpoint and reduce epithelial cell polarity by down-regulating E-cadherin expression in various carcinoma cells (75). In summary, Cdc42 and Rac1 regulate multiple cell functions that could affect tumor progression and metastasis.

Moreover, Cdc42 and Rac1 are frequently overexpressed or hyperactivated in epithelial cancers including ovarian cancer. Immunohistochemistry studies show that patients with a high clinical stage hepatocellular carcinoma (III-IV) had a higher tendency to express Rac1 which is associated with shorter disease-free survival, compared to patients with low pathologic grade hepatocellular carcinoma (76). Rac1 expression promotes EMT and the overexpression correlated with advanced stage of disease and early tumor recurrence in epithelial ovarian cancer patient (77). Rac1b is a Rac1 splice variant that adds 19 amino acids and causes hyperactivity through GEF-independent activation (78-80). Rac1b is overexpressed in breast, colorectal and lung cancer, and constitutes a marker of poor prognosis in KRAS/BRAF WT metastatic colorectal patients (81-85). Previous work by our group found that both Cdc42 and Rac1 were overexpressed or hyperactivated in advanced stages of ovarian cancer patients compared to benign or low grade tumor (86). Thus, Cdc42 and Rac1 GTPases could be potential pharmacologic targets for the treatment of ovarian and other epithelial cancers.

In addition to the described canonical Rho GTPases - Cdc42 and Rac1, other Rho GTPase isomers also play critical roles in cell proliferation, differentiation and cell migration (87). RhoA, -B and -C directly activate actin polymerization in stress fiber formation by interacting with ROCK-LIMP/actomyosin pathways. RhoA and RhoC have been found to promote cancer progress, whereas RhoB acts as a cancer suppressor with its antiproliferation and proapoptosis effects (88). A similar anti-tumor effect is also observed for RhoE targeted by p53 (89). RhoG regulates membrane dynamics involved in cell migration and spreading and microtubule dynamics critical for platelet granule secretion (90). RhoJ modulates the formation of focal adhesion and early endocytosis for endothelial chemotaxis, migration, proliferation and lumen formation, which is responsible for the angiogenesis (91).

Cancer growth and metastasis are directly correlated with the misregulation of Rho family GTPases that generally result in overexpression of Rho GTPases and aberrant activity of Rho GTPase regulators (e.g. GEF, GAP, GDI). Recently, mutationally active Rho GTPases have been identified using high-throughput exome sequencing techniques (92, 93). In about 5-10% melanoma, Rac1 (P29S) and Rac2 (P29L) mutants are found to activate the GTPases by enabling GEF-independent conversion to the GTP-bound form (93-95). In *C. elegans*, MIG-2 (S75F), which might be functionally equivalent to RhoG, and CED-10, which might be functionally equivalent to Cdc42, have been identified as gain-of –function mutations (96).

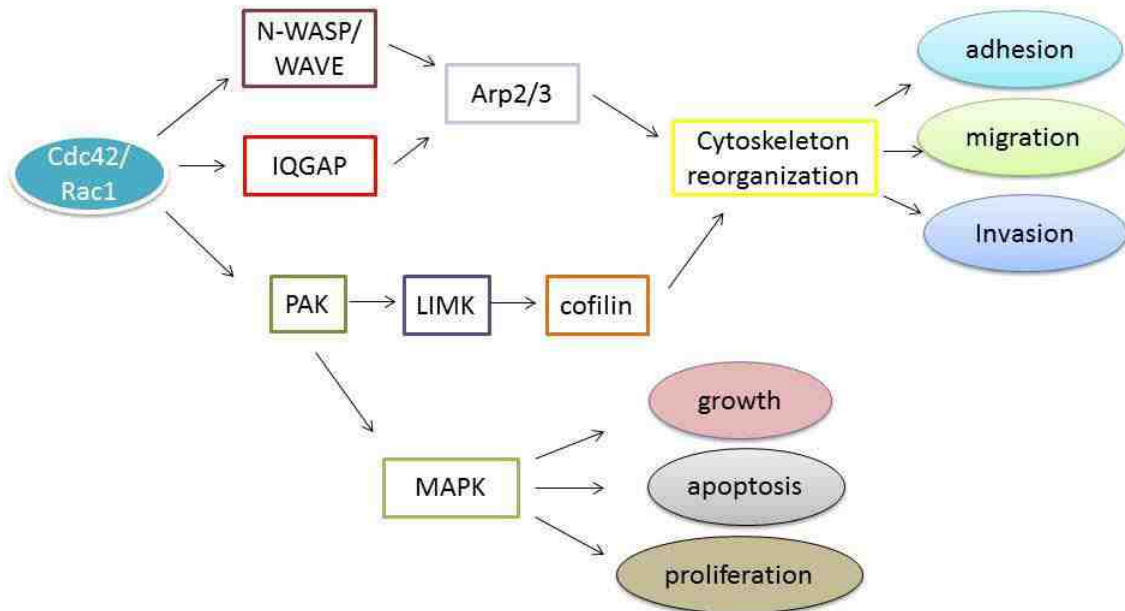


Figure 3. Cdc42 and Rac1 GTPases regulate multiple downstream signaling pathways. Cdc42 and Rac1 promote cytoskeleton reorganization through regulation of multiple effectors (e.g. N-WASP/WAVE, IQGAP, PAK) and associated subsequent signaling proteins (LIMK, Arp2/3), which are pivotal for cell adhesion, migration and invasion. Cdc42 and Rac1 also mediate the activation of MAPK signaling pathway through PAK, regulating cell growth, apoptosis and proliferation.

Rho GTPase Inhibitors

Since Cdc42 and Rac1 are potential high value therapeutic targets in ovarian and other cancers, numerous inhibitors targeting the Rho GTPases have been developed. Statins are 3-hydroxy-3-methylglutaryl-coenzyme A (HMG-CoA) reductase inhibitors that indirectly act as broad spectrum GTPase inhibitors by interfering with the prenylation required for membrane association and have been successfully used for the treatment of hypercholesterolemia (97). In recent years, statins have been found to induce apoptosis and inhibit proliferation in several cancer cell lines. Cancer risk reduction associated with statins use are reported for prostate, breast, colorectal, and pancreatic cancers in patients (98-101). The benefit in ovarian cancer is mixed and subtype specific (102), motivating the identification and testing of more selective GTPase inhibitors. Secramine inhibits Cdc42 binding to membranes in a RhoGDI-dependent manner, prevents membrane associated Cdc42 activation, and subsequently inhibits the formation of actin cytoskeleton mediated platelet integrin $\alpha 2\beta 1$ (103). CID2950007, an allosteric inhibitor of Cdc42 nucleotide binding, inhibits Cdc42-related filopodia formation and cell migration in cell based assays (104). NSC23766 was discovered as a Rac inhibitor and selectively inhibits the interaction between Dbl (a Rac GEF) and Rac (105). The compound has been shown to inhibit cell growth, proliferation and invasion in prostate cancer and hematopoietic stem cells (105, 106). Novel compounds (e.g. AZA1, AZA197, EHOp-016) based on structural information of NSC23766 have been synthesized and act as Cdc42 or Rac1 inhibitors to reduce cell migration and proliferation and tumorigenicity in a

xenograft mouse model in prostate and colorectal cancers (107-110). Although all these Rho GTPase inhibitors were designed and discovered with various modes of action and are predicted to be of great therapeutic benefit, the limitation of the Rho GTPase inhibitors lies in their poor selectivity between cancerous and normal cells. Therefore, these identified compounds may not be pharmacologically suitable for human use and none have as yet been translated to clinical application.

NSAIDs and Their Roles in Cancer Therapy

Non-steroidal anti-inflammatory drugs (NSAIDs) are potent cyclooxygenase (COX) inhibitors that cause reduced synthesis of prostaglandins from arachidonic acid. Many of the NSAIDs are marketed as racemates, composed of 1:1 mixtures of R and S-enantiomers. The two enantiomers often exhibit remarkable pharmacologic and toxicologic differences. The S-enantiomer has been shown to preferentially interact with COX (111) and is generally considered the active component in racemic drug formulations.

Recently, besides their analgesic function, several NSAIDs have been reported to have significant benefit for patient survival in various cancers. Growing evidence suggests that NSAIDs have a variety of molecular targets and may contribute to cancer prevention in both COX-dependent and COX-independent manners. For example, aspirin has been reported to reduce colon cancer risk by inhibiting the upregulated expression of COX-2, which promotes tumorigenesis in 40-45% of colon cancer (112). The evidence for COX-

independent pathways is that COX-2 negative epithelial cells exhibit similar IC_{50} values as COX-2 positive counterparts in terms of cell growth inhibition with celecoxib treatment (113). Furthermore, R-ibuprofen, which does not have COX inhibitory activity, is equally potent as the COX inhibitory S-ibuprofen in inhibiting PDGF-induced mitogenesis in colon cancer cells and colon cancer development in an animal model (114, 115). Numerous targets, in addition to COX, have been identified as potential mediators responsible for the chemopreventive action of NSAIDs, e.g. inhibition of I κ B kinase (IKK) β /NF- κ B mediated transcriptional activation and cell survival, reduction of protein kinase G (PKG) mediated angiogenesis, and downregulation of matrix metalloproteinase (MMP)2 and MMP9 mediated invasion (116-120). Although multiple targets have been identified for the anti-tumor effect of NSAIDs, there is no evidence of these potential targets being directly related to the clinically observed benefits on cancer patient outcomes.

Rationale of the Study

Using findings obtained from a high throughput screen of the 2007 Prestwick Chemical Library[®] (2007) of 100% off patent drugs contained 888 small molecules (Prestwick, Washington DC, USA) and cheminformatics approaches, the R-enantiomers of a limited number of NSAIDs, R-ketorolac and R-naproxen were identified as inhibitors of Cdc42 and Rac1 (121). Ketorolac is an FDA approved drug that is administered as a racemic mixture for post-surgery pain management. S-ketorolac inhibits COX-1 and COX-2 enzymes, whereas R-

ketorolac shows >100-fold less activity on both COX-1 and COX-2 (122). S-naproxen, but not R-naproxen is an FDA approved drug having analgesic, anti-inflammatory, and antipyretic activity. Such activity is also mediated via inhibition of the COX enzymes (123, 124).

The central goal of this study is to confirm and characterize the R-enantiomers of selected NSAIDs, ketorolac and naproxen, as bona fide Cdc42 and Rac1 GTPase inhibitors and establish their anti-tumor impacts in ovarian tumor cells and ovarian cancer patients. R-ketorolac, as a FDA-approved drug in racemic form, has potential to be repurposed as an anti-tumor drug for ovarian cancer therapy. Chapter 2 identifies the mechanism of R-ketorolac and R-naproxen on Cdc42 and Rac1 nucleotide binding using a flow cytometry based in vitro nucleotide binding assay. Chapter 3 utilizes cell-based assays to characterize the inhibitory effect of R-ketorolac on cell adhesion, migration and invasion using immortalized ovarian cancer cell lines and primary human ovarian cancer cells. Chapter 4 utilizes a clinical trial to establish a novel pharmacologic activity of ketorolac for therapeutic benefit in ovarian cancer patients.

Hypothesis

R-ketorolac inhibits Cdc42 and Rac1 GTPase activities and associated downstream cascades that are central to cell adhesion, migration and invasion, which will have beneficial effect in reducing ovarian tumor metastasis and progression.

Significance and Innovation

Compared to traditional drug development pipeline requirements, the overall time and cost of repurposing R-ketorolac will be greatly reduced because of the significant number of toxicology and safety assessments that have already been completed. The mechanistic study of signaling pathways inhibited by ketorolac will demonstrate Cdc42 and Rac1 as potential therapeutic targets for ovarian and other epithelial cancers therapies. Biochemical and structural studies of the mechanism of GTPase activity inhibition by selected NSAIDs will provide guidance for the development of new anti-tumor chemical entities.

CHAPTER 2

R-KETOROLAC INHIBITION OF CDC42 AND RAC1 NUCLEOTIDE BINDING

Abstract

Cdc42 and Rac1 GTPases are key regulators of actin reorganization, cell motility, cell-cell and cell-extracellular matrix (ECM) adhesion, whose activities are found closely correlated with tumor expansion and malignant progression. Despite a predicted benefit, targeting Cdc42 and Rac1 GTPases has not yet been translated to clinical practice. Through high throughput screening and computational shape homology approaches, we established the R-enantiomers of selected NSAIDs (ketorolac and naproxen) as Cdc42 and Rac1 inhibitors; distinct from the anti-inflammatory, cyclooxygenase inhibitory activity of S-enantiomer. In this chapter, a bead-based flow cytometry assay was used to establish that R-ketorolac and R-naproxen act as allosteric regulators of GTPase nucleotide binding by Cdc42 and Rac1. Molecular docking analyses are predicated on in vitro nucleotide binding assay results and GEF mediated nucleotide exchange mechanisms. R-enantiomers are suggested to preferentially interact with magnesium and exclude interaction with the guanine nucleotide phosphate residue. A preliminary structure-activity relationship study of ketorolac demonstrates that substituents on the phenyl ring are critical in modulating ketorolac inhibition of nucleotide binding by the GTPase, offering guidance for

generating more selective chemical entities. Taken together, the studies in Chapter 2 demonstrate that the R-enantiomers of selected NSAIDs (ketorolac and naproxen) act as Cdc42 and Rac1 inhibitors, which may have potential benefits for cancer therapy.

Introduction

The Rho-family (Ras homolog) GTPases are central to dynamic actin cytoskeleton assembly and rearrangement that are the underpinnings of normal cell-cell adhesion, cell migration and even transformation (54, 125). Among the Rho-family GTPases, Cdc42 and Rac1 are of particular interest due to their frequent overexpression or hyperactivation in epithelial cancers including ovarian cancer (73, 77, 86, 126, 127).

The conformational GTPase switch is regulated by the bound nucleotide (GTP or GDP) and determines the GTPase activation status. The conserved domain of Rho GTPases consists of a six-stranded β -sheet surrounded by five α -helices, known as the switch 1 and switch 2 regions (Figure 4) (58, 128). This domain includes the guanine nucleotide binding site that recognizes the guanine base as well as the β -phosphate and the Mg^{2+} . This domain is involved in the coordination of the β -phosphate and hydrolysis of GTP. For example, in Cdc42 nucleotide exchange (Figure 5), which is mediated by DOCK9 (a GEF for Cdc42), the nucleotide-binding site is first exposed via a conformational transition of switch 1. The movement of switch 1 triggered by DOCK9 (for Cdc42) and DOCK2 (for Rac1) GEFs facilitates release of GDP via rotation of P-loop Cys^{18C} and disrupts interaction with GDP by excluding Mg^{2+} (129, 130). Mg^{2+} is regarded as enhancing nucleotide affinity by neutralizing the negatively charged phosphate groups (128). During GTP hydrolysis, crystal structure analyses showed that Rich - a Rho GAP, hydrolyzes GTP by interacting with Cdc42 through the switch

1 and switch 2 regions. Specifically, Arg⁸⁵ of Rho GAP contacts the β - γ oxygens and catalyzes the GTP hydrolysis by interacting with P-loop (131, 132).

Since Cdc42 and Rac1 are potential high value, therapeutic targets in ovarian and other cancers, several GTPase targeted inhibitors have been identified with various modes of action. Irrespective of whether they affect GTPase membrane association by inhibiting protein prenylation (e.g. statins), GTPase regulator activity (e.g. NSC23766, secramine) or nucleotide binding ability (e.g. CID2950007), none have as yet been translated to human use (99, 103-105).

To investigate small molecules targeting Cdc42 and Rac1 which could be rapidly translated to clinical application, high-throughput screening and computational simulation of the 2007 Prestwick Chemical Library[®] of off-patent and FDA approved drug-like small molecules were conducted and identified R-enantiomers of selected NSAIDs, R-naproxen and R-ketorolac, as potential Cdc42 and Rac1 inhibitors; while S-enantiomers, which are identified as COX inhibitors, displayed little or no activity against GTPases.

In this chapter, a flow cytometry based *in vitro* nucleotide binding assay was used to establish the mechanism of inhibition of the R-enantiomer of selected NSAIDs on Cdc42 and Rac1. This approach enables distinction of allosteric or competitive inhibition of nucleotide binding.

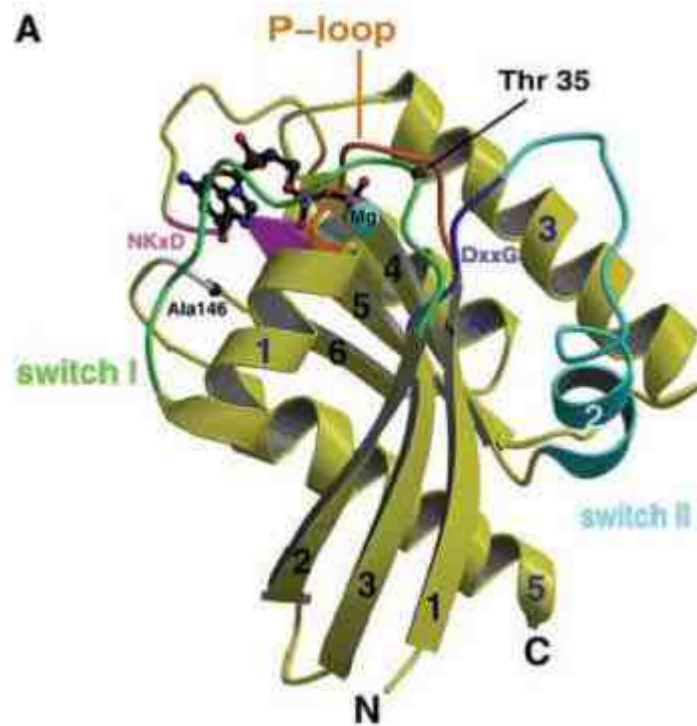


Figure 4. Structure of Rho GTPase. α -helix, β -sheet, switch 1, switch 2, and magnesium are indicated. (Vetter, IR et al., Science, 2001,294;1299-1304)

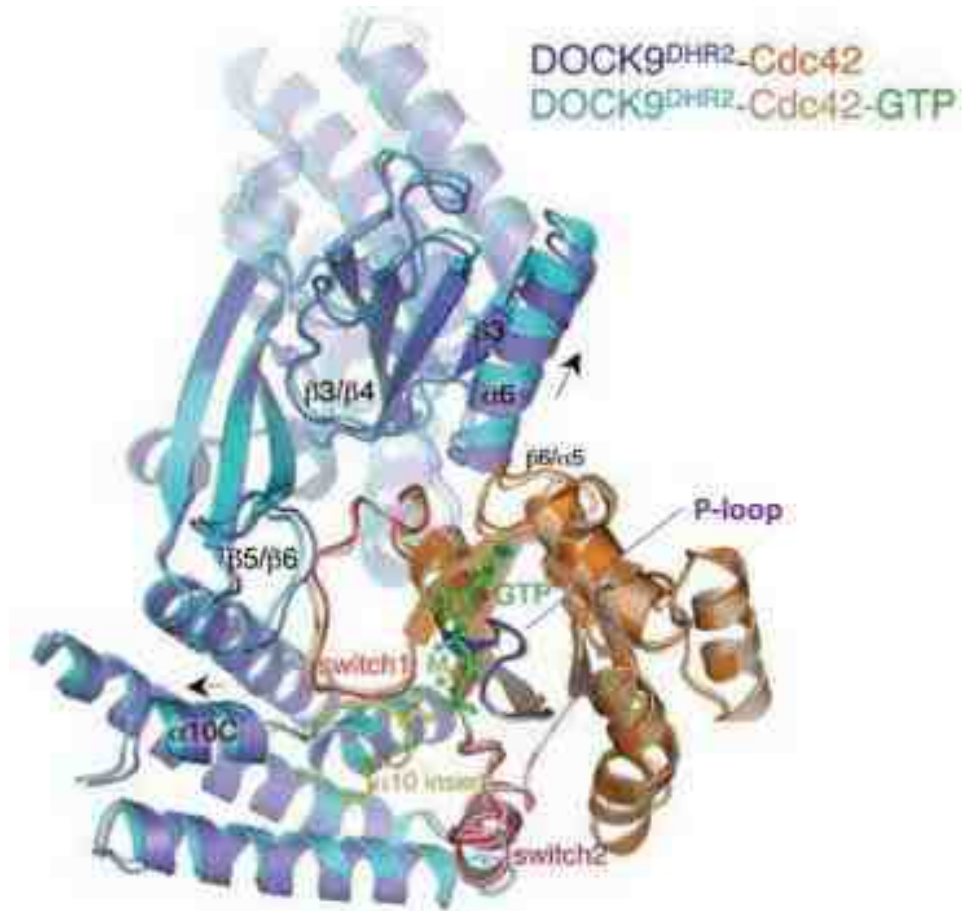


Figure 5. DOCK9 mediates the conformational changes in Cdc42 to facilitate nucleotide exchange. Cdc42 is colored orange/gold with switch 1 (red) and 2 (magenta) and P loop (blue). DOCK9 is colored in light blue/purple. GTP and magnesium are colored in green. DOCK9 interacts with Cdc42 and triggers the conformational change of switch 1, which facilitates Mg^{2+} exclusion and nucleotide exchange of GDP for GTP. The conformational change of DOCK9 includes $\alpha 6$ and $\alpha 10C$ helices (indicated by arrows) and $\beta 3/\beta 4$ and $\beta 5/\beta 6$ loops. (Kulkarni, K. et al., The Journal of Biological Chemistry, 2011; 286:25341-51)

Materials and Methods

Reagents

Superdex peptide beads (13 μm with an exclusion limit of 7kDa) were from Amersham Biosciences (custom-order). GST (glutathione S-transferase)-tagged GTPases (Cdc42/Rac1) were purified as described previously (133). Compounds for dose response assays were obtained as follows: R-ketorolac (K235600, Toronto Research Chemical Inc), S-ketorolac (K235605, Toronto Research Chemical Inc), R-naproxen (Acme Bioscience #A5026, Palo Alto, CA), S-naproxen sodium (N5160, Sigma-Aldrich), 6-methoxy-2-naphthalene acetic acid (6-MNA) (70620, Cayman Chemical, Ann Arbor, MI, USA), NSC23766 (204823, Santa Cruz, CA), CID2950007 (71203-35-5, Tocris). GST-PAK1 protein was from Millipore (14-864). BODIPY-GTP ((4,4-difluoro-4-bora-3a,4a-diaza-s-indacene or dipyrromethene boron difluoride) nucleotide analogue) was from Invitrogen Molecular Probes (Cat #: G22360). Ketorolac analogs (Screening Center Vial Barcode Number: SKCM101436, 101439, 100846, 104309, 104402, 104352, 100538, 100897, 102026, 100621, 101671, 103977, 103793, 103959) were synthesized by Dr. Jennifer Golden (Associate Director Medicinal Chemistry Center, Pharmaceutical Sciences Division, University of Wisconsin). CID2950007 analogs (44216842-CCCH₂CH₂NGtBoc(RS-II-16P), 44216842-Iodide(AG-II-106), 44216842-CCCH₂CH₂NH₂(RS-II-24C), 44216842-Heptynoic-Dioxy-HPY(490)) were synthesized by Dr. Jeffery Arterburn (Department of Chemistry, New Mexico State University). All compounds were dissolved in dimethyl sulfoxide

(DMSO) at 100 mM stock concentrations. Stocks should be aliquoted and multiple freeze-thaw cycles avoided.

Expression and Purification of GST-Cdc42/Rac1

GST-Cdc42/Rac1 protein was expressed in *E. coli* BL21 (DE3). Cultures were grown at 37°C to a bacterial density of 0.6-0.8 absorbance units at $\lambda=595$ nm. Bacteria were chilled on ice for 20 min and then induced by transfer to room temperature and addition of 0.2 mM isopropyl-beta-D-1-thiogalactopyranoside (IPTG) for 16-18 h to maximize yield of properly folded active fusion protein. Purification of GST-Cdc42/Rac1 was used for the flow cytometry based in vitro nucleotide binding assay according to standard procedures (133).

Synthesis of Glutathione (GSH) Beads for Flow Cytometry Assay

High density glutathione (GSH) conjugated beads were synthesized for flow cytometry assays by loading Superdex peptide beads with GSH as previously reported (134). Typical site occupancies of the beads at saturation are in the range of 1 to 4×10^6 ligand sites/bead (determined by the characteristic kinetic and equilibrium binding of GST fused green fluorescent protein (GFP) (135).

Immobilization of Cdc42/Rac1 on GSH Beads for Flow Cytometry

All in vitro nucleotide binding to GTPases and measurements were performed in HPS buffer (30 mM Hepes, pH 7.5, 20 mM NaCl and 100 mM KCl) containing 1 mM EDTA, 0.1% BSA (w/v) and 0.01% NP40 (v/v). A Becton Dickinson FACScan flow cytometer with a 488 nm excitation laser and standard

detection optics was used for all assays (133). Purified GST-tagged Cdc42/Rac1 protein was incubated in a 1.5 ml Eppendorf tube at 4°C overnight with 2×10^5 GSH beads in a total volume of 100 μ l of HPS buffer containing 1 mM EDTA, 1 mM dithiothreitol (DTT) added fresh and 0.1% BSA (w/v). Unbound protein was removed by centrifugation and washes by spinning GTPase bound beads twice at 800 g followed by resuspension of washed beads in fresh HPS buffer with 1 mM EDTA, 1 mM DTT added fresh and 0.1% BSA (w/v).

Flow Cytometric BODIPY-GTP Binding Assay

The nucleotide binding assays were carried out according to the protocols described previously (134). In order to measure BODIPY-GTP binding to Cdc42 and Rac1 GTPases, the in vitro nucleotide binding assay was performed in HPS buffer containing 1 mM EDTA in order to chelate the magnesium and facilitate GTPase nucleotide exchange. Briefly, individual GST-GTPases were allowed to bind to their respective GSH beads and combined. In the equilibrium assay, 2×10^3 GSH beads loaded with GST-GTPase were pre-incubated with either DMSO or a fixed compound concentration for 15 min followed by incubation with varying concentrations of BODIPY-GTP for 30 min at room temperature. A stock solution of ketorolac was prepared by dissolving to 10 mM concentration in DMSO. A three-fold serial dilution was made from the 10 mM stock in DMSO. In dose-response assays, 2×10^3 GSH beads loaded with GST-GTPase were pre-incubated with DMSO or increasing concentrations of the compounds for 15 min followed by incubation with a fixed concentration of BODIPY-GTP for 30 min at room temperature. Final DMSO concentrations were held constant in each

sample at 1%. For measurement, samples were diluted at least 10-fold and delivered and analyzed on a BD FACScan flow cytometer.

To measure the effect of a fluorescent CID2950007 analog (RS-II-79, synthesized by Dr. Arterburn and colleagues) on Cdc42 nucleotide binding, a single-plex dose-response assay was conducted. Diluted samples were measured on a BD FACScan flow cytometer. The fluorescence intensity of BODIPY-GTP was detected by FL-1 ($\lambda_{\text{ex}}=488$ nm, $\lambda_{\text{em}} = 530/30$ nm). FL-2 ($\lambda_{\text{ex}}=488$ nm, $\lambda_{\text{em}} = 585/42$ nm) was used to measure the fluorescence intensity of the fluorophore (HPY490) (136), which quantifies the bound RS-II-79 on GTPase. The non-specific binding of the RS-II-79 was measured by incubating GST-GSH beads with the fluorescent compound. The intensity of the bona fide bound RS-II-79 was calculated as: Mean Channel Fluorescence _(Cdc42-GSH beads) – Mean Channel Fluorescence _(GST-GSH beads).

Live Cell Imaging

GFP-actin-expressing MDCK cells were cultured on coverslips to 70-80% in DMEM media containing 10% FBS overnight. The next day the coverslip was transferred to NuncTM glass bottom dish (Thermo Scientific, Cat #: 150682) in DMEM-No Phenol Red (Gibco, Cat #: 31053-028) media with 10% FBS and loaded with 10 μ M RS-II-79. Confocal images were obtained using a Zeiss Axiovert 200M microscope and a 60x oil immersion objective. RS-II-79 (HPY-490) fluorescence was monitored with excitation at 480 nm and emission above 530 \pm 30 nm. GFP fluorescence was determined with excitation at 490 nm and

emission above 510 ± 10 nm. The fluorescence intensity of RS-II-79 was analyzed by Slidebook 5 software.

HPY490 Labeled RS-II-79 Penetration into MCA

For multicellular aggregate (MCA) assays, 2,000 SKOV3ip-GFP cells were seeded into each well of a Lipidure-coated 96 well plate (NOF America Corporation, White Plains, NY) and incubated for 48 hours to allow for the formation of MCA. MCAs were transferred to a Nunc Lab-Tek Chambered Coverglass 8-well imaging chamber (Thermo Scientific) and treated with fluorescently-labeled RS-II-79 ($10 \mu\text{M}$) to determine drug penetration. Confocal images through the center of the spheroid were captured at time points up to 66 minutes of treatment on a Zeiss Axiovert 200 M inverted confocal microscope equipped with a warming chamber to maintain the temperature at 37°C . Images were analyzed with Zeiss Zen software.

Statistical Analyses

Prism 5 software (GraphPad) was used to analyze all data to determine statistical significance. One-way ANOVA (Analysis of Variance) with Dunnett's test for multiple comparisons was performed to compare differences between the means of each group relative to the control group for all assays. P-values less than 0.05 were considered statistically significant. ANOVA was performed on these standardized values.

Results

R-ketorolac and R-naproxen Inhibit Cdc42 and Rac1 GTPase Nucleotide Binding as Allosteric Inhibitors

To test the capacity of ketorolac (Figure 6A) to inhibit GTPase nucleotide binding activity and determine the mechanism of inhibition, a bead based flow cytometry assay – which measures the *in vitro* GTPase nucleotide binding activity – was used. First, equilibrium nucleotide binding assays were performed under conditions where the tested compound concentration was held fixed against increasing concentrations of fluorescent nucleotide. In the presence of R-ketorolac, both the maximum fluorescence (B_{max}) and the apparent dissociation constant (K_d) of BODIPY-GTP for Cdc42 and Rac1 changed, which suggests a noncompetitive mechanism of action (Figure 6B, 6D, Table 1). S-ketorolac did not change the B_{max} and the K_d for Cdc42 (Figure 6C, Table 1) and exhibited a minor inhibition of Rac1 only at the maximum concentration of 100 μ M (Figure 6E). Single-plex dose-response measurements were used to verify the enantiomer selectivity of ketorolac for inhibiting nucleotide binding by Cdc42 and Rac1. The nucleotide concentrations in the assay were fixed at the determined dissociation constants ($K_d \approx 300$ nM). Increasing R-ketorolac concentrations reduced BODIPY-GTP binding, with respective EC_{50} (half-maximal effective concentration) values of 1.89×10^{-5} M for Cdc42 and 2.31×10^{-5} M for Rac1 (Figure 6F, 6G). The maximal inhibitory response was ~20% for both GTPases. S-ketorolac did not exhibit an inhibitory activity against either GTPase under the

tested conditions. Together, these findings suggest an enantiomer-selective, inhibitory activity of R-ketorolac against the nucleotide binding activity of Cdc42 and Rac1. Mechanistically, R-ketorolac action is consistent with an allosteric inhibition of GTPase nucleotide binding.

Moreover, single-plex dose-response measurements were used to test the effect of R-naproxen on Cdc42 and Rac1 nucleotide binding. The nucleotide concentration in this assay was fixed at the determined dissociation constant of 300 nM. As shown in Figure 7, nucleotide binding to the Cdc42 and Rac1 GTPases was inhibited by R-naproxen with an EC_{50} of 18 μ M. The maximal inhibitory response was ~30% for both GTPases. However, EC_{50} for the inhibition of Rac1 by S-naproxen was higher than 200 μ M. S-naproxen exhibited a similar EC_{50} for inhibition of Cdc42 but failed to reach the threshold of 20%. Together, these findings demonstrate R-naproxen, but not S-naproxen inhibits Cdc42 and Rac1 nucleotide binding, which is consistent with the enantiomer-selectivity of R-ketorolac.

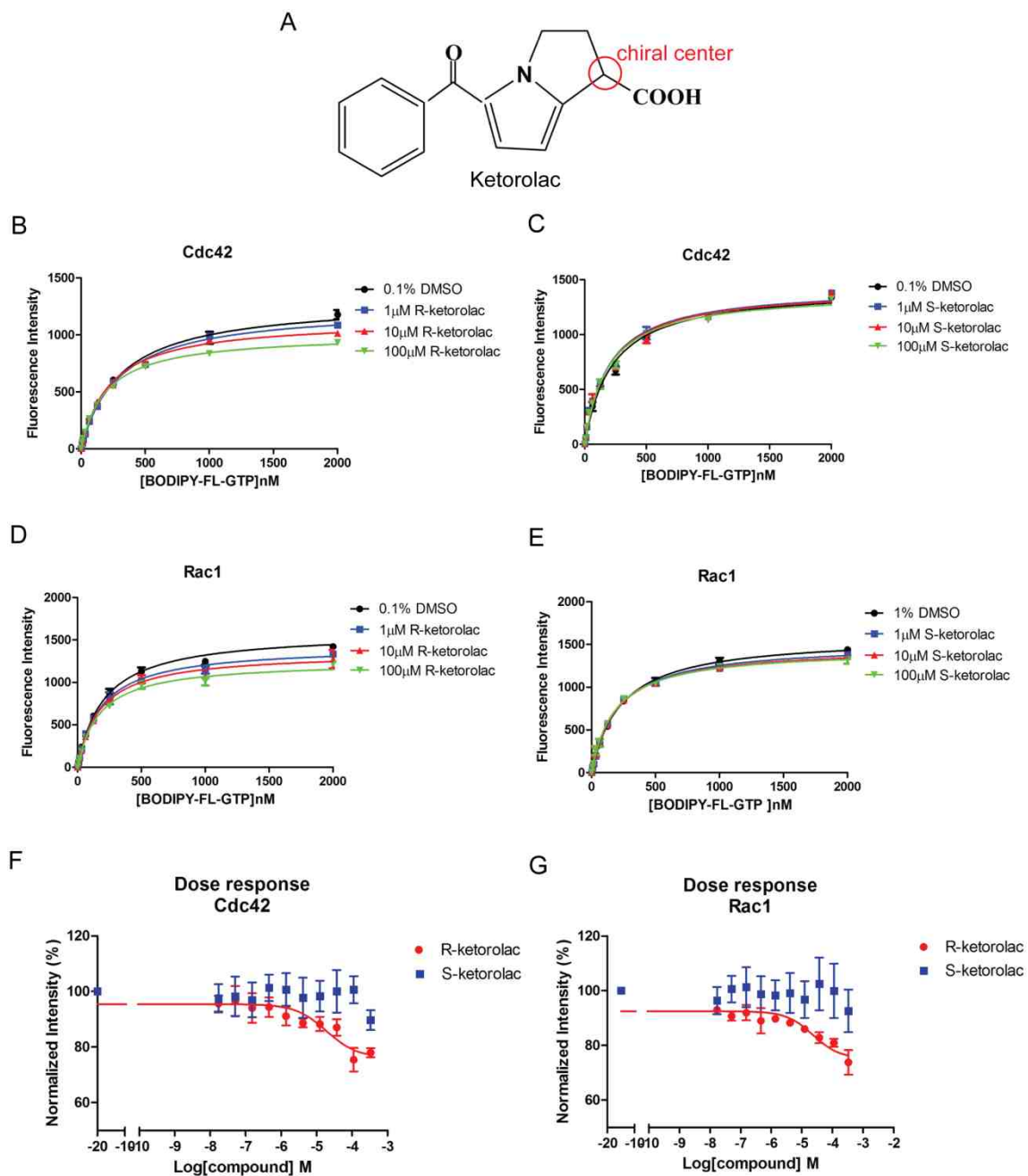


Figure 6. R-ketorolac acts as an allosteric inhibitor to selectively inhibit BODIPY-GTP binding to Cdc42 and Rac1 GTPases. (A) Chemical structure of R- and S-ketorolac with chiral center noted. (B-C) The presence of R-ketorolac changed both the B_{max} and the K_d (values are tabulated in Table 1) of BODIPY-GTP binding to Cdc42 measured under equilibrium binding conditions, while S-

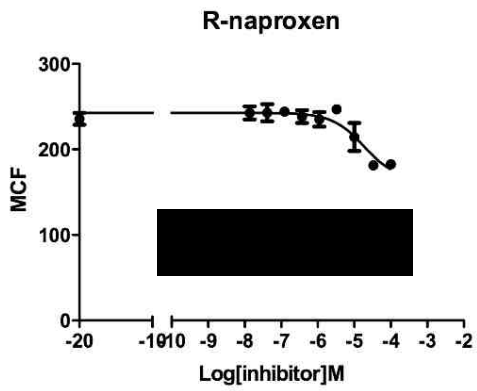
ketorolac did not affect BODIPY-GTP binding. (D-E) R-ketorolac changed the B_{\max} and the K_d of BODIPY-GTP binding to Rac1 measured under equilibrium binding conditions, while S-ketorolac did not affect BODIPY-GTP binding except at 100 μM . The equilibrium binding of BODIPY-GTP to the GTPases was measured in the presence of 0.1% DMSO or various concentrations of R- or S-ketorolac (1~100 μM). BODIPY-GTP binding curves were fitted to a hyperbolic one-site binding equation from GraphPad Prism 5. (F-G) R-ketorolac in contrast to S-ketorolac inhibited BODIPY-GTP binding to Cdc42 and Rac1 GTPases in a dose-dependent manner. BODIPY-GTP concentration was fixed at 300 nM for these experiments. The inhibition curves were fitted to the sigmoidal dose-response equation from GraphPad Prism5. In all experiments, GST-Cdc42 or Rac1 were immobilized on GSH beads and used to measure BODIPY-GTP binding. Bead-associated fluorescence intensity was quantified by flow cytometry and used to monitor drug treatment induced changes in nucleotide binding. Fluorescence attributed to nonspecific nucleotide binding was subtracted accordingly. Quantification of three independent measurements is plotted \pm SEM.

Table 1 Biochemical properties of Cdc42 and Rac1 nucleotide binding (BODIPY-GTP) with R- or S-ketorolac treatment

		Cdc42		Rac1	
		R-ketorolac	S-ketorolac	R-ketorolac	S-ketorolac
<i>B_{max}</i>	0.1% DMSO	1303 ± 38.45	1429 ± 49.49	1594 ± 28.08	1595 ± 23.75
	1 μM	1243 ± 22.98	1436 ± 48.54	1428 ± 21.17	1509 ± 19.02
	10μM	1134 ± 29.46	1426 ± 52.29	1355 ± 26.64	1471 ± 25.36
	100μM	1009 ± 13.20	1388 ± 38.97	1249 ± 23.76	1444 ± 27.02
<i>K_d</i>	0.1% DMSO	303.6 ± 26.56	219.6 ± 24.47	206.2 ± 13.66	230.7 ± 10.93
	1 μM	288.7 ± 16.03	195.8 ± 21.98	185.9 ± 10.59	204.4 ± 8.433
	10μM	226.6 ± 12.42	197.5 ± 23.90	176.1 ± 13.43	193.4 ± 11.06
	100μM	195.6 ± 8.465	186.7 ± 17.54	169.8 ± 11.94	180.6 ± 11.39

The B_{max} and K_d for the nucleotide binding (BODIPY-GTP) values were derived from data shown in Figure 6B-6E using Prism 5 software (GraphPad).

A. Rac1 nucleotide binding



B. Cdc42 nucleotide binding

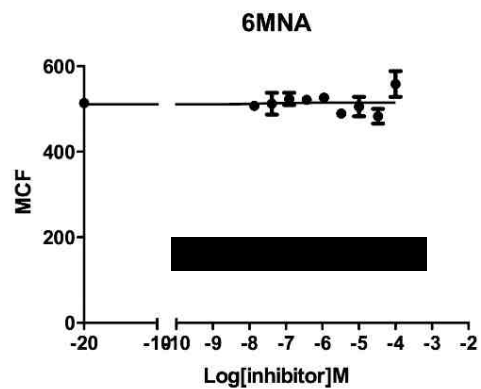
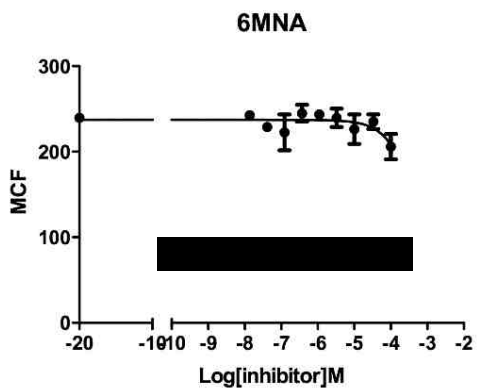
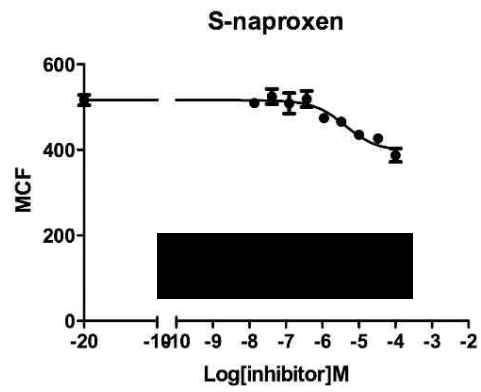
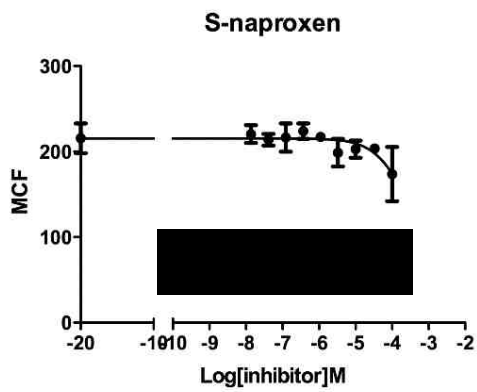
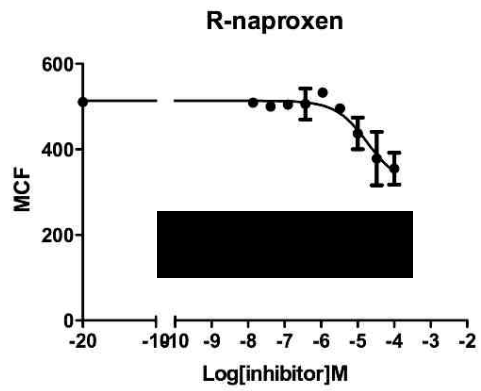


Figure 7. R-naproxen selectively inhibits BODIPY-GTP binding by Rac1 and Cdc42 in vitro. R-naproxen in contrast to S-naproxen and 6-methoxy

naphthalene acid (6MNA) inhibited BODIPY-GTP binding to GSH bead immobilized GST-Rac1 (A) and GST-Cdc42 (B) GTPase in a dose-dependent manner. BODIPY-GTP concentration was held constant at 100 nM for these experiments and drug concentrations varied from 10 nM to 100 μ M. Bead-associated fluorescence intensity was quantified by flow cytometry and used to monitor drug treatment induced changes in nucleotide binding. The inhibition curves were fitted to the sigmoidal dose-response equation using GraphPad Prism 5. Quantification of three independent measurements is plotted \pm SEM.

Molecular Docking of ketorolac and naproxen on Cdc42 and Rac1 GTP Bound Shows Enantiomer Selectivity of R-ketorolac-Magnesium Interaction

A recent structural study of guanine nucleotide exchange factor (GEF)-mediated nucleotide exchange on Cdc42 by Yang et al. demonstrated the importance of a valine residue (1951) in the nucleotide sensing domain of the DOCK9 GEF (129). The insertion of the sensing domain valine occludes the critical coordination of Mg^{2+} by the nucleotide and the consequent reduced charge shielding significantly decreases nucleotide affinity and leads to its release from the GTPase. The mechanism of Mg^{2+} exclusion to promote nucleotide release is distinct from that of other GEF proteins and is suggested to enhance DOCK GEF activity against a broader range of GTPases (129). Therefore, Mg^{2+} exclusion was considered as a possible mechanism for destabilization of nucleotide binding by R-ketorolac and R-naproxen through docking analyses. The carboxyl moiety has the potential to neutralize or displace Mg^{2+} from interacting with the nucleotide by forming a competing complex with the Mg^{2+} . In Figure 8, docking models based on Mg^{2+} exclusion used by DOCK9 GEF to promote nucleotide exchange on Cdc42 and Rac1 support the observed stereo-selectivity of R-ketorolac and R-naproxen, in which the carboxyl group is more favorably positioned than S-enantiomers to participate in Mg^{2+} exclusion.

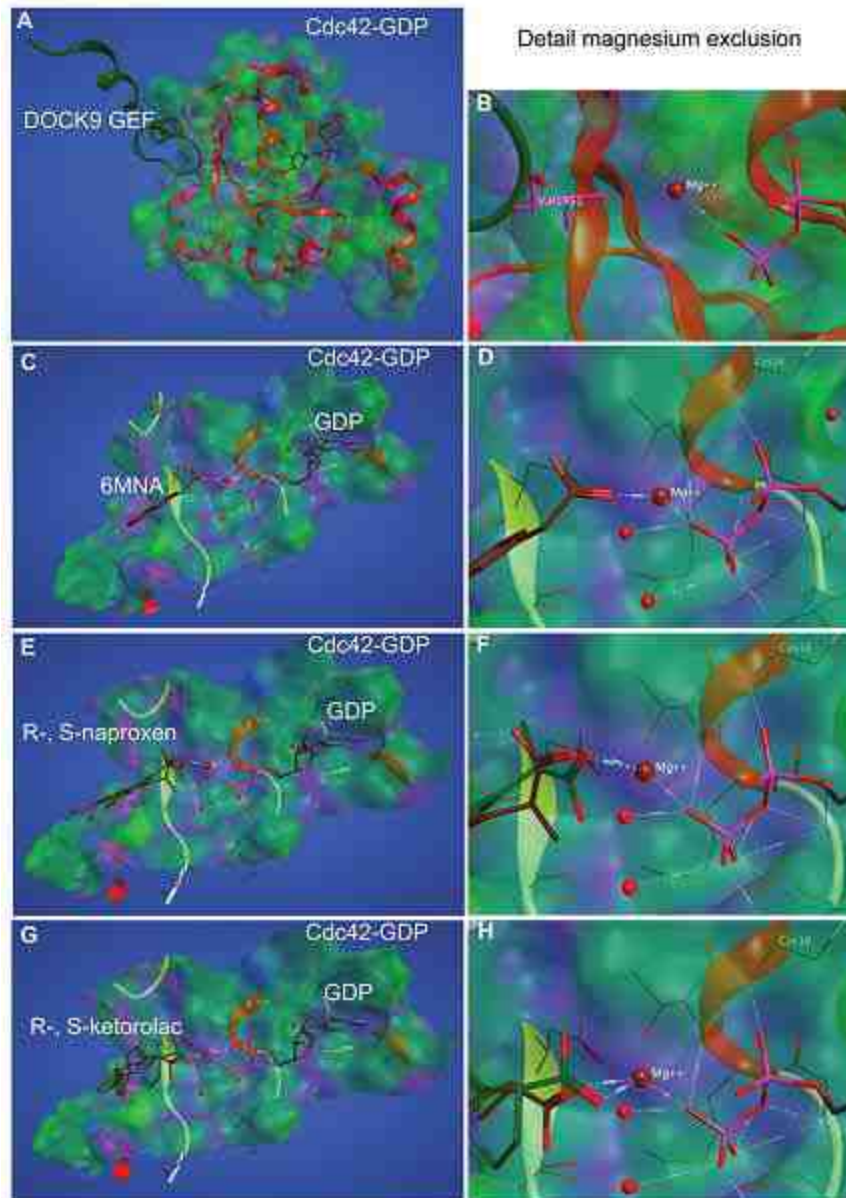


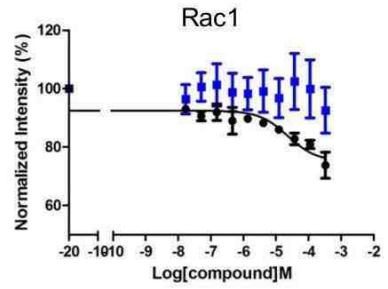
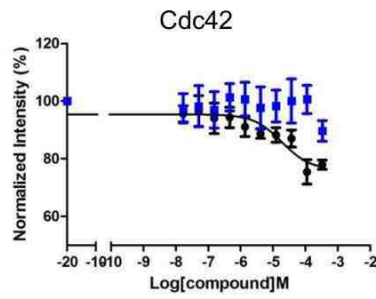
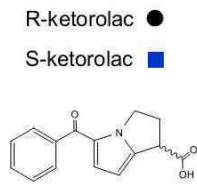
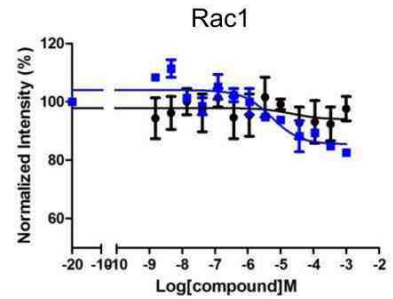
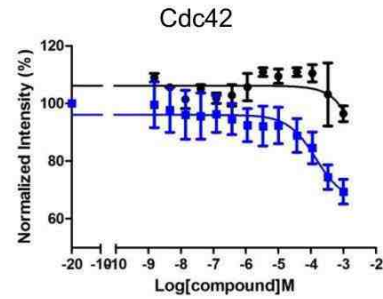
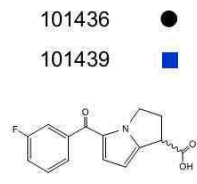
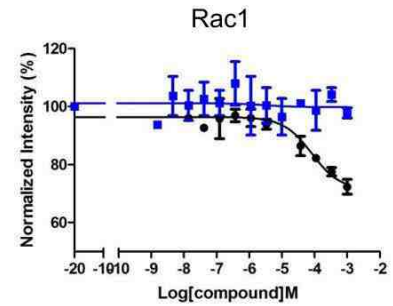
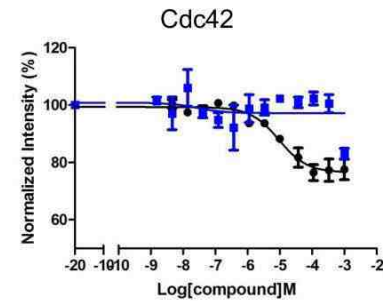
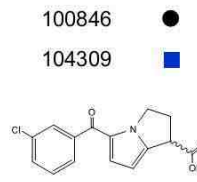
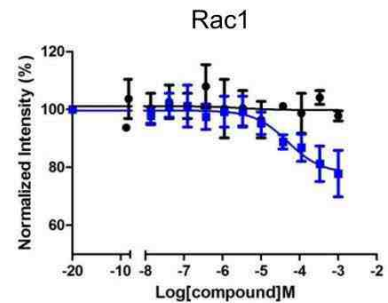
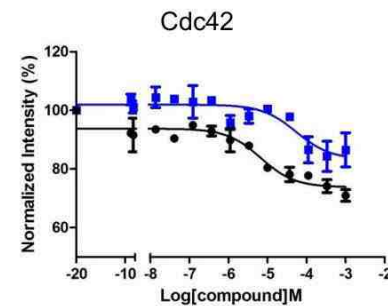
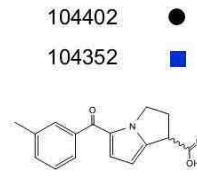
Figure 8. Compound docking to Cdc42 based on a magnesium exclusion model. The docking model is based on the work of Yang et al., 2009 (129) wherein Val1951 in the sensing domain of DOCK9 (dark green ribbon) was suggested to reduce nucleotide interaction with Mg^{2+} via steric hinderance or ‘exclusion’ and thereby destabilize nucleotide binding to cause release from the GTPase active site. (A-B) The crystal structure of Cdc42-GDP in complex with

the DOCK9 GEF (PDB ID 2WMN) was used to predict the active site docking of (C-D) 6-MNA, (E-F) R-, S-naproxen and (G-H) R-, S-ketorolac. (B, D, F, H) The carboxyl moiety in all compounds is proposed to interact with the Mg^{2+} , thereby precluding interaction with GDP and reducing binding affinity analogous to Val1951. R-naproxen and R-ketorolac are shown in green. 6-MNA, S-naproxen and S-ketorolac are shown in rust color. R-enantiomers show more favorable interaction with Mg^{2+} than S-enantiomers due to rotational constraints imposed on the carboxylate by the stereocenter. Images provided courtesy of Drs. T.I. Oprea and O. Ursu (Division of Translational Informatics, Department of Internal Medicine, University of New Mexico).

Structure-Activity Relationship (SAR) Determination Using Modified Ketorolac Analogs

The parent scaffold, represented by ketorolac, was modified on the phenyl group to afford the initial analogue collection. Analogs bearing changes to the phenyl ring moiety of the parent ketorolac were proposed since that functional group occupies a lipophilic area in the binding model that would benefit from a small appendage (e.g., Me, CF₃, or halogen). These small extensions from the phenyl ring were proposed to make key contacts within the binding site which might alter binding affinity. The activities of derivatives were tested in single-plex dose-response assays on Cdc42 and Rac1 GTPase nucleotide binding, and EC₅₀ values were determined (Figure 9 and Table 2). In comparison to the parent compounds, most compounds exhibited similar magnitudes of inhibition and EC₅₀ values on GTPase nucleotide binding. Interestingly, derivatives modified by trifluoromethyl (SKCM 102026) and 3-thiophene (SKCM 103793) resulted in an activation of nucleotide binding on Cdc42 with EC₅₀ values of 2.43×10⁻⁸ M and 2.28×10⁻⁸ M respectively. SKCM -101439, modified with a fluorine atom resulted in a 2.5-fold increased potency on Rac1 (EC₅₀=5.28×10⁻⁶ M), while reducing potency on Cdc42. 2-thiophene SKCM-103977 altered the compound activity from inhibition to preferential activation of Rac1 nucleotide binding with an EC₅₀ of 1.98×10⁻⁸ M. Similarly, 3-thiophene SKCM 103793 switched the activity from inhibition to preferential activation of Cdc42 nucleotide binding with an EC₅₀ value of 2.28×10⁻⁸ M. Notably, the potency of SKCM 103977 and SKCM 103793 were dramatically increased (~100-fold) as activators. The structure of the ketorolac

analogs are shown in Table 2 along with a tabulation of their efficacies and potencies against Cdc42 and Rac1 nucleotide binding activity. Although enantiomeric identity of each pair of compounds is unknown and it is difficult to conclude the relationship of enantiomeric selectivity observed between the analogs and the parent compound, the structural modification in the phenyl group is confirmed to have an effect on the overall GTPase nucleotide binding activity. Trifluoromethyl (SKCM 102026) and 3-thiophene (SKCM 103793) resulted in an activation of Cdc42 nucleotide binding. This finding supports that lipophilic areas play a key role in modulating GTPase activity, possibly by affecting property of carboxyl group at the chiral center.

A**B****C****D**

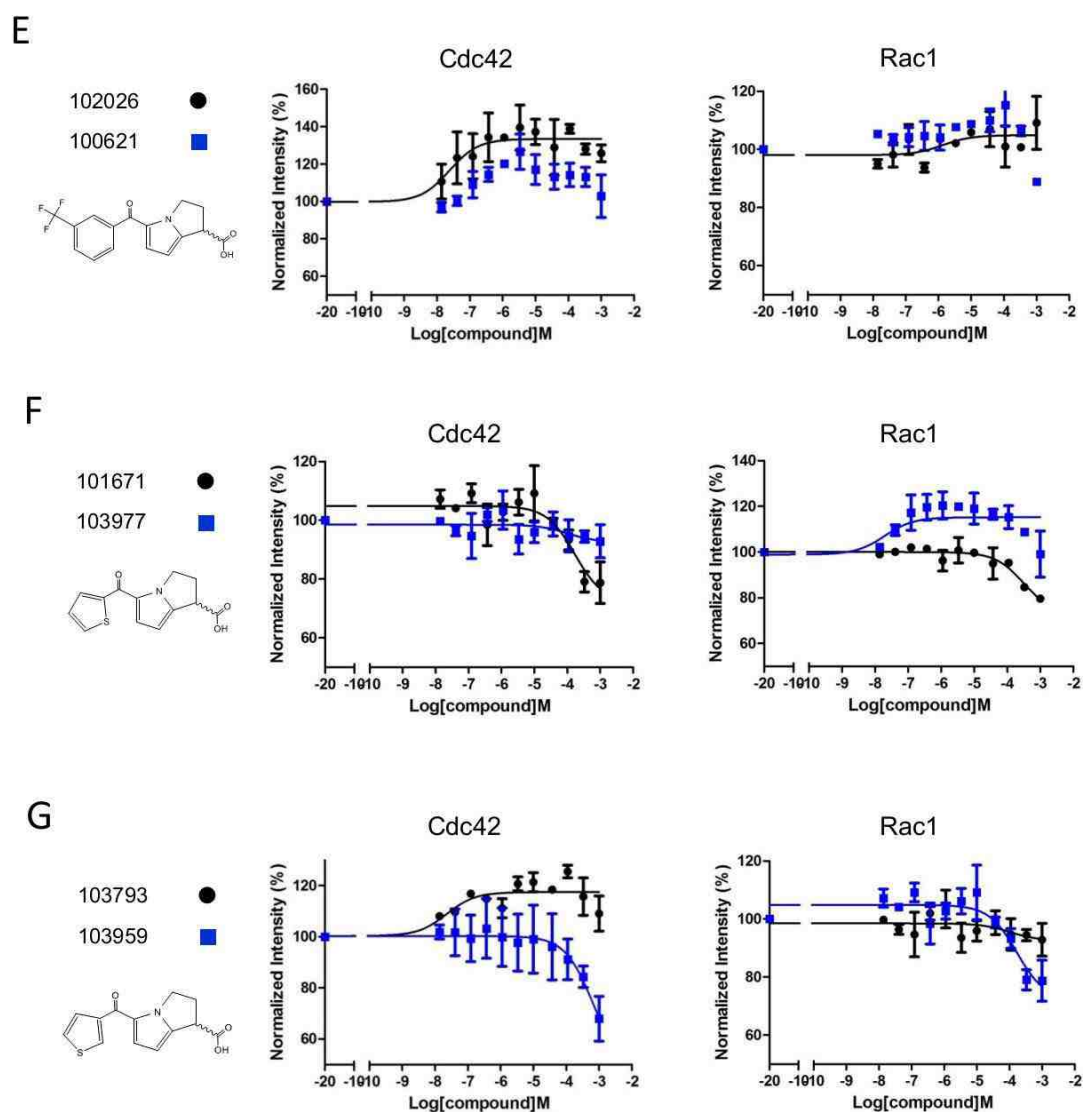
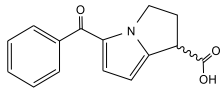
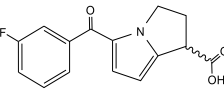
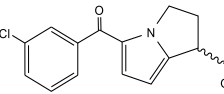
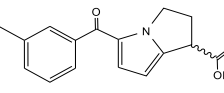
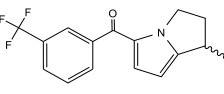
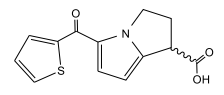
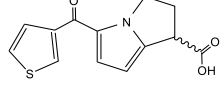


Figure 9. The impact of ketorolac analogs on Cdc42 and Rac1 nucleotide binding. Parent compounds – ketorolac (A) were modified on the phenyl with a fluorine atom (B), a chlorine atom (C), a methyl group (D), or a trifluoromethyl group (E). Alternatively, the phenyl ring was replaced by 2-thiophene (F) or 3-thiophene (G) rings. These analogs were tested by a single-plex dose-response assay to evaluate their activities of nucleotide binding on Cdc42 and Rac1 GTPases. BODIPY-GTP concentration was fixed at 300 nM. The inhibition

curves were fitted to the sigmoidal dose-response equation from GraphPad Prism5. In all experiments, GST-Cdc42 or Rac1 were immobilized on GSH beads and used to measure BODIPY-GTP binding. Bead-associated fluorescence intensity was quantified by flow cytometry and used to monitor drug treatment induced changes in nucleotide binding. Quantification of two independent measurements is plotted \pm SEM,

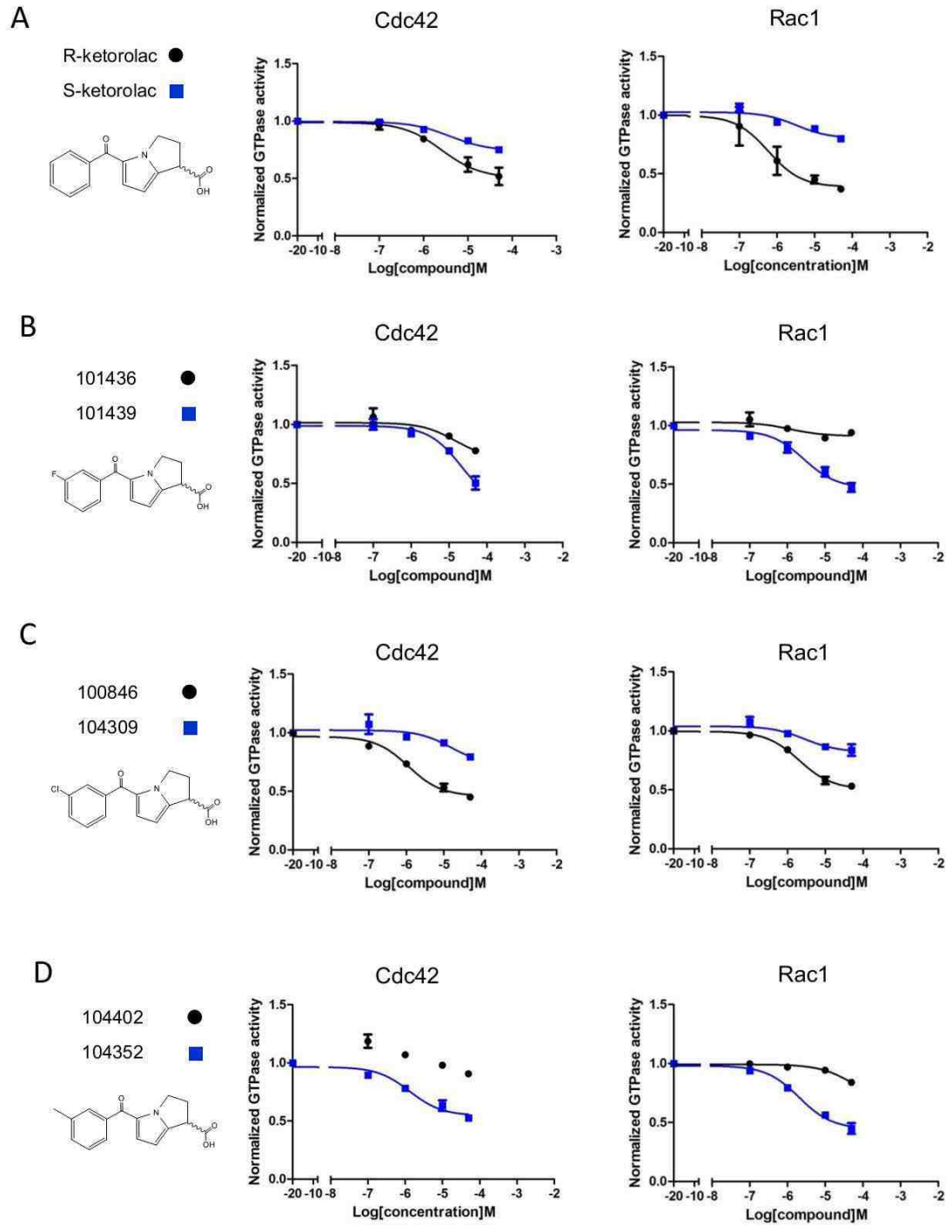
Table 2 Impact of ketorolac analogs on in vitro Cdc42 and Rac1 nucleotide binding

Structure	Screening Center Vial Barcode Number	Cdc42		Rac1	
		Inhibition(-) /Activation(+) magnitude	EC ₅₀	Inhibition(-) /Activation(+) magnitude	EC ₅₀
	R-ketorolac	~ 20% (-)	1.89×10 ⁻⁵	~ 20% (-)	2.31×10 ⁻⁵
	S-ketorolac	<10% (-)		<10% (-)	-
	SKCM 101436	< 10% (-)	-	< 10% (-)	-
	SKCM 101439	~ 30% (-)	1.42×10 ⁻⁴	~ 20% (-)	5.28×10 ⁻⁶
	SKCM 100846	~ 20% (-)	9.38×10 ⁻⁶	~ 25% (-)	8.17×10 ⁻⁵
	SKCM 104309	< 10% (-)	-	< 10% (-)	-
	SKCM 104402	~ 20% (-)	5.46×10 ⁻⁵	< 10% (-)	-
	SKCM 104352	~ 20% (-)	6.75×10 ⁻⁶	~ 20% (-)	4.99×10 ⁻⁵
	SKCM 102026	~ 25% (+)	2.43×10 ⁻⁸	< 10% (-)	-
	SKCM 100621	< 10% (-)	-	< 10% (-)	-
	SKCM 101671	~ 31% (-)	1.72×10 ⁻⁴	~ 20% (-)	3.21×10 ⁻⁴
	SKCM 103977	< 10% (-)	-	< 10% (+)	1.97×10 ⁻⁸
	SKCM 103793	~ 15% (+)	2.28×10 ⁻⁸	< 10% (-)	-
	SKCM 103959	~ 32% (-)	6.75×10 ⁻⁴	~ 20% (-)	1.03×10 ⁻⁴

The Effect of Ketorolac Analogs on Cdc42 and Rac1 Activation in SKOV3ip Cells

A flow-based GTPase effector binding assay (G-trap, detects and quantifies GTPases in the GTP-bound conformation) (135) was performed to test the impact of ketorolac analogs on Cdc42 and Rac1 activation in SKOV3ip cells. Cells were starved for 2 h, treated with each compound for 2 h, and finally stimulated with EGF (10 ng/ml). As shown in Figure 10, in comparison to the parent compounds, most derivatives did not alter ketorolac activity, which showed similar inhibition efficacies and EC₅₀ values on Cdc42 and Rac1 GTPase activation. Notably, the 2-thiophene modified analog (SKCM 101671 and SKCM 103977) exhibited less enantiomer selectivity on the inhibition of Cdc42. The trifluoromethyl (SKCM 102026 and SKCM 100621) resulted in loss of inhibition against Rac1 for both enantiomers. SKCM 102026 behaved as an inhibitor in cells, having been clarified as an activator in vitro (Figure 9E); behavior is similar to screening studies that identified R-naproxen as an activator, while cell based studies demonstrated inhibitory activity against Rac1 and Cdc42 (Ref PLoS One). The different observed behaviors of SKCM 102026 under different assay conditions may be due to the experimental context such as the local concentration of Mg²⁺, nucleotide, and other regulatory proteins (e.g. GEFs, GAPs). Thus, compounds identified as activators only through in vitro nucleotide binding assays, warrant further study in cell-based assays (137). Importantly, 3-thiophene (SKCM 103793 and SKCM 103959) exhibited more enantiomeric selectivity in the inhibition of both Cdc42 and Rac1 GTPases and the active

enantiomer retained the inhibition efficacy (~50%) and similar EC_{50} values compared to the parent compound. Taken together, these results suggest trifluoromethyl and 2-thiophene alter ketorolac activity, which may be due to changed properties of the carboxyl group at the chiral center. One possibility is that the trifluoromethyl group, as a strong electron-withdrawing group, may enhance the interaction between the $-COOH$ and Mg^{2+} by decreasing the electron density of the carboxyl group. 3-thiophene, as a strong electron-donating group, may reduce the interaction between $-COOH$ and Mg^{2+} by decreasing the acidity of the $-COOH$. The other possibility is that the trifluoromethyl group might actually improve lipophilic stabilization of the parent compound and decrease carboxyl magnesium interaction through an electron donating activity, which induces the observed increased nucleotide binding on GTPase. In addition, thiophene may also interact with Mg^{2+} directly through the cation- π interaction. According to the results of the GTPase nucleotide binding assay and the G-trap assay, 3-thiophene modification in the phenyl ring was tolerated and provides guidance for developing improved ketorolac derivatives with higher affinity, efficacy and enantiomeric selectivity.



-continued

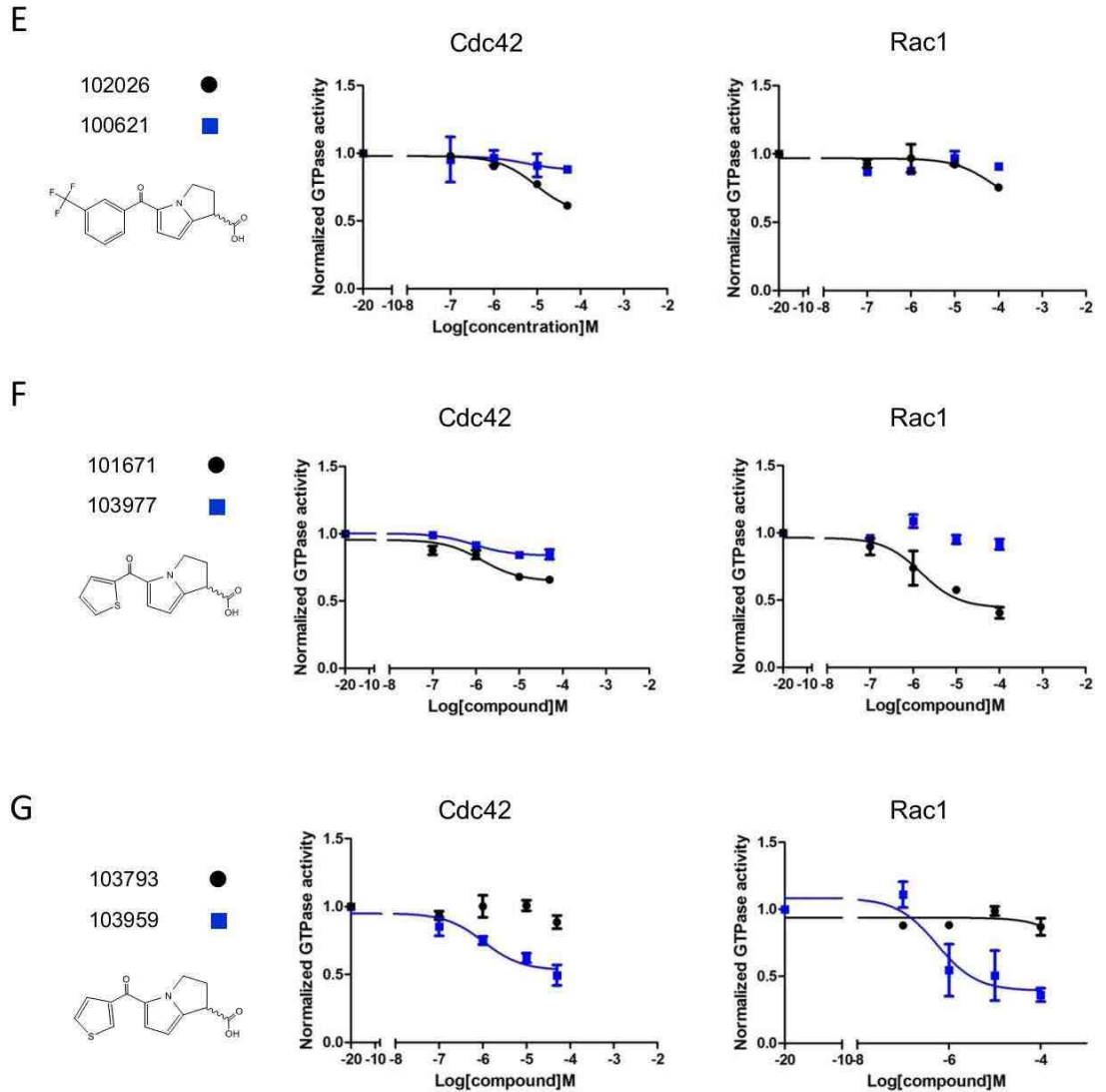
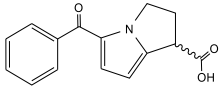
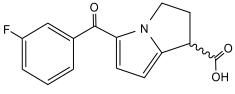
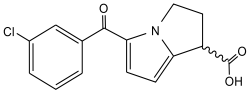
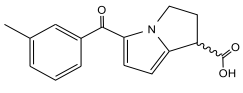
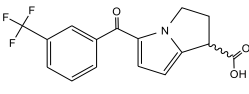
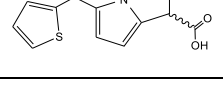
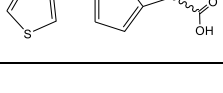


Figure 10. Ketorolac derivatives exhibit different inhibitory effects on Cdc42 and Rac1 activation in SKOV3ip cells. Parent compound – ketorolac (A) was modified on the phenyl with a fluorine atom (B), a chlorine atom (C), a methyl group (D), or a trifluoromethyl group (E). Alternatively, the phenyl ring was replaced by 2-thiophene (F) or 3-thiophene (G) rings. These analogs were tested by a GTPase effector binding (G-trap) assay to evaluate their activities on

epidermal growth factor mediated Cdc42 and Rac1 activation in SKOV3ip cells. In all experiments, SKOV3ip cells were starved in 0% FBS media for 2 h and pretreated with individual drugs for 2 h prior to EGF (10 ng/ml) stimulation. Activated Cdc42 and Rac1 levels in cell lysates were measured using a flow cytometry based GTPase effector binding assay. Flow intensities were normalized to untreated controls. Quantification of two independent measurements is plotted \pm SEM.

Table 3 Impact of ketorolac analogs on Cdc42 and Rac1 activation in cell-based assay

Structure	Screening Center Vial Barcode Number	Cdc42		Rac1	
		Inhibition(-) /Activation(+) magnitude	EC ₅₀	Inhibition(-) /Activation(+) magnitude	EC ₅₀
	R-ketorolac	~ 50% (-)	2.58×10 ⁻⁶	~ 50% (-)	5.87×10 ⁻⁷
	S-ketorolac	<10% (-)	-	<10% (-)	-
	SKCM 101436	~ 20% (-)	1.42×10 ⁻⁵	< 10% (-)	-
	SKCM 101439	~ 50% (-)	2.15×10 ⁻⁵	~ 50% (-)	2.71×10 ⁻⁶
	SKCM 100846	~ 50% (-)	1.13×10 ⁻⁶	~ 50% (-)	2.03×10 ⁻⁵
	SKCM 104309	~ 20% (-)	1.54×10 ⁻⁵	< 10% (-)	-
	SKCM 104402	< 10% (-)	-	< 10% (-)	-
	SKCM 104352	~ 50% (-)	2.02×10 ⁻⁶	~ 50% (-)	1.32×10 ⁻⁵
	SKCM 102026	< 10% (-)	9.25×10 ⁻⁶	~ 20% (-)	7.10×10 ⁻⁵
	SKCM 100621	< 10% (-)	-	< 10% (-)	-
	SKCM 101671	~ 30% (-)	1.41×10 ⁻⁶	~ 50% (-)	1.52×10 ⁻⁶
	SKCM 103977	< 10% (-)	-	< 10% (-)	-
	SKCM 103793	< 10% (-)	-	< 10% (-)	-
	SKCM 103959	~ 50% (-)	1.04×10 ⁻⁶	~ 50% (-)	5.48×10 ⁻⁷

CID2950007 Analogs Inhibit GTP Binding to Cdc42

CID2950007 has been identified as a noncompetitive allosteric Cdc42 inhibitor (Avg EC_{50} 2.6 μ M), which binds to guanine nucleotide-bound Cdc42, induces dissociation of nucleotide, and locks the protein in an inactive conformation (104, 138). The related structural analog CID44216842 differs by the replacement of phenyl and 4-methoxyphenyl groups of CID2950007 with 3-methoxyphenyl and 4-bromophenyl substituents at the 3- and 5-positions of the 4,5-dihydro-1*H*-pyrazole core, respectively. CID44216842 exhibited a slightly improved EC_{50} (0.4 μ M) although the aqueous solubility was decreased (104, 138). In preparation for fluorescent modification, three analogs were synthesized with modifications to the phenyl ring in the pyrazole 5-position as shown in Figure 11. The 4-bromophenyl substituent of CID44216842 was selected as the site for the introduction of a linking alkylamine moiety that could be conjugated to amine-reactive fluorophores. The 4-iodophenyl analog AG-II-106 was synthesized as a more reactive substrate for the palladium catalyzed carbon-carbon coupling chemistry that was envisioned for the installation of a linkage. The latent chemical linkage was installed using a Sonogashira coupling reaction with *tert*-butyl but-3-yn-1-ylcarbamate to give RS-II-16P. The *tert*-butylcarbamate protecting group was removed using trifluoroacetic acid to give the free amine RS-II-24C. The effect of each of these new analogs on the binding of BODIPY-GTP to Cdc42 was assessed in a bead based flow cytometry assay. In this assay, the concentration of BODIPY-GTP was fixed at the K_d concentration of Cdc42 (K_d =100 nM). Compared to the parent compound (CID2950007, EC_{50} = 1.04×10^{-6} M),

AG-II106 and RS-II-16P showed improved EC_{50} values of 2.90×10^{-7} M and 1.06×10^{-7} M, respectively, and RS-II-24C exhibited a similar EC_{50} of 1.23×10^{-6} M. Taken together, all three analogs retained inhibitory activity toward Cdc42 nucleotide binding with either improved or similar EC_{50} values and similar inhibition efficacies.

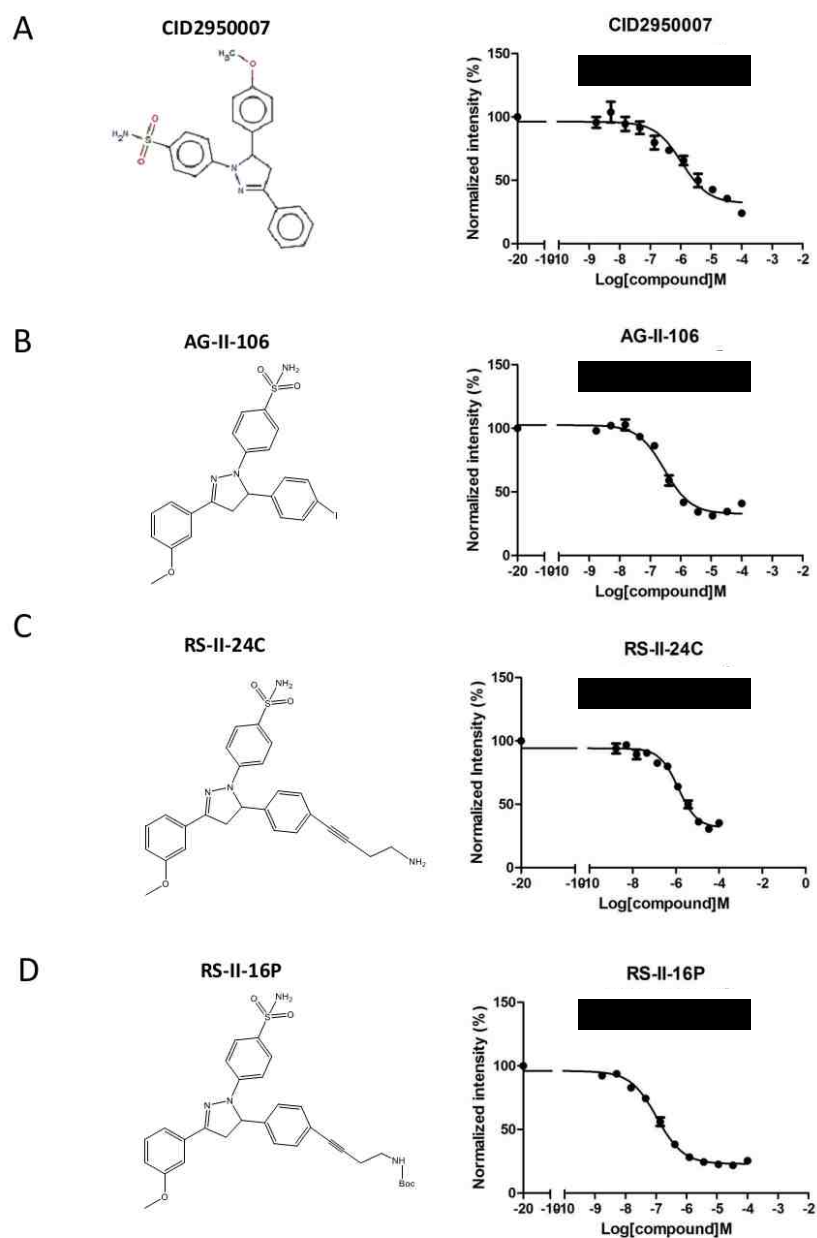


Figure 11. CID2950007 analogs inhibit BODIPY-linked nucleotide binding to Cdc42. All analogs - AG-II-106 (B), RS-II-24C (C) and RS-II-16P (D) exhibited similar potencies and efficacies against Cdc42 nucleotide binding in comparison to the parent compound-CID2950007 (A).

Fluorescent Analog of CID2950007 (RS-II-79) Inhibits Cdc42 Nucleotide Binding

A fluorescent analog of CID2950007 and CID44216842 - RS-II-79 was synthesized by modifying AG-II-106 with a linkage connected to a fluorescent dye. The amine-reactive N-hydroxysuccinimide ester of a hydrazinylpyridine based fluorescent HPY-dye was first reacted with *N*-(2-(2-(2-aminoethoxy)ethoxy)ethyl)hept-6-ynamide to give 2-(9*H*-fluoren-9-ylidene)-3,3-difluoro-6-((2-(2-(2-(hept-6-ynamido)ethoxy)ethoxy)ethyl)carbonyl)-2,3-dihydro-[1,2,4,3]triazaborolo[4,5-*a*]pyridin-2-ium-3-uide. This hept-6-ynamido compound was coupled with the iodophenyl analog AG-II-106 using the Sonogashira coupling procedure to give the desired product RS-II-79 in good yield. This one-step coupling approach for introduction of a fluorescent label was analogous to the synthesis of RS-II-16P described in the previous section. RS-II-79 exhibits absorption spectra with $\lambda_{\text{abs}} = 472\text{-}490$ nm and emission spectra with $\lambda_{\text{emi}} = 551\text{-}563$ nm with characteristically large Stokes shifts (136). Based on the efficacy of the model compounds RS-II-16p and RS-II-24C possessing alkynyl linkages in that position, RS-II-79 was expected to be a functional probe. RS-II-79 was tested for efficacy as a probe for inhibiting guanine nucleotide binding and as well for comparatively measuring small molecule interaction and affinity for the Cdc42 GTPase. Using a single-plex dose response assay, RS-II-79 inhibited BODIPY-GTP nucleotide binding in a dose-dependent manner with EC_{50} of 1.07×10^{-6} M and maximum inhibition of ~80% (Figure 12). In comparison to the parent CID2950007, the inhibitory activity of RS-II-79 against nucleotide binding to

Cdc42 was unchanged, though was slightly reduced compared to CID44216842. Additionally, the direct binding of RS-II-79 to Cdc42 was tested by following the HPY-dye fluorescence intensity bound to GTPase, which showed an K_d of 1.90×10^{-7} M and maximum binding efficacy of 80%. Taken together, these results suggest that the fluorescent analog, RS-II-79 retains a similar inhibitory effect on the nucleotide binding to Cdc42 in comparison to the parent compound, CID29500007. The binding curve of the RS-II-79 demonstrates that the compound reduces nucleotide binding by direct binding to Cdc42. These data are consistent with CID29500007 being identified as an allosteric inhibitor of Cdc42 (104, 139).

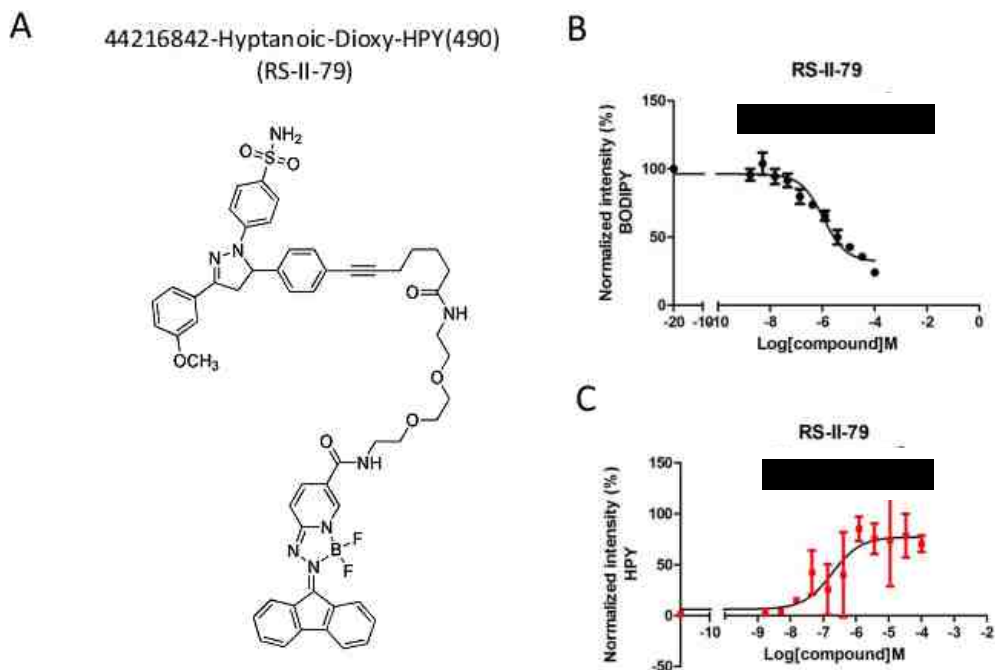


Figure 12. Fluorescent analog of CID2950007 - RS-II-79 (44216842-Hyptanoic-Dioxy-HPY(490)) inhibits BODIPY-linked nucleotide binding to Cdc42. (A) Structure of RS-II-79. (B) RS-II-79 reduced BODIPY-GTP nucleotide binding to Cdc42 in a dose-dependent manner with an EC_{50} of 1.07×10^{-6} M. (C) Fluorescent RS-II-79 specifically interacted with Cdc42 in a dose-dependent manner. Based on the one-site binding curve, the K_d was determined as 1.90×10^{-7} M. In the flow cytometry assay, the fluorescent intensity of BODIPY-GTP was detected by FL-1 ($\lambda_{ex}=488$ nm, $\lambda_{em} = 530/30$ nm), which quantified the nucleotide binding. The fluorescent intensity of the fluorophore (HPY) was detected by FL-2 ($\lambda_{ex}=488$ nm, $\lambda_{em} = 585/42$ nm) (136), which quantified bound RS-II-79 on GTPase. GST-GSH beads were used in the control experiment and represented non-specific binding of the compound. The intensity of the bona fide bound RS-II-79 was calculated as: Mean Channel Fluorescence_(Cdc42-GSH beads) – Mean Channel Fluorescence_(GST-GSH beads).

Penetration of Multicellular Aggregates (MCA) by RS-II-79

Since the fluorescent analog RS-II-79 was identified as a Cdc42 specific inhibitor interacting at an allosteric binding site of GTPase, a live cell imaging study was conducted to test the cellular permeability of RS-II-79. In order to investigate the rate of RS-II-79 uptaken by the cell, 2 μ l of 10 mM stock (dissolved in DMSO) was added to 2 ml of the media. Figure 13 shows GFP-actin-expressing MDCK cells before and after the addition of RS-II-79 with excitation at 488 nm and emission detection in the range 530 \pm 30 nm. These cells started to take up the RS-II-79 within 2-3 min and continue to rise steadily over 10 min. Therefore, RS-II-79 was found to have good permeability in cultured cells. However, due to the diffuse distribution and low signal-to-noise ratio of the fluorescent compound, the exact subcellular localization needs to be further confirmed.

Moreover, the penetration of RS-II-79 into MCA was investigated to evaluate the drug diffusion processes that mimic the extracellular microenvironment in actual solid tumors. The MCA was formed by 2000 SKOV3ip cells. Appendix A shows representative images of penetration of an MCA by RS-II-79, observed by confocal microscopy. A steady increase in penetration depth within the MCA was observed from the periphery toward the core of the MCA over time. In addition, the MCA penetration assay was also conducted in Doxorubicin at 6 μ M and Doxil (liposome-encapsulated doxorubicin) at 6 μ M. The result (data not shown) shows the penetration ability of RS-II-79 is similar to Doxil, but not as good as Doxorubicin. These observations suggest that

the fluorescent analog of CID2950007, RS-II-79 penetrates within the MCA in a time-dependent manner. A gradually diffused and decreased fluorescence pattern from the periphery to center region of the MCA was evident. Penetration experiments with longer incubation time (up to 24 h) will need to be performed to test whether the RS-II-79 could fully penetrate into the MCA.

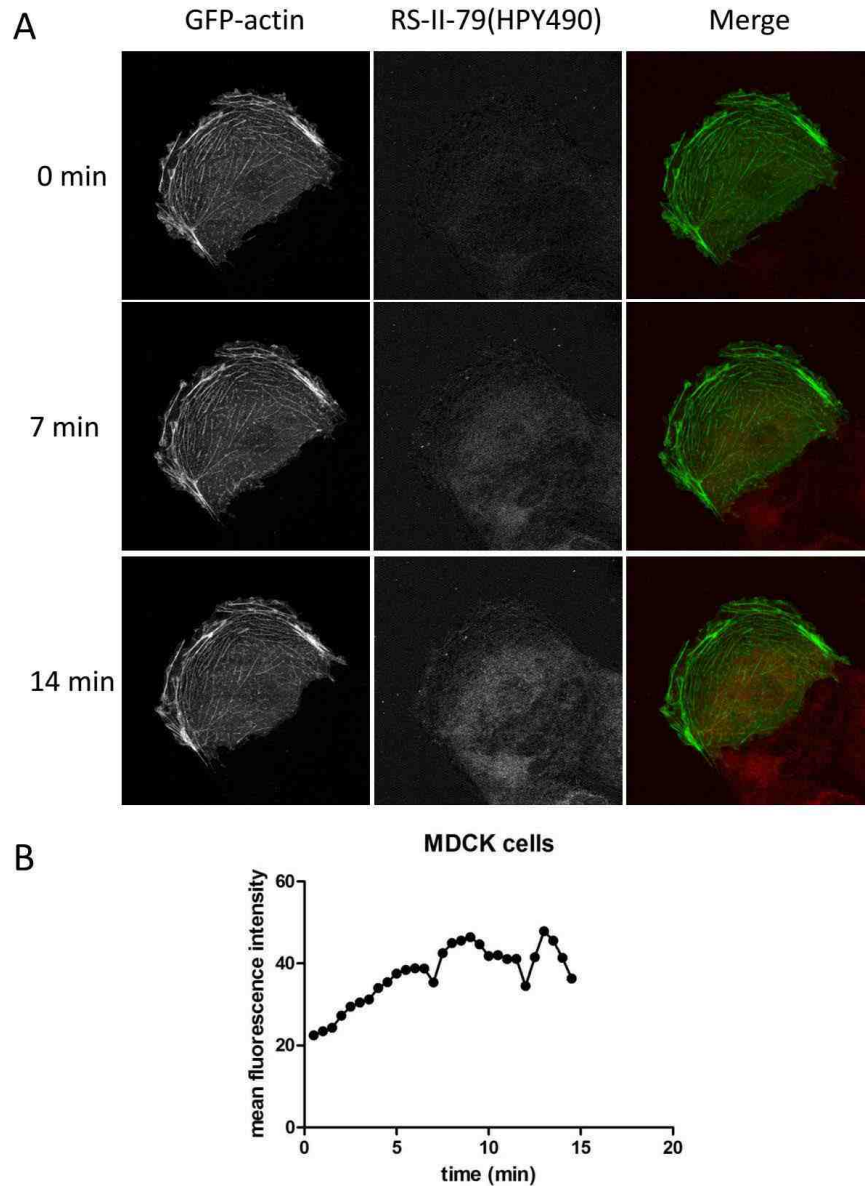


Figure 13. Distribution of fluorescent RS-II-79 in living cells in a time-dependent manner. GFP-actin expressing MDCK cells were treated with fluorescent RS-II-79 at 10 μ M final concentration. (A) Representative images of GFP-actin expressing MDCK cell in 10 μ M RS-II-79 at 0, 7, and 14 min after loading the RS-II-79. (B) Quantification of the uptake of RS-II-79 in MDCK cell over time.

Conclusion and Discussion

In this chapter, R-ketorolac and R-naproxen identified from high throughput screening and computational simulation are shown to inhibit *in vitro* BODIPY-GTP nucleotide binding to Cdc42 and Rac1. Equilibrium binding and single-plex dose-response studies demonstrated that the R-enantiomers, but not the S-enantiomers of selected NSAIDs (ketorolac and naproxen) act as allosteric, non-competitive inhibitors. A computational simulation was conducted and confirmed the enantiomer-selective activity of these NSAIDs. We suggest that [R] α -Me carboxylates preferentially interact with magnesium and reduce stabilization and promote nucleotide release. Using ketorolac analogs, an SAR analysis was initially conducted, which suggests that the phenyl ring plays a key role in modulating ketorolac activity on GTPase nucleotide binding, possibly by affecting the properties of the carboxyl group at the chiral center. In addition, CID2950007 derivatives with modifications on the phenyl ring were well tolerated and enabled the synthesis of a fluorescent derivative. The fluorescent analog, RS-II-79 has similar properties as CID2950007 and is able to permeabilize into single cells and penetrate into 3-D tumor MCA.

The biochemical basis for GTPase inhibition by R-ketorolac and R-naproxen is provided by computational and experimental approaches. The model is enantiomer-selective, with S-ketorolac being poorly positioned to exert the same magnesium exclusion and therefore could explain the observed differences in EC_{50} values measured for R- and S-ketorolac in the *in vitro* nucleotide binding

assay. The model is further supported by X-ray crystallography data, which identified the preferential binding of S-naproxen to COX-2 (111). R-naproxen, like R-ketorolac, exhibits Cdc42 and Rac1 inhibitory activity, albeit with less potency. Naproxen, like ketorolac has a constrained alpha methyl carboxyl that may account for the stereo-selective activities of the R- and S-enantiomers (140).

In preliminary SAR studies, ketorolac analogs were synthesized with modifications to the phenyl ring of the parent compound; including additions of a methyl group (Me), halogens (F, Cl), trifluoromethyl (CF₃) and replacement of phenyl with a thiophene. The analogs were tested in vitro using a GTPase nucleotide binding assay and in cells using GTPase effector binding assay. Because the enantiomeric identity is unknown and the initial compound set was fairly limited with modification in a lipophilic area (the phenyl ring), we are unable to define a clear SAR trend that improves the activity profile of the parent compound in this preliminary study. The fluorine derivatives showed interesting trends toward increased Rac1 selectivity over Cdc42 and provide a very sensitive nucleus that can be effectively exploited in 1D NMR experiments to probe direct binding of small molecule inhibitors to unlabeled GTPase samples and assess stoichiometry. However, the 3-thiophene analog shows the most promising results with improved affinity, efficacy and enantiomeric selectivity on both Cdc42 and Rac1 GTPases. This finding indicates that 3-thiophene modification could be a good starting point for further analog syntheses and screening. Further SAR work is required to evaluate the substituents on the adjacent carbon of the phenyl ring, modifications to the ketone, or alterations to the fused ring system in order

to identify the key structures and improved chemical entities for developing effective GTPase regulators.

The identification of R-ketorolac and R-naproxen as allosteric regulators of Cdc42 and Rac1 presents a novel mechanism of action based on stabilization of the GDP-bound GTPase that may in part be promoted through interference with GEF-mediated activation or by making nucleotide exchange independent of regulatory proteins. This potential mechanism is distinct from the currently known inhibitors that interfere directly with GEF, GAP or GDI interaction or block GTPase membrane association, e.g. farnesyl-transferase (FTI), geranylgeranyl-transferase (GGTI) and prenyl-transferase inhibitors, which display poor selectivity for individual Rho GTPases (141-143). The identified R-ketorolac and R-naproxen have been shown to specifically inhibit Cdc42 and Rac1 activation, but have no effect on RhoA in cell based GTPase effector binding (G-trap) assays (See Chapter 4, Figure 35) (138, 140). Naproxen is clinically only available as the S-enantiomer. In contrast, ketorolac is an FDA-approved drug and is in active clinical use as the racemic mixture. Thus, R-ketorolac is an ideal candidate for drug repurposing and development for cancer therapy. In the following chapters, the anti-tumor effect of ketorolac was investigated in cell-based assays and clinical trials, which confirm Cdc42 and Rac1 as novel targets of R-ketorolac and demonstrate benefit in patient outcomes in ovarian cancer therapy.

CHAPTER 3

R-KETOROLAC TARGETS CDC42 AND RAC1 AND ALTERS OVARIAN CANCER CELL BEHAVIORS CRITICAL FOR INVASION AND METASTASIS

Abstract

Cdc42 and Rac1 are attractive therapeutic targets in ovarian cancer based on established importance in tumor cell migration, adhesion and invasion. Despite a predicted benefit, targeting GTPases has not yet been translated to clinical practice. R-ketorolac is an established allosteric inhibitor of Cdc42 and Rac1. In this chapter, cell-based assays were utilized to determine R-ketorolac activity against Cdc42 and Rac1 activation and subsequent biological functions. Studies on immortalized human ovarian adenocarcinoma cells (SKOV3ip), and primary, patient-derived ovarian cancer cells show R-ketorolac is a robust inhibitor of growth factor or serum dependent Cdc42 and Rac1 activation with a potency and cellular efficacy similar to small molecule inhibitors of Cdc42 (CID2950007/ML141) and Rac1 (NSC23766). Furthermore, GTPase inhibition by R-ketorolac reduces downstream p21-activated kinases (PAK1/PAK2) effector activation by >80%. Multiple assays of cell behavior using SKOV3ip and primary patient-derived ovarian cancer cells show that R-ketorolac significantly inhibits cell adhesion, migration and invasion. In sum, the evidence demonstrate R-ketorolac is a direct inhibitor of Cdc42 and Rac1 that is capable of modulating

downstream GTPase-dependent, physiological responses, which are critical to tumor metastasis. The findings demonstrate the selective inhibition of Cdc42 and Rac1 GTPases by an FDA approved drug-racemic ketorolac that can be used in humans.

All the work in this chapter are published: Guo, Y, et al., 2015 Oct;14(10):2215-27.

doi: 10.1158/1535-7163.MCT-15-0419. Epub 2015 Jul 23.

Introduction

PAK1- Effector of Cdc42 and Rac1

Serving as molecular switches, Cdc42 and Rac1 control a variety of signaling pathways that are central to dynamic actin cytoskeletal assemblies and rearrangements that are the underpinnings of cell-cell adhesion, cell migration and even transformation (62). P21 activated kinases (PAKs) are well known downstream effector proteins of Cdc42 and Rac GTPases. As shown in Figure 14, inactive PAKs form dimers, where the auto-inhibitory domain (AID) binds to the kinase domain which prevents auto-phosphorylation. Cdc42 and Rac interact with PAK at the Cdc42/Rac interacting binding motif (CRIB) to disrupt the interaction between the AID and the dimer PAK, which in turn leads to a conformational change of PAK to an activated monomer and causes auto-phosphorylation of PAK (144). Activated Group A PAK (PAK1, 2, 3) proteins phosphorylate regulatory myosin light chain (MLC) or LIM Kinase (LIMK1) which leads to formation of polymerized actin structure, such as focal adhesion complex, lamellipodia and filopodia (64, 145). However, other types of PAK (e.g. PAK4) lead to the dissolution of stress fiber by decreasing myosin light-chain kinase (MLC) phosphorylation (63).

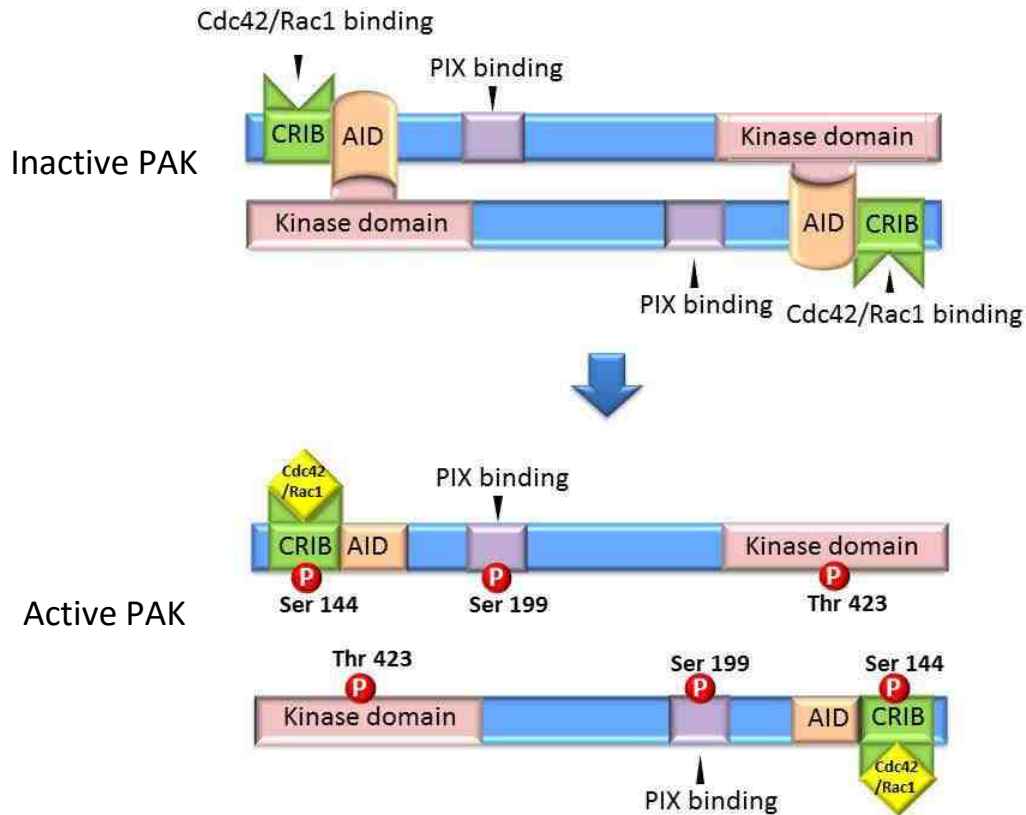


Figure 14. A model for PAK1 activation. Based on the published structure (145), PAK1 contains a N-terminal regulatory domain, including Cdc42/Rac1 interaction/binding (CRIB) and auto-inhibitory domain (AID), a PAK-interacting exchange factor (PIX) and a kinase domain. In inactive state, the PAK is auto-inhibited through the formation of dimers between the AID and the kinase domain to prevent auto-phosphorylation. In the presence of GTP-Cdc42/Rac1, the GTPase CRIB complex catalyzes phosphorylation of Serine144 at AID, which disables the AID-kinase domain interaction and activates the monomeric PAK auto-phosphorylation kinase domain at Threonine 423. The phosphorylation of Serine 199 is activated by a PAK-interacting exchange factor (PIX).

Rho GTPases Mediated Cell Motility

Extracellular matrix (ECM) is composed of multiple fibrous protein, including collagen, fibronectin, and laminin, providing structural support and the biochemical and biomechanical environment for cell division, growth and development (146). Cdc42 and Rac1 are involved in cellular signaling pathways that transduce extracellular signals to the assembly of integrin-mediated focal adhesion complexes (147). In early adhesion events, integrins through G-protein coupled signaling mediate focal adhesion kinase (FAK)-Src kinase complex to activate Rac for nascent adhesion to the ECM. Later, activated Rac coordinates extensive crosstalk between integrin (particularly $\alpha 5\beta 1$), Src kinases and other Rho GTPases, which leads to formation of mature focal adhesions involved in cell spreading (60, 148-150) (Figure 15). Downstream effectors of Rho GTPases, such as PAK1 and IQGAP are responsible for cadherin-mediated cell-cell adhesion, which are significant for the formation of MCA, cell migration and EMT (151, 152). Cell-matrix and cell-cell adhesion play critical roles during cancer metastasis which is required for the anchoring of malignant MCA to the ECM of target abdominal organs (19).

During tumor metastasis, cell migration is another critical step of cell movement that is controlled by Rho GTPases (Figure 15). Activated by extracellular stimuli, Rho GTPases stimulate actin polymerization for lamellipodium extension and filopodia formation. Lamellipodia are thin, sheet-like membrane protrusions at the leading edge. Filopodia are finger-like protrusions

that extend from lamellipodium (153). Both are regulated by Cdc42 and Rac1 through Rho GTPase-PAK-LIM kinase (LIMK) and Rho GTPase-WASP/WAVE-Arp2/3 signaling pathways for actin reorganization and serve to establish cell-cell and cell-matrix contact (125, 154). Once the lamellipodia and filopodia contact the ECM, focal adhesions form to stably anchor cells to the matrix. At the same time, when cells migrate in a 3-D ECM, activated Rho GTPases and Src kinase are involved in the formation of invadopodia which are membrane protrusions that concentrate matrix metalloproteinases (MMP), e.g. MMP2 and MMP-9, at their tips and based on their matrix degradative properties enable cell invasive behaviors (149, 155, 156).

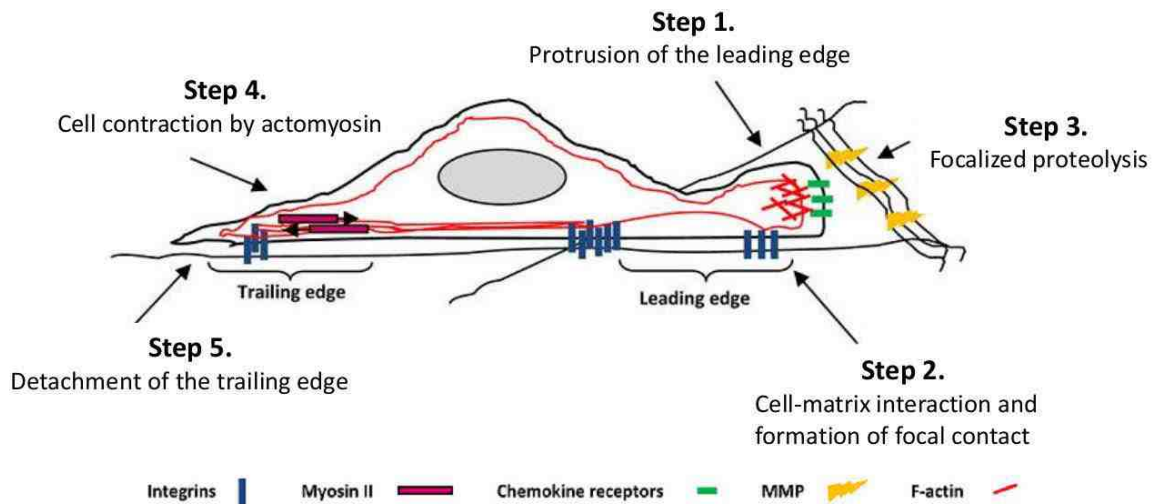


Figure 15. Cell migration model. Cell migration on 2-D and in 3-D ECM is schematized in five steps: (1) Lamellipodium extension at the leading edge – actin polymerization at the leading edge of cell. Rac, Cdc42 and Arp2/3 involved. (2) Formation of new focal adhesion complex – integrins interact with ECM ligands and mediate focal adhesion complex formation. Rac involved. (3) Secretion of surface proteases at sites of ECM contact leads to focal proteolysis and enables invasion of 3-D matrices; (4) Cell body contraction by actomyosin complexes; (5) Tail detachment. (Parri, M., Cell Communication and Signaling. 2010;8:23)

Materials and Methods

Cell and Reagents

Compounds for dose response assays were obtained as follows: R-ketorolac (K235600, Toronto Research Chemical Inc), S-ketorolac (K235605, Toronto Research Chemical Inc), R-naproxen (Acme Bioscience #A5026, Palo Alto, CA), S-naproxen sodium (N5160, Sigma-Aldrich), 6-methoxy-2-naphthalene acetic acid (6-MNA) (70620, Cayman Chemical, Ann Arbor, MI, USA), NSC23766 (204823, Santa Cruz, CA), CID2950007 (71203-35-5, Tocris). GST-PAK1 protein was from Millipore (14-864). Rat tail type I collagen was obtained from BD Biosciences (Cat #: 354265). A polyclonal antibody directed against Tks5 (Src tyrosine kinase substrate 5) was obtained from Dr. Rytis Prekeris (University of Colorado, Denver) (157). The following commercial antibodies were used: mouse mAb (monoclonal antibody) directed against Rac1 from BD Transduction Laboratories (Cat #: 610651), mouse mAb directed against Cdc42 from Santa Cruz (Cat #: sc-8401), FITC (fluorescein isothiocyanate)-conjugated mouse mAb directed against EpCAM (epithelial cell adhesion molecule) (clone Ber-EP4) from Dako (Cat #: F0860); rabbit polyclonal Cy5-conjugated anti-CA125 (cancer antigen 125) from Bioss Inc.(Cat #: bs-0091R-Cy5), mouse mAb PE (Phycoerythrin)-conjugated anti-CD45 (lymphocyte common antigen 45) from eBioscience (Cat #: 12-9459), rabbit polyclonal antibodies directed against phospho-PAK1 (Ser144)/PAK2(Ser141) (Cat #: 2606), phospho-PAK1(Ser199/204)/PAK2(Ser192/197) (Cat #: 2605), phospho-

PAK1(Thr423)/PAK2(Thr402) (Cat #: 2601) and PAK1 (Cat #: 2602) from Cell Signaling Technology. Alexa 488 goat anti-mouse antibody (Cat #: A-11029) and Alexa 647 goat anti-rabbit antibody (Cat #: A-21235) from Life Technology, all used per manufacturers' instructions.

Patient Information

A Phase 0 trial investigating the use of postoperative ketorolac was reviewed and approved by the University of New Mexico Health Sciences Center Human Research Review Committee (NCT01670799 clinicaltrials.gov) (158). Informed patient consent was obtained prior to surgery. Eligible patients having suspected advanced stage ovarian, fallopian tube or primary peritoneal cancer underwent planned optimal cytoreductive surgery. Upon surgical entry into the abdomen, ascites fluid was retrieved and residual material was recovered and sent fresh to the investigators for processing. Ascites material used for this study was from patients confirmed to have stage III or IV at final pathologic diagnosis. Nine patient samples were included in the study (Table 4).

Table 4 Patient Information

Patient number	Tumor stage	Assay application				
		Cdc42 activity	Rac1 activity	Filopodia formation	Cell adhesion	Gelatin degradation
INST1115-24	IIIC	•				
INST1115-29	IIIC	•	•			
INST1115-30	IV	•	•			
INST1115-31	IV*	•	•			
INST1115-35	IIIC	•	•			
INST1115-36	IIIC	•	•			
INST1115-42	IIIC			•	•	•
INST1115-43	IIIC			•	•	•
INST1115-44	Unstaged* *			•	•	
INST1115-49	IIIC					•

All except for two patients had ovarian serous carcinoma.

* Patient #30 had stage IV uterine serous carcinoma.

** Patient #44 had mucinous ovarian cancer.

Isolation and Cell Culture of Ascites-Derived Primary Ovarian Cancer Cells

Peritoneal ascites were obtained at the time of debulking surgery with an average volume of 200 ml. Cells were collected by centrifugation at 300g for 5 min. The Ficoll-Paque (1.073 ± 0.001 g/ml) PREMIUM density gradient media (GE Healthcare) was used to pellet and remove erythrocytes and polymorphonuclear cells. The mononuclear white cells and tumor cells found at the top of the Ficoll interface were transferred to a sterile tube and washed with RPMI 1640 media with 5% FBS. To deplete leukocytes and further enrich tumor cells, samples were incubated with CD45-coated Dynabeads[®] (Life technologies, Cat #: 11350D) for 1.5 h at 4 °C, washed and collected by centrifugation according to the manufacturer's protocol. Isolated tumor cells were cultured as described by T. Shepherd *et. al* (159). Briefly, enriched ovarian cancer cells were cultured on collagen-coated (20 µg/cm²) tissue culture dishes. After 3-4 d, when most of the tumor cells had adhered, the media was replaced and continued to be changed every 2-3 d until cells grew to confluence. The expanded cells were used for filopodia formation, cell adhesion, migration and extracellular matrix degradation assays.

Flow Cytometric GTPase Effector Binding Assay for Quantification of Cellular, Active GTPase Levels

The assay was carried out according to the protocols described previously (135). Ketorolac treated and vehicle-control cells were lysed in RIPA (high stringency cell lysis buffer) buffer (50 mM Tris-HCl, 150 mM NaCl, 1 mM EDTA,

0.25% (w/v) Na-deoxycholate, 1 mM Na₃VO₄, 1 mM NaF, 1% (v/v) NP-40 (nonyl phenoxyethoxyethanol), 1 mM PMSF (phenylmethylsulfonyl fluoride) and protease inhibitors consisting 10 µg/ml each of chymostatin, leupeptin, pepstatin and antipain). Insoluble debris was removed by centrifugation and the supernatants were incubated with GTPase effector coated beads (PAK1-PBD for Cdc42 and Rac1) for 1 h. Primary antibodies directed against Cdc42 or Rac1 and secondary antibody Alexa 488 were incubated with the beads for 1 h. Fluorescence intensity MCF (mean channel fluorescence) was used to measure the amount of active intracellular GTPase. MCF was measured by flow cytometry (Accuri C6, BD Biosciences). GTPase activity was calculated as $(MCF_{\text{sample group}} - MCF_{\text{unstimulated negative control}}) / MCF_{\text{stimulated positive control}}$.

Quantification of Filopodia Formation

The assay was conducted as described previously (104). Cells were cultured on coverslips to 50% confluence and serum-starved for 2 h, treated with individual drugs and stimulated with 10 ng/ml EGF for 20 min. Cells were gently rinsed 3x with ice cold PBS and fixed with 3% paraformaldehyde. Rhodamine phalloidin (ThermoFisher Scientific, Cat #: R415) was used to label the actin. Images were collected using a Zeiss LSM (laser scanning microscope) 510 confocal microscope equipped with a 63× oil immersion lens. For each experiment, a battlement pattern was used to select 30 images at random. Length and number of filopodia per cell were quantified using Slidebook 5.5 software.

Cell Adhesion Assay

The adhesion assay was modified from the method described by M.J. Humphrie (160). Cells were cultured at least 48 h and disassociated with 0.05% trypsin/EDTA. Suspended cells were rested in 0% FBS RPMI media for 1 h and treated with individual drugs. Cells stimulated with 5% serum were seeded on a 96-well plate (5×10^4 cells/well) coated with $0.5 \mu\text{g}/\text{cm}^2$ fibronectin or collagen and permitted to attach for 1 h. The 96-well plate was gently washed with PBS and cells were fixed with 3% paraformaldehyde. Samples were stained with crystal violet and lysed with 10% acetic acid and absorbance ($\lambda=595 \text{ nm}$) quantified using on a plate reader.

Cell Migration Assay

SKOV3ip cells were plated at 1×10^5 cells/well in 24-well Boyden chambers and allowed to attach for 4 h. Ketorolac enantiomers were added from 10 mM DMSO stocks to growth media at final concentrations ranging from 1 to 300 μM . After 48 h, inserts were removed and stained with DAPI (4',6-diamidino-2-phenylindole). Final DMSO concentration should be no higher than 0.1%. Membrane filters were imaged on a Zeiss inverted microscope using a 20x objective. Three representative fields were counted from each treatment group.

Gelatin Degradation Assay

The commercial gelatin degradation kit (Millipore, Cat #: ECM671) was used per manufacturer's instructions and modified to incorporate drug treatment and

EGF stimulation as follows. Briefly, according to the manufacturer's instruction, poly-L-lysine was diluted for coating pre-cleaned (e.g. acid washed with 15 min sonication in waterbath) 12 mm diameter round coverslips (50 μ l/coverslip) for 20 min. 50 μ l diluted glutaraldehyde was next placed on coverslips for 15 min. Cy3-gelatin and unlabeled gelatin were mixed and 25 μ l/coverslip was placed on parafilm and glutaraldehyde coated coverslip placed carefully face down on top of the drop – taking care to avoid trapping air bubbles – and allowed to set for 10 min in a humidified chamber. Coated coverslips were lifted gently by adding 500 μ l PBS underneath and then incubated with 70% ethanol for 30 min to sterilize, protected from light. To quench residual free aldehydes, 500 μ l growth media per well was added and incubated for 30 min. Cells were seeded on fluorescent coverslip and allowed to adhere for 6 h and then treated with individual drugs for 24 h. Cells were fixed with 3% paraformaldehyde, permeabilized with 0.1% Triton X-100 and immunostained for Tks5. Actin was visualized with FITC-phalloidin. Fifteen fields per coverslip were imaged on a Zeiss LSM 510 META with a 63x oil immersion objective. Gelatin degradation by invadopodia was analyzed using Slidebook 5.5 software. Percent degradation was quantified as: (degradation area)/(total cell area) for each image.

Western Blot

SKOV3ip cells were serum-starved for 2 h and treated with individual drugs for 1 h. After stimulation with 10 ng/ml EGF for 20 min, cells were washed with ice cold PBS and lysed with RIPA buffer. Cell lysates were processed for SDS-

PAGE, transferred to polyvinylidene fluoride membranes and individual proteins were detected with specific antibodies directed against PAK and phospho-PAK.

Statistical Analyses

Prism 5 software (GraphPad) was used to analyze all data to determine statistical significance. One-way ANOVA (Analysis of Variance) with Dunnett's test for multiple comparisons was performed to compare differences between the means of each group relative to the control group for all assays. P-values less than 0.05 were considered statistically significant. For some assays conducted on primary ovarian patient samples (GTPase activity measurements and gelatin degradation assays), standard z-scores of the values were calculated for each patient to minimize large ranges of values and to compare across groups on a uniform scale. ANOVA was performed on these standardized values.

Results

R-ketorolac Inhibits Cdc42 and Rac1 Activation in Immortalized and Primary Human Ovarian Cancer Cells

A flow cytometry based assay for quantitatively assessing the levels of active GTPases in cell lysates was developed in the Wandinger-Ness and Buranda laboratories (135). The assay was used to test the cellular impact of ketorolac isoforms on GTPase activation. Maximal Cdc42 and Rac1 activation in SKOV3ip cells treated with 10 ng/ml EGF occurred at different times; 20 min for Cdc42 and 5 min for Rac1 (Figure 16). Growth factor stimulated activation of Cdc42 and Rac1 was differentially inhibited in an enantiomer-selective manner (Figure 17). R-ketorolac substantially inhibited growth factor dependent activation of Cdc42 and Rac1 in a dose-dependent manner with an EC_{50} value of 2.577 μ M for Cdc42 and 0.587 μ M for Rac1 (Figure 17, circles). In contrast, even at the highest dose of 100 μ M, S-ketorolac exhibited limited inhibition (less than 30% of maximum by R-ketorolac) of Cdc42 and Rac1 (Figure 17, squares). Enantiomer-selective inhibition was also found in HeLa cells treated with R-ketorolac (140). Control cytotoxicity measurements in three different cell lines (SKOV3ip, OVCA 429, and OVCA 433) showed <10% inhibition of cell proliferation induced by either enantiomer of ketorolac at the highest tested dose and treatment (300 μ mol/L for 96 hours) (data not shown).

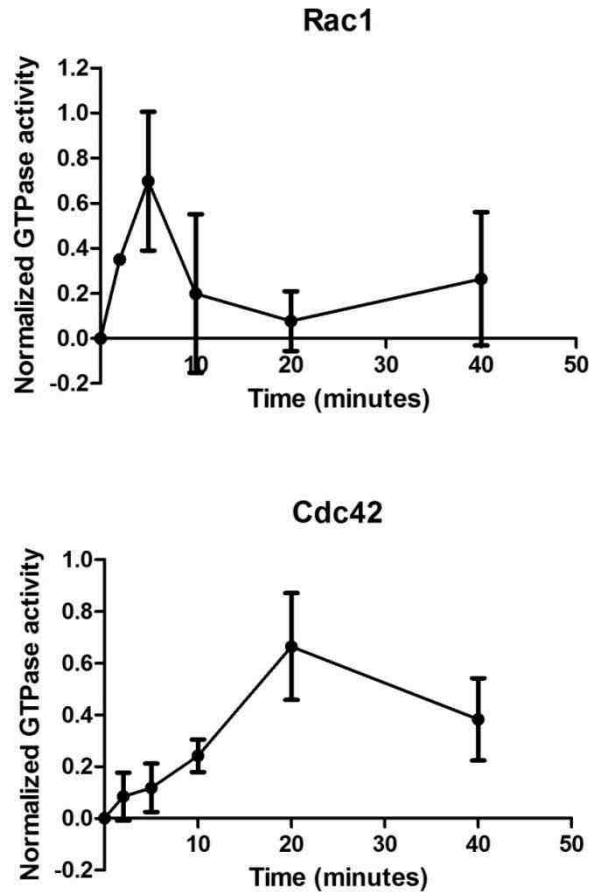


Figure 16. Time course of maximal Cdc42 and Rac1 activation in SKOV3ip cells upon growth factor stimulation. SKOV3ip cells were cultured overnight to reach ~80% confluence, then stimulated with 10 ng/ml EGF for different time length (0 - 40 min). The activation was terminated by washing with ice cold PBS. Cells were lysed with RIPA buffer and the activated GTPase levels were measured using a flow cytometry based GTPase effector binding assay. Normalized activities are expressed relative to unstimulated controls.

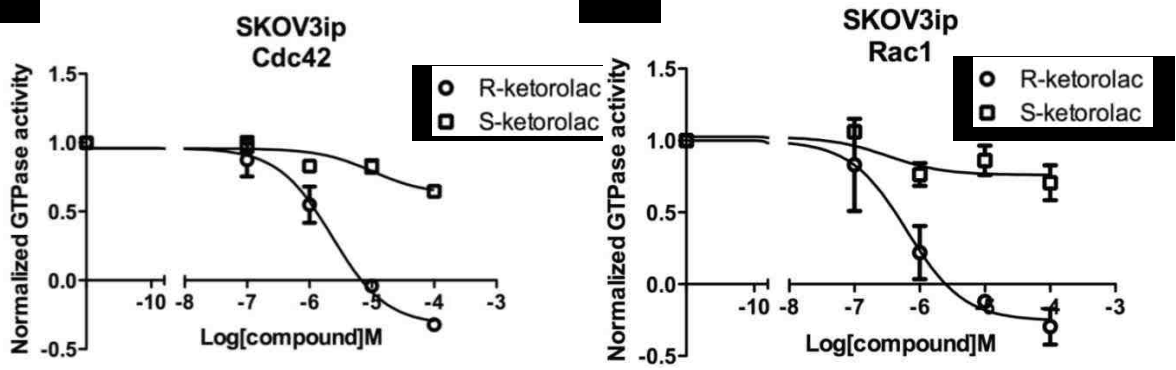


Figure 17. R-ketorolac preferentially inhibits Cdc42 and Rac1 activities in SKOV3ip cells. R-ketorolac causes a dose-dependent, enantiomer selective inhibition of growth factor stimulated Cdc42 and Rac1 activation in SKOV3ip cells. SKOV3ip cells were starved in 0% FBS media for 2 h and pretreated with individual drugs for 2 h prior to EGF (10 ng/ml) stimulation. Activated Cdc42 and Rac1 levels in cell lysates were measured using a flow cytometry based GTPase effector binding assay. Flow intensities were normalized to untreated controls. All experiments were repeated three times independently. Results are normalized as [(sample MCF—negative control MCF)/positive control MCF], where the negative control is the MCF reading obtained using lysates from unstimulated cells, and the positive control is the MCF reading obtained from the stimulated cells treated with DMSO. Values below zero represent inhibition of GTPase activity in cells to below the basal levels (resting cells without EGF stimulation).

The effect of ketorolac was also examined in primary ovarian cancer cells purified from patient ascites. Surgery samples were obtained and analyzed as part of an approved clinical study (see Materials and Methods and Table 4). Primary human ovarian cancer cells were enriched via Ficoll gradient centrifugation and depletion of lymphocytes using CD45 Dynabeads. Purified primary human ovarian cancer cells were positive for CA125 and EpCAM, which are commonly overexpressed in epithelial ovarian carcinomas (Figure 18) (161, 162). Isolated tumor cells were treated with individual ketorolac isoforms or specific Cdc42 and Rac1 inhibitors and the endogenous Cdc42 and Rac1 activities were tested. Because of the heterogeneity in activity levels of the GTPases for individual patient samples, z-scores were used to comparatively evaluate the impact of ketorolac on tumor cell GTPase activities from different patients. Treatment with 10 μ M R-ketorolac reproducibly inhibited both Cdc42 and Rac1 in a statistically significant manner (Figure 19). The magnitude of R-ketorolac inhibition of Cdc42 or Rac1 was similar to the inhibition observed in positive controls treated with CID2950007, an allosteric Cdc42 inhibitor, or NSC23766, a Rac1 inhibitor that interferes with GEF-mediated GTPase activation (104, 105). S-ketorolac exhibited limited inhibition and was not statistically significant (Figure 19). Taken together, the results demonstrate that R-ketorolac is a potent, enantiomer-selective inhibitor of Cdc42 and Rac1 in primary human ovarian cancer cells.

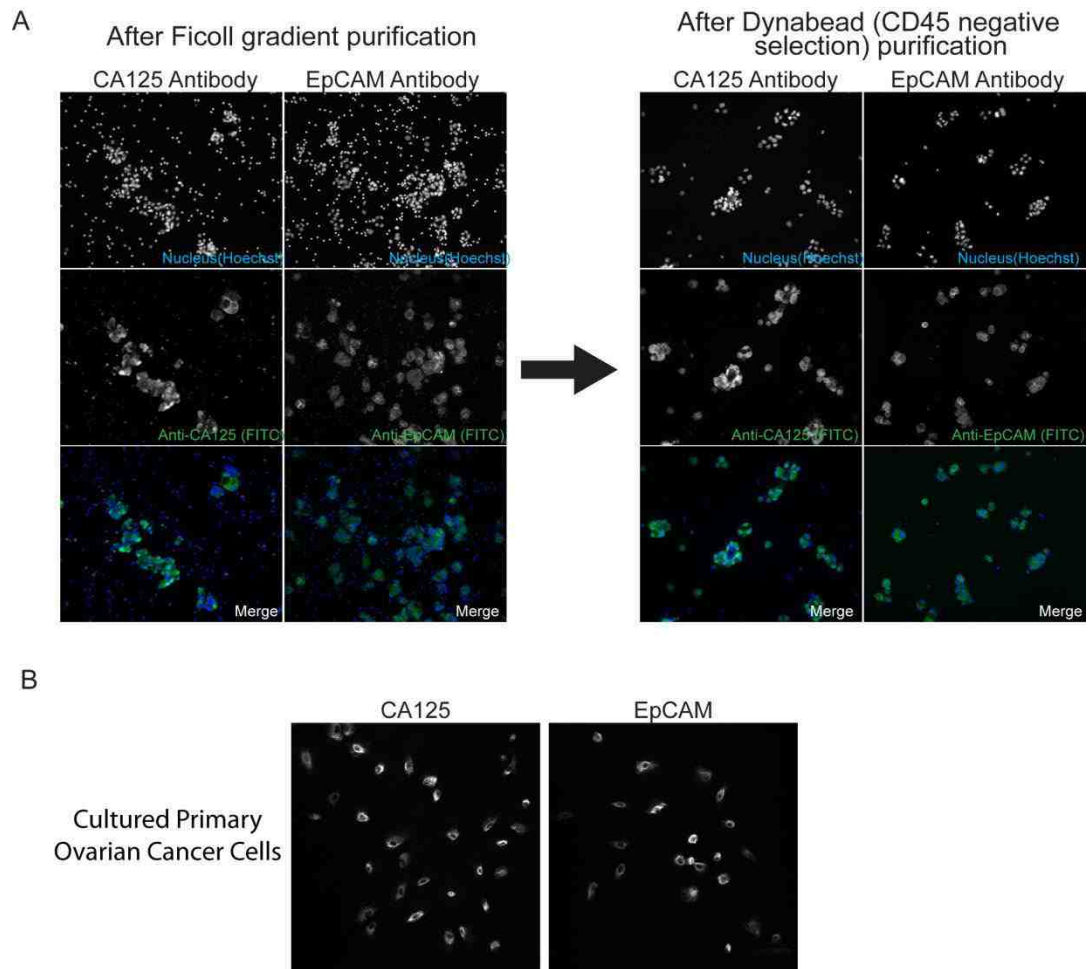


Figure 18. Characterization of primary ovarian cancer cell marker expression by immunofluorescence. (A) Cells were purified via Ficoll gradient and negative selection using CD45-Dynabeads. Cells were stained for CA125 and EpCAM (clone Ber-EP4). (B) Isolated cells were expanded by brief cell culture and stained for CA125 and EpCAM (clone Ber-EP4).

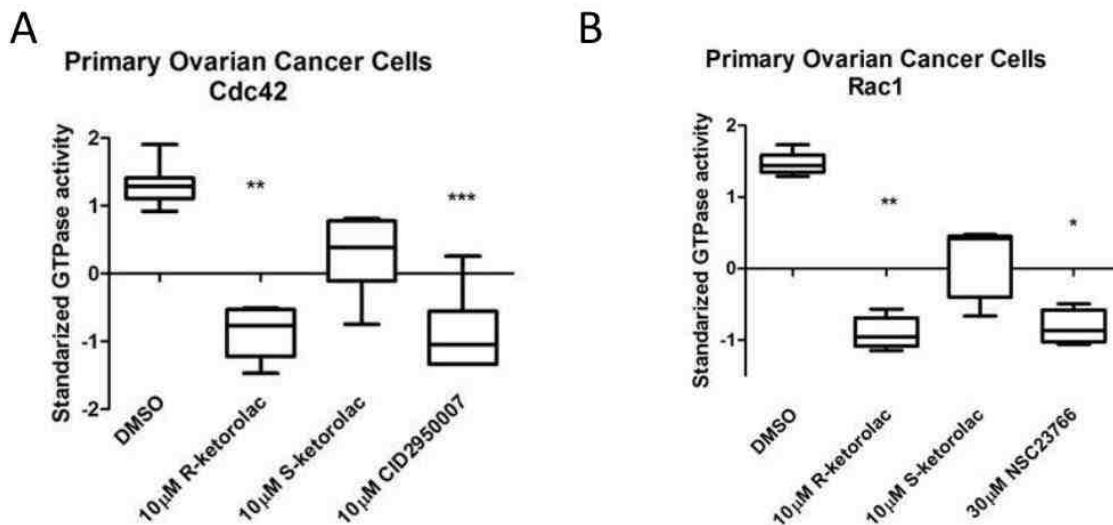


Figure 19. R-ketorolac preferentially inhibits Cdc42 and Rac1 activities in ascites derived primary human ovarian cancer cells. R-ketorolac causes a dose-dependent, enantiomer-selective inhibition of endogenous Cdc42 and Rac1 activities in primary ovarian cancer cells. Isolated primary ovarian cancer cells from three independent patients were treated with drugs for 1 h and processed for flow cytometry GTPase effector binding assays to measure the GTPase activity. Six patient samples were tested for Cdc42 activity and five patient samples were tested for Rac1 activity in response (Table 4). CID2950007 and NSC23766 served as Cdc42 and Rac1 specific inhibitors respectively. Plotted are z-scores. For individual patient sample, z-score is defined as $z=(X - \mu)/\sigma$, where X is MCF, μ is the mean of X, and σ is the standard deviation of X. Quantification of three independent measurements is plotted \pm SEM. Statistically significant differences are indicated: * $p<0.05$, ** $p<0.01$, *** $p<0.001$.

Inhibition of Cdc42 and Rac1 by R-ketorolac Decreases Activation of Downstream p21 Activated Kinases (PAK1/PAK2)

The impact of R-ketorolac on PAK1/PAK2 effector signaling directly downstream of the Cdc42 and Rac1 GTPases was examined (Figure 20). Cells stimulated with 10 ng/ml EGF exhibited robust phosphorylation of the Ser144/141 residues compared to unstimulated control cells. In contrast, there was a dose-dependent suppression of p-PAK1/PAK2 following R-ketorolac treatment that was similar to positive controls treated with Cdc42 or Rac1 specific inhibitors. S-ketorolac on the other hand had limited effect on p-PAK1/PAK2 levels at either 1 μ M or 10 μ M (Figure 20). The expression of total PAK1 was not affected by either R- or S-ketorolac treatment (Figure 20). These results demonstrate the suppression of p-PAK1/PAK2 paralleled the inhibition of Cdc42 and Rac1 in a dose-dependent manner following R-ketorolac treatment; and S-ketorolac exhibited no significant inhibition of p-PAK1/PAK2.

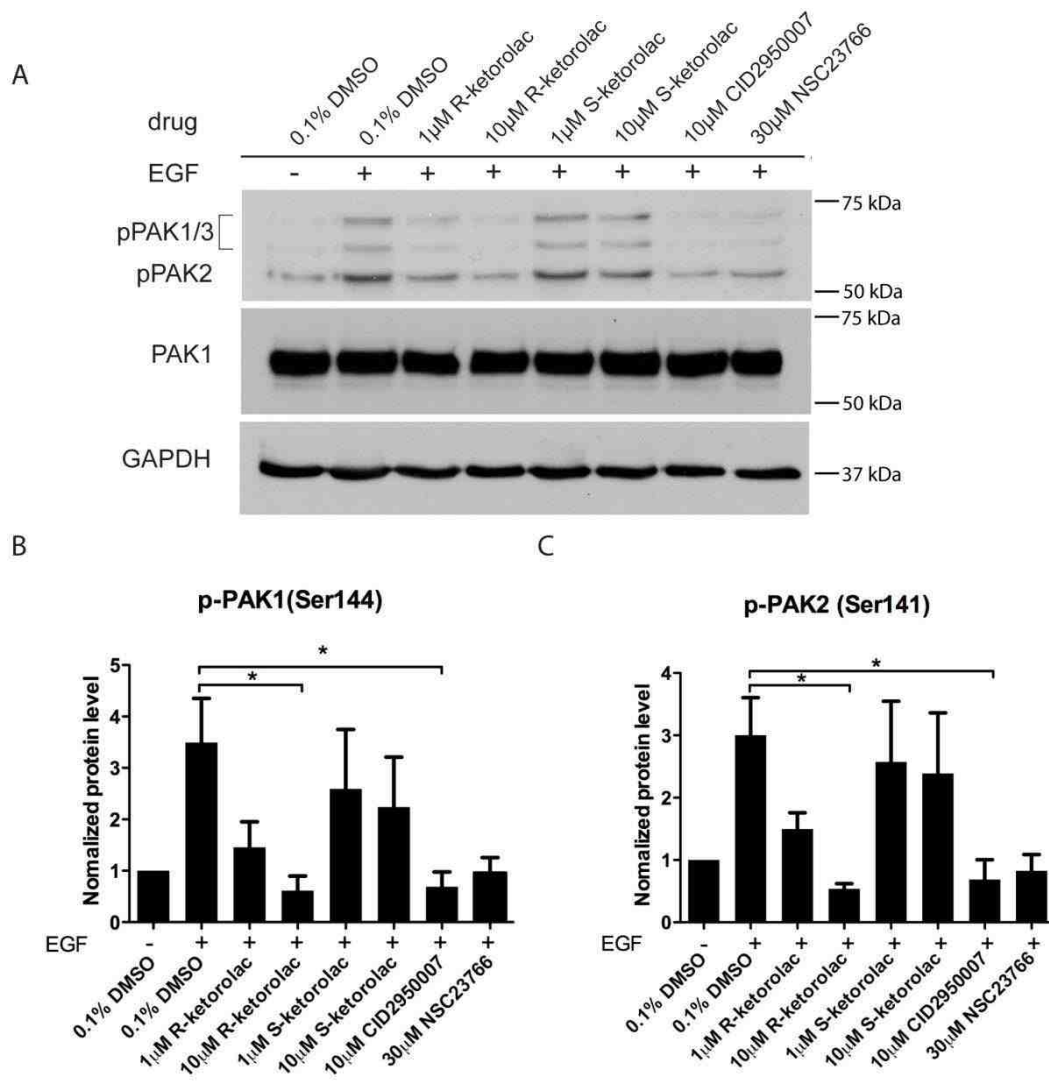


Figure 20. R-ketorolac decreases the phosphorylation of PAK1(Ser144)/PAK2(Ser141) without affecting total PAK levels. (A) SKOV3ip

cells were cultured overnight, then starved in 0% FBS media for 2 h and pretreated with individual drugs for 2 h followed by EGF stimulation (10 ng/ml) for 20 min. Representative blots from one of three independent experiments are shown. Equal amounts of cell lysate protein were resolved by SDS-PAGE and immunoblotted for p-PAK1(Ser144)/PAK2(Ser141). GAPDH served as the loading control. Cdc42 inhibitor, CID2950007 and Rac1 inhibitor, NSC232766

were used as positive controls. (B-C) Films from three independent experiments were quantified by ImageJ analysis. p-PAK1/PAK2 levels were normalized to unstimulated controls. Quantification of three independent measurements is plotted \pm SEM. Statistically significant differences are indicated: * $p < 0.05$, ** $p < 0.01$, *** $p < 0.001$.

Phosphorylation of PAK1/PAK2 on two further residues (Thr423/402 or Ser199/204 / Ser192/197) that are downstream of other signaling pathways were also examined. Interestingly, p-PAK1(Thr423)/PAK2(Thr402) and p-PAK1(Ser199/204)/PAK2(Ser192/197) were reduced by R and S-ketorolac with greater variability and less pronounced enantiomeric selectivity (Figure 21). For example, R-ketorolac consistently inhibited the phosphorylation at pPAK1/PAK2 (Thr423) with statistical significance at 1 μ M though more variably at 10 μ M. S-ketorolac exhibited statistically significant inhibitory effects at 10 μ M against Thr432/402, but not against Ser199/204 / Ser192/197. Inhibition of phosphorylation by the Rac1 inhibitor NSC23766 and the Cdc42 inhibitor CID2950007 was also more modest and failed to reach statistical significance in some instances. The explanation for the differences in responsiveness of individual phosphorylation sites is likely due to the fact that Ser144/141 is localized in an N-terminal regulatory domain and directly interacts with Cdc42 and Rac1 (Figure 14). While Thr423/402 residues in the catalytic kinase domain and Ser199/204/ Ser192/197 adjacent to auto-inhibitory domain are targeted by other regulatory molecules in a GTPase-independent manner (145, 163). For example, S-ketorolac may inhibit phosphorylation on these sites by affecting lipid-dependent stimulation of PAK1/PAK2 (e.g. sphingosine) or through crosstalk between COX-1/COX-2 and PI3K signaling and the GTPase-PAK1/PAK2 pathway (164, 165).

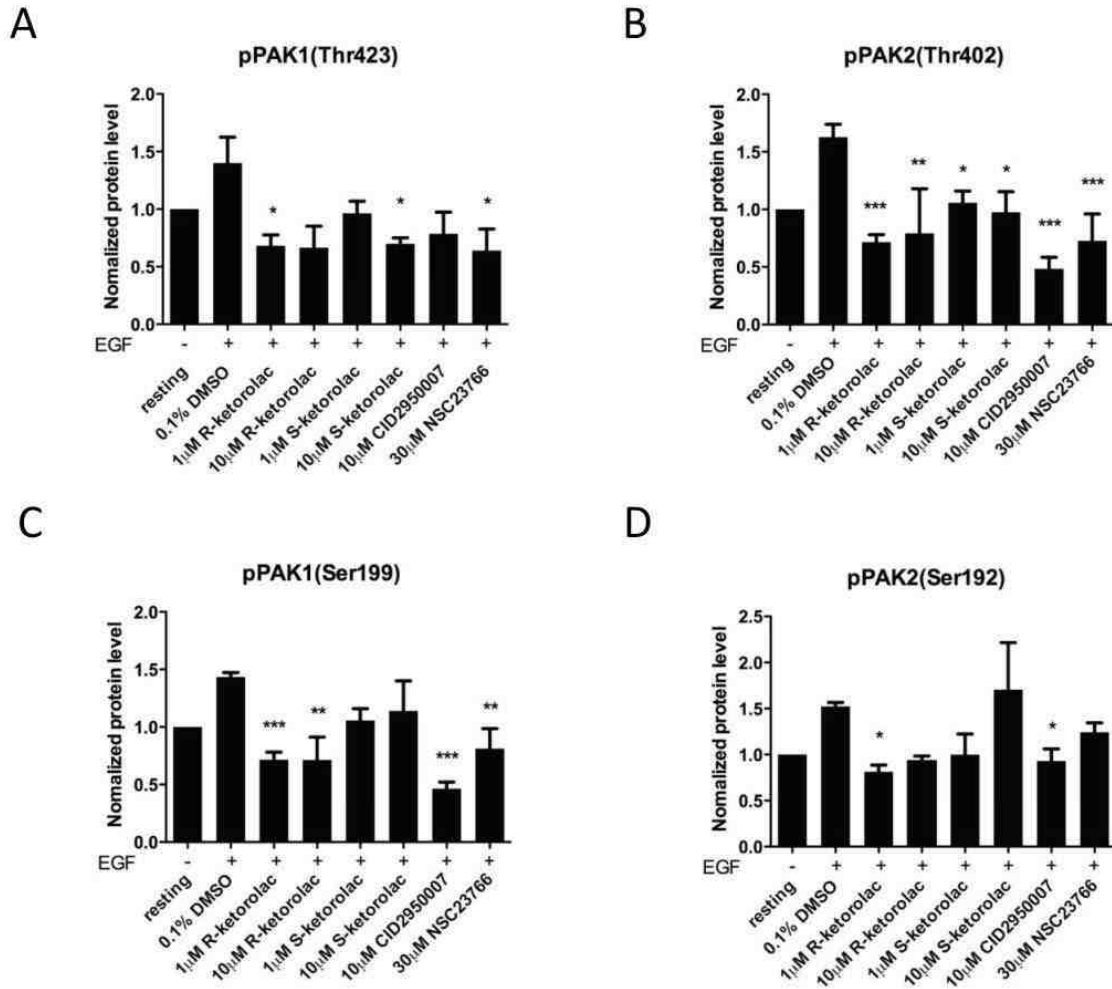


Figure 21. Ketorolac inhibition of p-PAK1 (Thr423)/PAK2(Thr402) and p-PAK1(Ser199)/PAK2(Ser192). (A-D) Quantification of three independent measurements of the expression of p-PAK1(Thr423)/PAK2(Thr402) and p-PAK1(Ser199)/PAK2(Ser192) levels in SKOV3ip cells +/- drug treatments as indicated. p-PAK1/PAK2 levels were normalized to unstimulated controls.

R-ketorolac Inhibits Cdc42-Dependent Filopodia Formation in SKOV3ip Cells and Primary Ovarian Cancer Cells

Filopodia are membrane protrusions that are constructed of bundled actin filaments and directly regulated by Cdc42 (166). Therefore, we tested filopodia formation, including numbers and length of filopodia to evaluate the effect of ketorolac on cell behaviors. When resting cells were stimulated with 10 ng/ml EGF, both numbers and length of filopodia increased with the most striking activation seen 20 min post-stimulation. Two concentrations of R-, and S-ketorolac were tested to take into consideration differential sensitivities of Cdc42 to the two enantiomers. In comparison to the vehicle treatment group, R-ketorolac (at both 1 μ M and 10 μ M concentrations) decreased numbers length of filopodia to basal levels and similar to CID2950007; while S-ketorolac only showed a significant inhibition on filopodia length at 10 μ M and did not significantly inhibit filopodia numbers at either 1 μ M or 10 μ M. (Figure 22). These results demonstrate that R-ketorolac impedes filopodia formation, which depends on the upstream activation of Cdc42.

Filopodia formation assays performed using primary ovarian cancer cells yielded similar results and reinforced the finding of the enantiomer-selective effect. R-ketorolac treated primary ovarian cancer cells exhibited significantly decreased filopodia numbers and length; while S-ketorolac exerted no inhibitory effect (Figure 23).

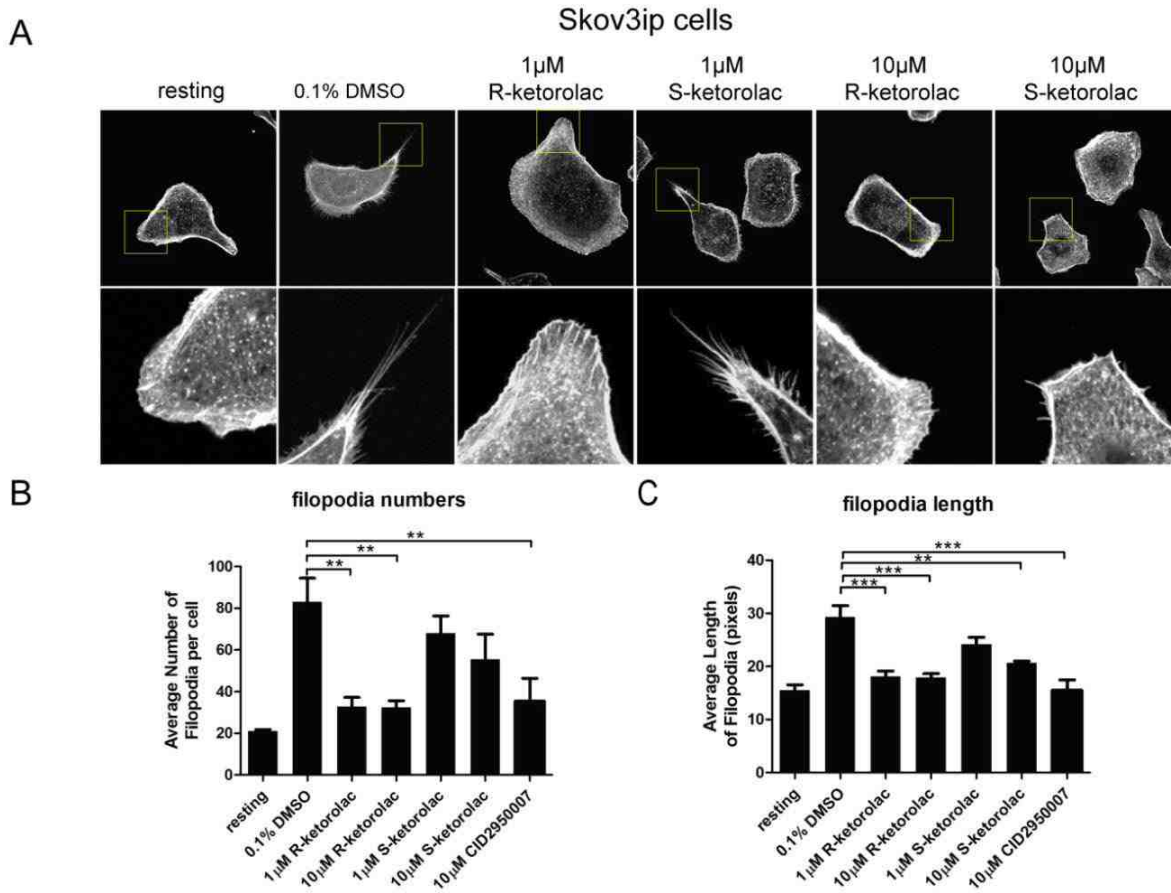


Figure 22. R-ketorolac decreases Cdc42 dependent filopodia formation in SKOV3ip cells following EGF stimulation. (A) Representative confocal images of filopodia formation for each treatment group in SKOV3ip cells are shown. Lower panels are magnified images of the boxed regions. (B-C) Quantification of numbers and length of filopodia on each cell. For all experiments, cells were plated on coverslips and cultured overnight, then starved in 0% FBS media for 2 h and pretreated with drug or 0.1% DMSO vehicle for 2 h, followed by EGF (10 ng/ml) stimulation for 20 min. Cells were permeabilized and stained with rhodamine-phalloidin. Confocal images were taken on a Zeiss LSM 510 META confocal microscope. All quantification is based on three independent

trials with 30 cells imaged in a battlement pattern and analyzed using Slidebook 5.5 software. Mean lengths or numbers of filopodia are plotted \pm SEM. Statistically significant differences are indicated: * $p < 0.05$, ** $p < 0.01$, *** $p < 0.001$.

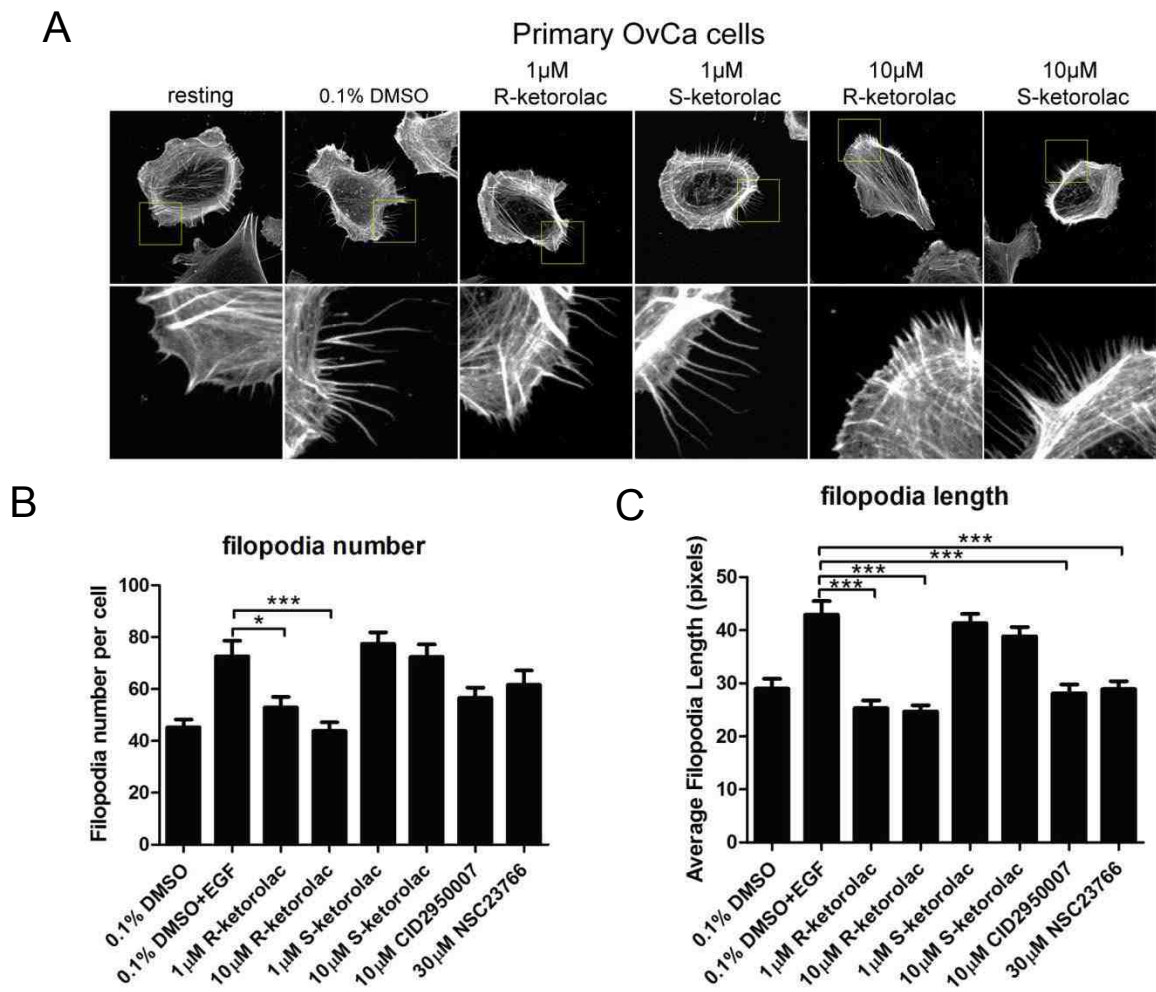


Figure 23. R-ketorolac decreases Cdc42 dependent filopodia formation in primary human ovarian cancer cells following EGF stimulation. (A) Representative confocal images of filopodia formation for each treatment group in primary human ovarian cancer cells are shown. Lower panels are magnified images of the boxed regions. (B-C) Quantification of numbers and length of filopodia per cell in primary human ovarian cancer cells. For all experiments, cells were plated on coverslips and cultured overnight, then starved in 0% FBS media

for 2 h and pretreated with drug or 0.1% DMSO vehicle for 2 h, followed by EGF (10 ng/ml) stimulation for 20 min. Cells were permeabilized and stained with rhodamine-phalloidin. Confocal images were taken on a Zeiss LSM 510 META confocal microscope. All quantification is based on three independent trials with 30 cells imaged in a battlement pattern and analyzed using Slidebook 5.5 software. Mean lengths or numbers of filopodia are plotted \pm SEM. Statistically significant differences are indicated: * p <0.05, ** p <0.01, *** p <0.001.

R-ketorolac Inhibits Cdc42- and Rac1-Mediated Cell Adhesion, Migration and Invasion

Cell Adhesion - A cell attachment assay was used to test the effect of ketorolac on cell adhesion. Stimulated cells were allowed to adhere to matrix-coated substrates. R-ketorolac reduced SKOV3ip cell adherence to both fibronectin and collagen, and S-ketorolac had no significant effect (Figure 24A-B). R-ketorolac also inhibited human primary ovarian cancer cell adhesion to collagen; while S-ketorolac had no significant effect (Figure 24C). This observation suggests that the R-enantiomer of ketorolac inhibits cell-substrate adhesion likely as a biological consequence of its inhibitory effect on upstream Cdc42 and Rac1 activation.

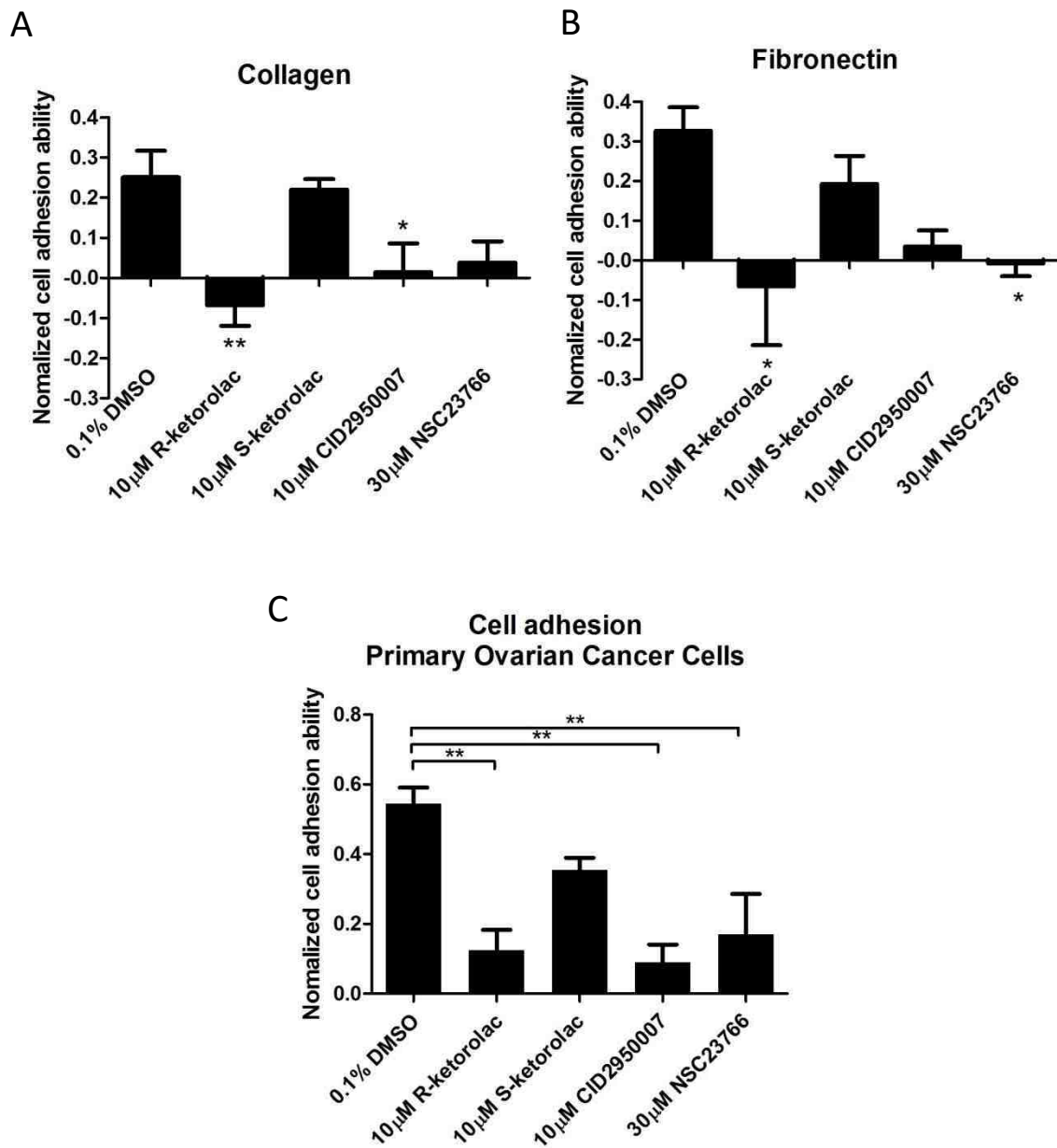


Figure 24. R-ketorolac inhibits cell-substrate adhesion in SKOV3ip cells and primary human ovarian cancer cells. (A-B) R-ketorolac significantly inhibits cell adhesion in SKOV3ip cells compared to S-ketorolac. SKOV3ip cells were trypsinized, starved in 0% FBS media for 1 h, pretreated with drug for 1 h,

followed by serum stimulation (5% (v/v) final concentration) and seeded on matrix pre-coated 96-well plate for 1 h. Cells were fixed and stained with crystal violet and finally lysed with acetic acid. Cell substrate adhesion was quantified based on absorbance of cell lysates at 595 nm and normalized to unstimulated controls. (C) Similar to SKOV3ip cells, R-ketorolac significantly inhibits cell substrate adhesion in primary human ovarian cancer cells as well. Primary ovarian cancer cells were purified, cultured and used for the cell attachment assays to test the effect of drugs on cell substrate adhesion. CID2950007 and NSC23766 served as positive controls. Each group was normalized to unstimulated controls as $[(\text{sample absorbance} - \text{negative control absorbance}) / \text{positive control absorbance}]$, where the negative control is the absorbance reading obtained using lysates from unstimulated cells, and the positive control is the absorbance reading obtained from the stimulated cells treated with DMSO. Value zero represents the basal level (resting cells without serum stimulation) of adhesion. Data represented three independent trials. Each data point represents the mean of measured values \pm SEM. Statistically significant differences are indicated: * $p < 0.05$, ** $p < 0.01$, *** $p < 0.001$.

Cell Migration - Activated by extracellular stimuli and dependent on GTPase activation, cell migration is initiated by the formation of membrane protrusions, including Cdc42-dependent filopodia and Rac1-mediated lamellipodia (125). SKOV3ip cell migration in the presence of R- or S-ketorolac was tested in a Boyden chamber assay. Migration was inhibited in a dose-dependent manner with R-ketorolac beginning to impinge on cell migration at 1 μ M. The inhibitory effect increased in a dose-dependent manner with maximum inhibition of 80% at 300 μ M R-ketorolac (Figure 25). Modest inhibition by S-ketorolac was detected at about 50 μ M with a maximum inhibition less than 50% at 300 μ M. The results demonstrate that cell migration was inhibited as a direct biological consequence mediated by Cdc42 and Rac1 inhibition by R-ketorolac, whereas S-ketorolac was 50-fold less potent.

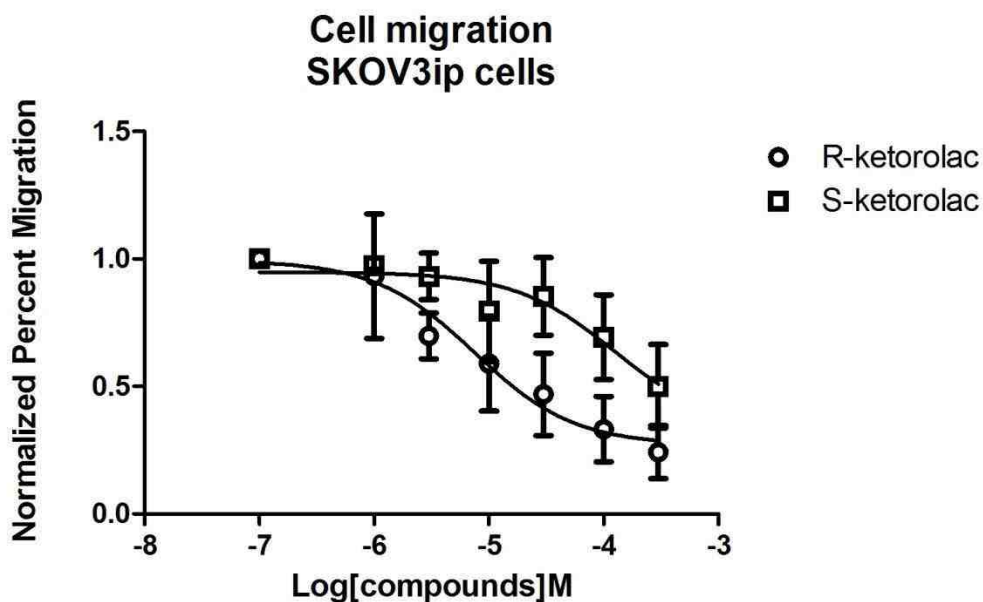


Figure 25. R-ketorolac selectively inhibits cell migration in a dose-dependent manner. SKOV3ip cells were seeded in Boyden chambers in the presence of drug for 48 h. Cell migration was normalized to no treatment controls. Three fields of view were counted for each treatment group. Data represented three independent trials. Each data point represents the mean of measured values \pm SEM. Statistically significant differences are indicated: * $p < 0.05$, ** $p < 0.01$, *** $p < 0.001$. Data provided courtesy of Dr. S.R. Kenney (Department of Pharmaceutical Sciences, University of New Mexico).

Cell Invasion - Invadopodia are membrane protrusions that are dependent on activated Cdc42 and Src kinase. Invadopodia concentrate matrix metalloproteinases at their tips and based on their matrix degradative properties serve as surrogates for cell invasive behaviors (155). To study the effect of ketorolac on invadopodia formation, the invadopodia-mediated degradation of gelatin matrices was quantified. In Skov3ip cells, invadopodia were observed as puncta of F-actin and Tks5-positive structures, which colocalized with the degradation sites on the gelatin matrix (Figure 26A). R-ketorolac treatment also resulted in reduced gelatin degradation in a dose-dependent manner with 70 to 80% inhibition at 1 and 10 μ M. However, S-ketorolac did not exert any obvious inhibition of gelatin degradation at 1 μ M and the reduction of gelatin degradation with 10 μ M S-ketorolac treatment was ~50% but failed to reach the statistical significance (Figure 26 B, C). Tks5 is an early marker of invadopodia formation that precedes matrix metalloprotease localization to the tips of mature structures. To distinguish whether R-ketorolac had a direct inhibitory effect on metalloprotease activity or whether the observed effect on gelatin degradation was primarily due to inhibition of invadopodia formation, the impact on metalloproteinase activity secreted into the culture medium was also measured and found to be similar \pm ketorolac. Therefore, we conclude that the primary effect of R-ketorolac is to prevent Cdc42-dependent invadopodia formation. When the gelatin degradation assay was conducted in primary ovarian cancer cells, the standardized z-scores showed the degradation of matrix by tumor cells

was also significantly decreased in a dose-dependent manner by R-ketorolac treatment, while the inhibition by S-ketorolac was less and reached significance only at the highest dose (Figure 27). Z-scores were used to account for large differences in absolute GTPase activity levels observed for individual patient samples (Figure 19), likely related to known differences in GTPase overexpression seen in ovarian cancer (77, 86). The inhibitory effect of R-ketorolac in primary ovarian cancer cells is consistent with the observations in SKOV3ip cells.

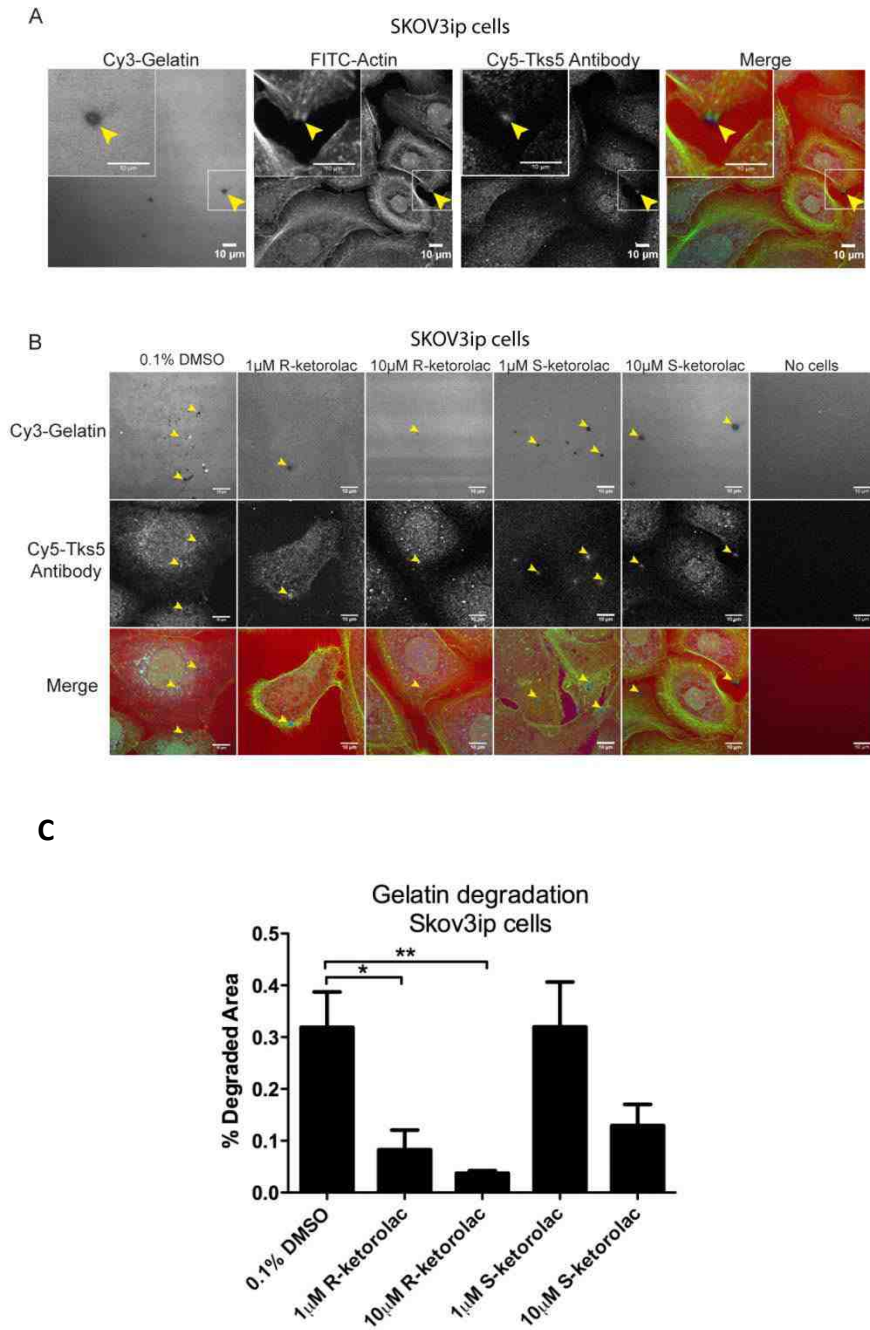


Figure 26. R-ketorolac inhibits invadopodia formation and gelatin degradation in SKOV3ip. (A) Colocalization of gelatin degradation, actin and Tks5 antibody in SKOV3ip cells. Insets are magnified images of the boxed

regions. Arrowheads denote points of invadopodia formation that are coincident with gelatin degradation. (B) Representative confocal images of gelatin degradation for each treatment group in SKOV3ip cells are shown. Lower panels are magnified images of the boxed regions. Arrowheads denote the gelatin degradation sites. (C) Quantification of the gelatin degradation area in SKOV3ip cells. For all experiments, SKOV3ip cells were seeded on Cy3-gelatin labeled coverslips for 24 h in the presence of different drugs, including two enantiomers of ketorolac, and Cdc42 and Rac1 specific inhibitors (CID2950007 and NSC23766, respectively) as positive controls. DMSO (0.1%) served as the vehicle control treatment. Results are normalized as $[(\text{sample degraded area} - \text{negative degraded area}) / \text{positive control degraded area}]$, where the negative control is the degradation of unstimulated cells, and the positive control is the degradation of the stimulated cells treated with DMSO. Value zero represents the basal level (resting cells without EGF stimulation) of gelatin degradation. All quantification is based on three independent trials with 15 representative fields counted for each treatment. Each data point represents the mean of measured values \pm SEM. Statistically significant differences are indicated: * $p < 0.05$, ** $p < 0.01$, *** $p < 0.001$.

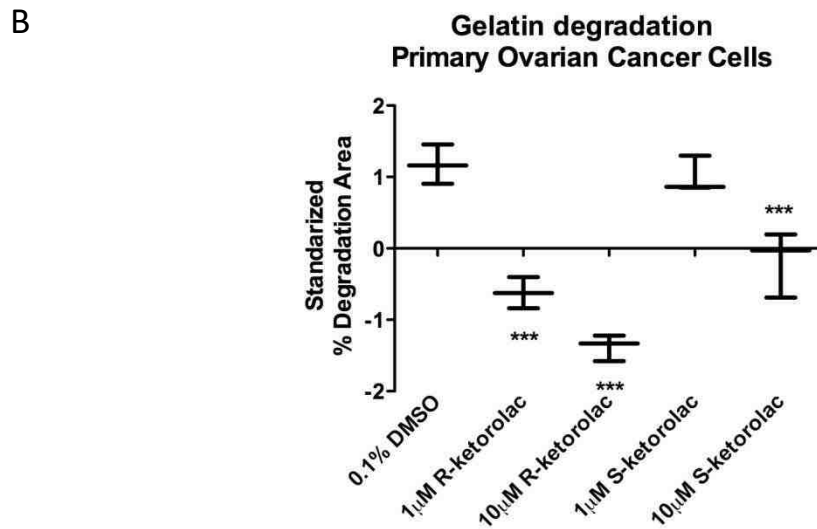
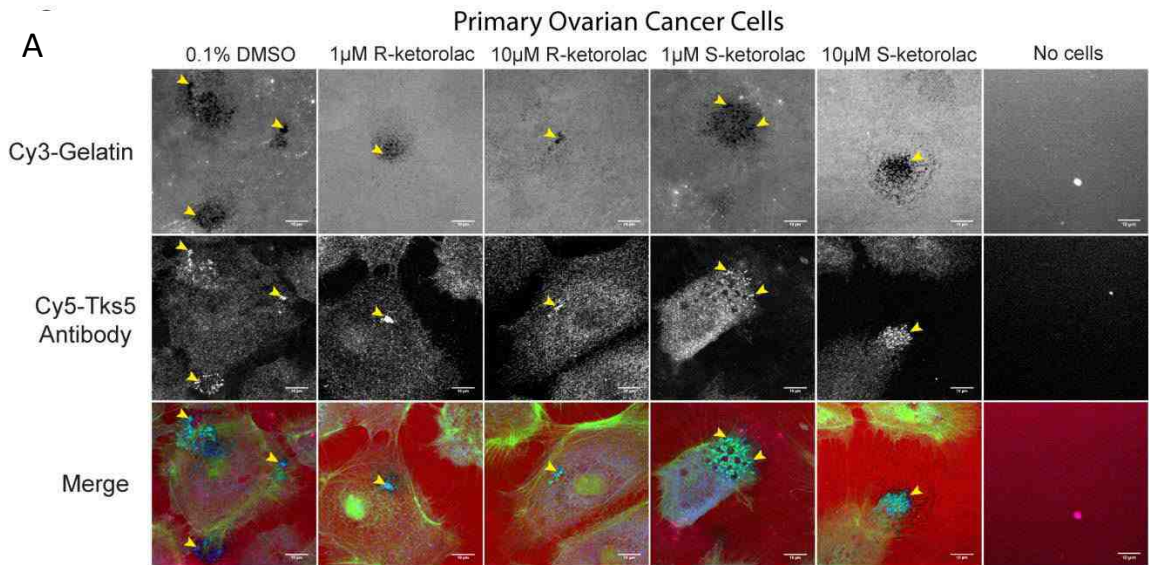


Figure 27. R-ketorolac inhibits invadopodia formation and gelatin degradation in primary human ovarian cancer cells. (A) Representative confocal images of gelatin degradation for each treatment group in primary ovarian cancer cells are shown. Lower panels are magnified images of the boxed regions. Arrowheads denote the gelatin degradation sites. (B) Quantification of the gelatin degradation area in primary ovarian cancer cells. Due to the variability

of the extent of gelatin degradation observed with primary human ovarian cancer cells, z-scores are plotted. For all experiments, primary ovarian cancer cells were seeded on Cy3-gelatin labeled coverslips for 24 h in the presence of different drugs, including two enantiomers of ketorolac, and Cdc42 and Rac1 specific inhibitors (CID2950007 and NSC23766, respectively) as positive controls. DMSO (0.1%) served as the vehicle control treatment. Plotted are z-scores. For individual patient sample, z-score is defined as $z=(X - \mu)/\sigma$, where X is the gelatin degraded area for each treatment, μ is the mean of X , and σ is the standard deviation of X . All quantification is based on three independent trials with 15 representative fields counted for each treatment. Each data point represents the mean of measured values \pm SEM. Statistically significant differences are indicated: * $p<0.05$, ** $p<0.01$, *** $p<0.001$.

Conclusion and Discussion

In this chapter, R-ketorolac is shown to inhibit Cdc42 and Rac1 activation and associated cell functions, including adhesion, migration and invasion in both SKOV3ip cell and primary human ovarian tumor cells. In its clinical application, ketorolac is given for its potent analgesic activity. It is administered as a racemic mixture via diverse routes (intravenous, injectable, oral, intranasal) and is known as ToradolTM. The pain relieving activity is ascribed primarily to the S-enantiomer, which is a known non-selective cyclooxygenase (COX-1/COX-2) inhibitor (122, 167). The R-enantiomer lacks significant activity against cyclooxygenases (e.g. $IC_{50} > 100 \mu M$ against COX1 and COX2 and ~3 orders of magnitude greater than the IC_{50} of S-ketorolac) and has until now been considered inert (122, 167). The previously unrecognized and novel mechanism of action for the R-enantiomer has important ramifications when considering the efficacy and novel activities of clinically administered ketorolac. For example, breast cancer patients treated with ketorolac perioperatively had a decreased rate of early breast cancer relapse (53). Collaborative studies from Hudson and Wandinger-Ness laboratories with colleague Muller and Cook demonstrate ovarian cancer patients receiving ketorolac exhibit an enrichment of R-ketorolac in the peritoneum, a reduction in GTPases activation of residual tumor cells, and improved 5-year survival (86). The cell based studies using human immortalized and primary human ovarian cancer cells presented here, demonstrate that R-ketorolac treatment alters tumor cell adhesion, migration and invasion—all behaviors that

are central to ovarian cancer metastasis. The findings offer unprecedented mechanistic insights regarding the R-ketorolac activity against GTPases, which may explain the clinically observed survival benefit in patients treated perioperatively with racemic ketorolac.

In ovarian cancer, cyclooxygenases are upregulated and have been considered as potential targets, however, clinical trials have been mixed and do not support significant benefit in combinatorial treatment with chemotherapy and a cyclooxygenase inhibitor versus treatment with chemotherapy alone (168). Although the survival benefit of ketorolac use in breast cancer was postulated to be due to possible inhibitory roles in anti-angiogenesis, inhibition of prostaglandin synthesis and decreased immune suppression as compared to opioids and other analgesics (169, 170), there was previously no precedence for other pharmacologic activities associated with R- or S-ketorolac. A recent structural study identifies a new hydrophobic ligand binding site on intestinal fatty acid binding protein that can interact with ketorolac (all deposited structures show protein complexed to R-ketorolac though not explicitly stated in publication – Ursu and Oprea, unpublished observation), though functional consequences are unknown (170). We speculate that the slight inhibitory effects of S-ketorolac on GTPase activation and actin dependent cell behaviors may arise from crosstalk between COX-2 and PI3K and integrin regulated pathways. COX-2 dependent crosstalk has been shown through knockout and pharmacologic means to regulate Cdc42 and Rac1 activation, and adhesion and migration of macrophages and endothelia (165, 171). Because R-ketorolac is a much less

potent COX inhibitor than S-ketorolac, its more pronounced effect on GTPase activation and downstream cell behaviors indicates that it is primarily targeting Cdc42 and Rac1 through a direct mechanism. Furthermore, pharmacokinetic analyses show that S-ketorolac is more rapidly excreted, leading to an increased prevalence of R-ketorolac *in vivo* (86, 122, 167). Taken together, our identification of R-ketorolac as a GTPase inhibitor helps to explain the significant benefits of racemic ketorolac in human breast and ovarian cancer patient survival, and why other NSAIDs that preferentially target COX have not yielded similar benefit (53, 86, 172).

Ketorolac is an FDA (Food and Drug Administration)-approved drug for human use and is in active clinical use as the racemic mix. Therefore, R-ketorolac has significant potential for rapid repurposing. Implementation of R-ketorolac in human clinical trials would offer the first opportunity to directly test the predicted benefit of a Cdc42 and Rac1 selective inhibitor for cancer patients. Such an application could circumvent current renal and hematologic toxicities that limit racemic ketorolac use to a maximum of 5 days. Analyses of Rac1 inhibition in cancer cell lines and animal models with NSC23766 treatment suggests benefit for inhibiting metastasis and angiogenesis (173). Additionally, Rac1 inhibition may mitigate Trastuzumab resistance in breast cancer cell lines, thus suggesting that the availability of a clinically accessible selective Cdc42 and Rac1 inhibitors could offer new paradigms for combinatorial therapies (173). We envision that the use of R-ketorolac in the perioperative window and thereafter presents a unique opportunity to block tumor reseeding and spread, as well as

angiogenesis, which may enhance the efficacy of combined chemotherapies or targeted therapies.

CHAPTER 4

A NOVEL PHARMACOLOGIC ACTIVITY OF KETOROLAC FOR THERAPEUTIC BENEFIT IN OVARIAN CANCER PATIENTS

Abstract

Previous studies identified the R-enantiomer of ketorolac as an inhibitor of the Rho family GTPases Cdc42 and Rac1. Cdc42 and Rac1 regulate cancer-relevant functions including cytoskeleton remodeling necessary for tumor cell adhesion and migration. In this chapter, elevated expression and activity of Cdc42 and Rac1 are reported in ovarian cancer patient tissues, confirming target relevance. A clinical trial is performed in eligible patients to measure the bioavailability of R- and S-ketorolac in serum and peritoneal fluid, and GTPase activity in peritoneal cells. The results show ketorolac in peritoneal fluids is enriched in the R-enantiomer and GTPase activity is inhibited in ascites-derived primary ovarian tumor cells after ketorolac administration when R-ketorolac is at peak levels. In addition, a retrospective study suggest that women given perioperative ketorolac have a lower hazard of death (Hazard Ratio=0.30 [95%CI 0.11-0.88]). Thus, ketorolac has a novel pharmacologic activity conferred by the R-enantiomer and R-ketorolac achieves sufficient levels in the peritoneal cavity to inhibit Rac1 and Cdc42, potentially contributing to the observed survival benefit in women who received ketorolac.

All the work in chapter 4 are published Guo, Y and Kenney SR, et al., Clin Cancer Res. 2015 Jun 12. [Epub ahead of print] PMID: 26071482

Introduction

Ovarian cancer is the leading cause of death from gynecologic malignancies and the second most common gynecologic cancer (174). Five year patient survival remains less than 50% and the mortality rate hasn't changed appreciably in two decades (174). The majority of women are diagnosed with metastatic disease, and although a substantial proportion of women respond to initial treatment, recurrence is common (16). Despite concerted efforts, identification of effective targeted therapies has remained elusive in this disease (6). There remains a great need to identify new strategies to treat and manage ovarian cancer.

The Rho family of small GTPases (Cdc42, Rac and Rho) are key regulators of cancer-relevant cellular functions including actin reorganization, cell motility, cell-cell and cell-ECM adhesion and invasion (54, 149, 153). In many human tumors (including colon and breast), there is clinical and experimental evidence that aberrant Rho-family signaling contributes to tumor growth, survival, invasion and metastasis (54, 68, 175-177). On the basis of these functions, Cdc42 and Rac1 have been recognized as attractive therapeutic targets (173, 178) and inhibitors are effective in experimental systems (104, 107-110, 179, 180), but specific inhibitors of Cdc42 or Rac1 have not been translated to clinical use.

A Cdc42 selective inhibitor effectively blocked migration of two ovarian tumor cell lines (104, 181), suggesting that Rho-family GTPases may be potential

therapeutic targets in ovarian cancer. Using findings obtained from a high throughput screen of the Prestwick library of off patent, FDA-approved drugs and cheminformatics approaches, we identified the R-enantiomers of a limited number of NSAIDs as inhibitors of Cdc42 and Rac1. The corresponding S-enantiomers are considered the active component in racemic drug formulations acting as NSAIDs with selective activity against cyclooxygenases (COX). One candidate, R-ketorolac, inhibited ovarian tumor cell migration and adhesion without causing cytotoxicity (182, 183). Our data indicate that the clinically administered racemic ketorolac (Toradol[®]) has two distinct pharmacologic activities; the well-established inhibition of COX 1 and 2 by S-ketorolac serving as the basis of the FDA-approved indication for pain management, and a previously unrecognized property of Cdc42 and Rac1 inhibition conferred by the R-enantiomer. Cell based measurement of GTPase activity demonstrated that R-ketorolac specifically inhibits EGF-stimulated Cdc42 and Rac1 activation at low micromolar concentrations. The GTPase inhibitory effects of R-ketorolac in cells mimic those of established Cdc42 (CID2950007/ML141) and Rac1 (NSC23766)-specific inhibitors (104, 183).

In this chapter, R-ketorolac is shown to achieve an effective concentration in peritoneal fluids and inhibited Cdc42 and Rac1 activity in cells retrieved from the peritoneal compartment of post-surgical ovarian cancer patients following administration of the racemic drug for postoperative pain management. A medical record review to compare the ovarian cancer-specific survival of ovarian cancer patients who did or did not receive ketorolac for post-operative analgesia

revealed increased survival of patients receiving ketorolac. This observation is in keeping with reports for improved clinical outcomes associated with ketorolac usage, as compared with other NSAIDs, in breast cancer patients (53, 169, 184). Although it has been long recognized that R-enantiomers of NSAIDs are poor inhibitors of COX activity (167, 185, 186), potential pharmacologic activities or benefits of the R-enantiomers have remained largely unexplored. The findings show that Cdc42 and Rac1 are unrealized therapeutic targets in ovarian cancer and use of ketorolac may benefit ovarian cancer patients.

Materials and Methods

Immunohistochemical Analyses of GTPase Targets

Immunohistochemical staining was performed using standard procedures. Rac1 was stained with mAb (clone 102, BD Biosciences, 10155-1-AP) and Cdc42 was stained with rabbit pAb (Protein Tech Group). A Vectastain Ready-to-Use (RTU) ABC-peroxidase kit and ImmPact DAB (SK-4105) were used to visualize primary antibody labeling with hematoxylin nuclear counterstain (H-3401) for tissue staining and samples were mounted in VectaMount (H-5000); (all from Vector Laboratories).

For large scale ovarian tumor profiling, tissue microarrays were purchased from US BioMax, Inc. (Rockville, MD, cat# OV1005 061 and OV8010 009). In total 180 unique tissue samples were included in the evaluation; ranging from stage I-IV and grades 1-3 (Appendix A). All tumor types were validated and staining was scored by a pathologist with gynecologic pathology specialty (Dr. Lomo) and evaluated for location (nuclear and cytoplasmic), as well as intensity of positive staining. Scoring was based on the product of the percentage of cells stained and the intensity of the staining in each localization (3+: strong, 2+: intermediate, 1+: weak and 0: no staining), resulting in a minimum of 0 (100% cells x 0) and a maximum of 300 (100% cells x 3+).

qPCR of Ovarian Cancer cDNA Arrays

qPCR was performed using Origene SYBR Green I master mix solution diluted to a final concentration of 1X with primers at a concentration of 0.33 μ M. PCR mix was added to each well of the microarray plate and incubated on ice for 15m to dissolve the cDNA. qPCR was conducted using a Bio-Rad iCycler (Hercules, CA) under the following conditions; 95° for 5m, 30 cycles of (95° for 15s, 60° for 30s, 72° for 1m), followed by melt curve analysis, hold at 4°. Rac1b levels were measured using custom primers synthesized by Invitrogen. Rac1b forward primer, 5'-TCCGCAAACAGTTGGAGA-3', was coupled with Rac1 reverse primer, 5'-CTACATGTTTGC GGATAGGATAGGG-3'. The identity of the PCR product as Rac1b was confirmed by sequence analysis.

qPCR of Ovarian Cancer cDNA Arrays

Rac1b levels were measured using custom primers synthesized by Invitrogen. Rac1b forward primer, 5'-TCCGCAAACAGTTGGAGA-3', was coupled with Rac1 reverse primer, 5'-CTACATGTTTGC GGATAGGATAGGG-3'. The identity of the PCR product as Rac1b was confirmed by sequence analysis.

Quantitative PCR (qPCR) of Ovarian Cancer cDNA Arrays

qPCR analysis of Rho family GTPases was performed using Tissuescan Ovarian Cancer cDNA microarrays (Appendix B) from Origene (Rockville, MD, cat# HORT301, HORT302,HORT303) and standard techniques. qPCR amplification utilized Qiagen Quantitect primers for Cdc42 (Valencia, CA,

QT01674442), Rac1 (QT00065856), and RhoA (QT00044723), and β -actin (Origene), and custom Rac1b primers from Invitrogen (Carlsbad, CA). Primer information for Rac1b, additional information on the Ovarian Cancer cDNA arrays is presented in Appendix B. Analysis of serous cancer only is shown in Figure 32. CT values obtained using iCycler software. Relative expression levels were determined using $\Delta\Delta$ CT values.

Patients, Study Design and Treatment

A Phase 0 trial investigating the use of postoperative ketorolac was reviewed and approved by the University of New Mexico Health Sciences Center Human Research Review Committee (clinicaltrials.gov -NCT01670799). Patients presenting with a new diagnosis of ovarian, fallopian tube or primary peritoneal cancer were screened for eligibility. Eligible women were at least 18 years old, an ECOG Performance Status <2 and had consented to a planned debulking surgery- Consent was obtained prior to surgery if primary eligibility was met. Secondary eligibility after surgery included confirmed histologic diagnosis of epithelial ovarian, fallopian tube or primary peritoneal cancer; optimal cytoreduction and placement of an intraperitoneal port for planned chemotherapy; adequate renal function and no postoperative complications prohibiting ketorolac use. Patients with known bleeding disorders or other contraindications to NSAID use were excluded.

Subjects received a single IV dose of Toradol[®] (15 or 30 mg based on the patient age and creatinine clearance) within the first 72 h of surgery when all

clinical safety parameters were met. Use of other NSAIDs during the trial was not permitted; however narcotic regimens were allowed for postoperative pain management. All study protocols were reviewed by an independent data and safety monitoring board. Baseline ascites samples were obtained at surgery. Subsequent peritoneal fluid samples were collected from the intraperitoneal port prior to dosing and at 1, 6, and 24 h after single dose ketorolac administration. Peripheral blood was collected at the same time points. Serum and peritoneal fluid were separated from cellular material via low speed centrifugation. Tumor cells were further purified on Ficoll gradients to red blood cells and negative selection with anti-CD45 beads to remove lymphocytes. The resulting tumor cell fractions were analyzed by flow cytometry for EpCAM and MUC16/CA125 (see Figure 28 for representative purity).

Analysis of Patient Derived Cells

To purify ovarian cancer cells from ascites, cells were recovered from ascites samples by low speed centrifugation at 1000 rpm. The cell pellets were gently resuspended and overlaid on a Ficoll (density 1.077 ± 0.001 g/ml; GE Healthcare 17-5442-02) to separate red blood cells from lymphocytes and tumor cells per manufacturer's instructions. Anti-CD45 beads (ThermoFisher Scientific, 11153D) were used to deplete lymphocytes and the resulting tumor cell fraction was analyzed visually and by flow cytometry. For flow cytometric analysis, cells suspended in phosphate buffered saline (PBS) were fixed with formaldehyde (2-4% final concentration) for 10 min, chilled for 20 min and then processed for immunostaining as described by Cell Signaling Technology

([http://www.cellsignal.com/contents/resources-protocols/flow-cytometry-protocol-\(flow\)/flow](http://www.cellsignal.com/contents/resources-protocols/flow-cytometry-protocol-(flow)/flow); webpage Accessed July 22, 2014). Briefly, non-specific mAb binding to human Fc receptor was blocked by pretreatment for 10 min at room temperature with human Fc receptor binding inhibitor (14-916, Affymetrix eBioscience). Conjugated primary antibody staining was performed in PBS containing 0.5% BSA using $0.5-1 \times 10^6$ cells / assay for 1 h at room temperature. Cells were washed with 500 μ M PBS containing 0.5% BSA once and resuspended in 500 μ l PBS for flow cytometry measurement (BD FACSCalibur)

Tumor cell fractions were positive for EpCAM (detected with mAb against EpCAM clone Ber-EP4, Dako) and MUC16/CA125 (detected with a Cy5-labeled rabbit pAb directed against human MUC16/CA125; bs-0091R-Cy5, Bioss Antibodies) and negative for CD45 (detected with a PE-labeled rabbit pAb directed against human CD45/LCA, 12-9459, Affymetrix eBioscience) (Figure 28).

For analysis of GTPase activity in patient-derived cells, active RhoA was quantified based on binding to GST-Rhotekin (RT01, Cytoskeleton, Inc.). Antibodies specific for Cdc42 (sc-8401, Santa Cruz Biotechnology, Inc.), Rac1 (610650, BD Transduction Labs) or RhoA (26C4, sc-418, Santa Cruz Biotechnology, Inc.) and Alexa Fluor 488 donkey anti-mouse IgG (A21202, Life Technologies) were also used.

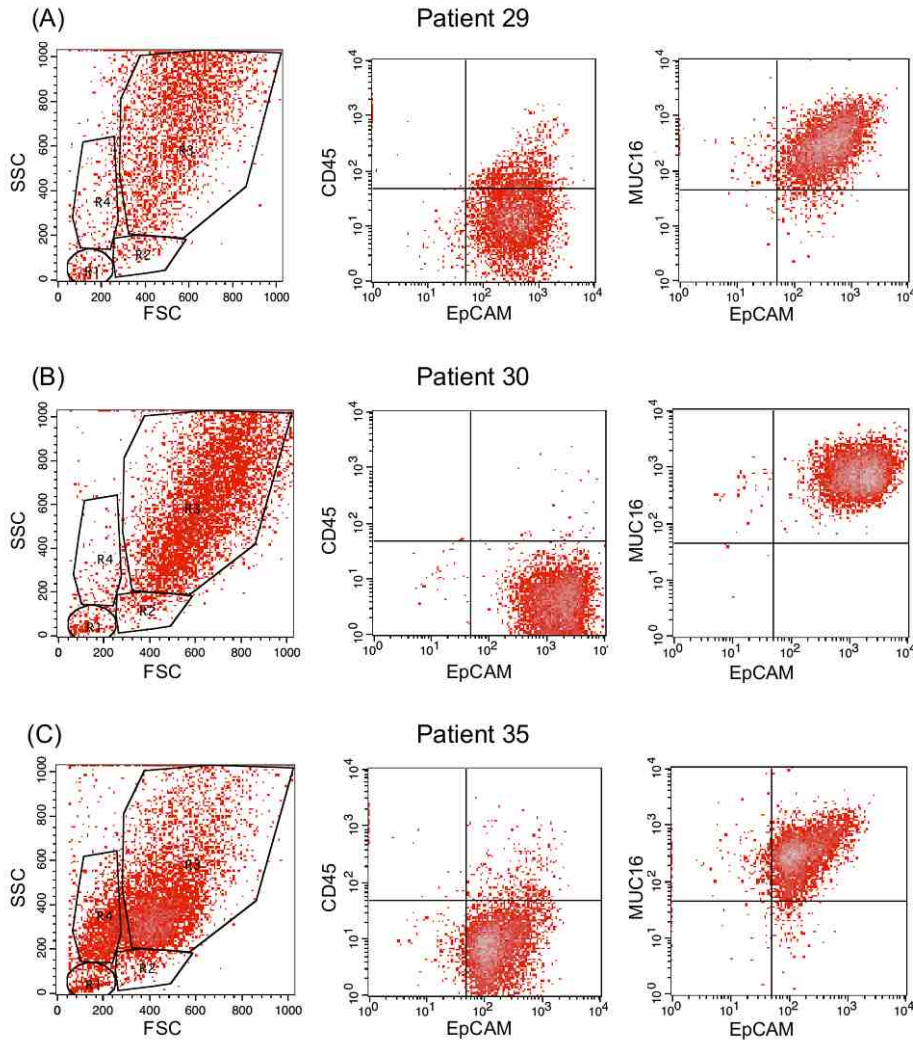


Figure 28. Purified ovarian tumor cells express EpCAM and MUC16/CA125.

Ovarian tumor cell identification by flow cytometry using patient ascites samples from three individuals (designated 29, 30, and 35). Tumor cells were purified from ascites using Ficoll gradients to remove red blood cells and CD45 Dynabeads negative selection to remove leukocytes. The resulting cells (gated as R3) were negative for CD45 and positive for EpCAM and MUC16/CA125. Markers were tracked by flow cytometry on a Becton Dickinson FACSCalibur Flow Cytometer.

High Performance Liquid Chromatography

R- and S-enantiomers of ketorolac were analyzed by high performance liquid chromatography (HPLC) using published procedures (186, 187). See Appendix C for additional information. The R-value for the standard curve of total ketorolac was 0.9997 and represented a concentration range that spanned established human serum concentrations (0.092 µg / ml to 6.0 µg / ml).

Analysis of GTPase Activity

Two methods were used to assess GTPase activity in cells based on effector binding. Commercial GLISA kits from Cytoskeleton, Inc., analyzed Rac1 (Denver, CO, cat# BK-128), Cdc42 (BK-127) or RhoA (BK-124) per manufacturer's instructions. Alternatively, Rac1, Cdc42 and RhoA activities were measured using a flow cytometric effector binding assay (G-trap) (135, 140). Briefly, $\sim 10^5$ purified primary tumor cells were lysed in 200 µl RIPA buffer for each assay. GST-PAK1 protein (Millipore, 14-864) was immobilized to the GSH-beads according to the methods reported in previous work (180). Cell lysates were normalized to the same concentration and incubated with pre-labeled beads for 1 h at 4°C. Primary antibody and conjugated secondary antibody staining were performed in HPS buffer containing 1% BSA for 1 h at 4°C. Stained beads were resuspended in 500 µl HPS buffer. Fluorescence intensity (mean channel fluorescence, MCF) was measured by flow cytometry (Accuri C6). GTPase activity was calculated by (MCF of sample group – MCF of unstimulated

group) / MCF of stimulated group. Equal amounts of protein were used for each assay.

Retrospective Patient Outcomes Review

A medical record review was conducted under institutional review board approval with a waiver of patient consent. Ovarian cancer patients were identified from the New Mexico Tumor Registry [NMTR] a member of the population-based Surveillance, Epidemiology, and End Results [SEER] Program of the National Cancer Institute (34). Inclusion criteria were as follows: invasive, epithelial ovarian cancer (any histology), age 40-79 years at diagnosis, years of diagnosis 2004–2006, and receipt of surgery at an Albuquerque, NM hospital (only three hospitals in the metropolitan area provide this level of surgery). Diagnosis years of 2004-2006 ensured at least 6 years follow-up (mortality followed through Dec 31, 2012) for each patient. We abstracted the surgical medical records for all analgesics and anesthesia medications used before hospital admission, during surgery and hospital stay, and given at discharge. Of the 138 potential cases, 6 women did not undergo surgery because of advanced disease/severe comorbidities or desired palliative care only, 1 woman had her surgery in another state, 2 women died before surgery, and medical records were not located for 6 women, leaving 123 women in the final analysis.

Statistical Analysis

qPCR findings for GTPase expression levels were analyzed using one-way ANOVA followed by Dunnett's Multiple comparisons test to determine

differences between ovarian cancer grade. IHC data was analyzed using one-way ANOVA followed by Tukey's post test to determine significant differences between groups. Data obtained from patient fluid and cell samples was analyzed as a repeated measure ANOVA followed by Dunnett's multiple comparisons test to determine significant differences between groups. For the retrospective medical record review, information from the medical record was merged with information from the NMTR for final analysis. Clinical and treatment characteristics of patients who did and did not receive peri-operative ketorolac were compared with chi-square tests and t-tests. In a preliminary, crude analysis the Kaplan-Meier method was used to estimate the survival probabilities. The difference in survival based on receipt of peri-operative ketorolac was examined using the stratified log-rank test to adjust the effect of a single categorical factor such as age group, AJCC stage, etc. Because this was an observational study and not a randomized controlled trial, the final analysis was based on a Cox proportional hazards model to adjust for clinical and treatment characteristics that may have differed between those who did and did not receive peri-operative ketorolac. We estimated the hazard ratio (HR) for ovarian cancer-specific mortality comparing those who did and did not receive peri-operative ketorolac while adjusting for age at diagnosis (<50, 50-64, >65) AJCC stage (I, II, III, IV), completion of chemotherapy as planned (yes, no), and receipt of neoadjuvant chemotherapy (yes, no). Based on the Cox proportional hazards regression, an example survival plot is presented in Figure 36. Additional survival plots are presented in Appendix C-F.

Results

Expression of Rac1 and Cdc42 in Ovarian Cancer

On the basis of the established functions of Rho-family GTPases, ovarian cancer metastasis is predicted to be strongly dependent on Rac1/Cdc42-regulated pathways for exfoliation, formation of multicellular aggregates, mesothelial adhesion, and localized invasion into the interstitial collagen-rich submesothelial matrix (6, 16, 188). To test whether these GTPases are dysregulated in ovarian cancer, we examined grade-dependent expression of Cdc42 and Rac1 protein by immunohistochemical staining of human tumor samples (Figure 29) and GTPase mRNA using quantitative PCR analysis of ovarian cancer tissue cDNA arrays (Figure 30 and Figure 31). Cdc42 protein overexpression levels were highly significant for malignant, high grade tumors ($p < 0.001$) compared to lower grade tumors without an apparent increase in mRNA levels. In contrast, there was little evidence of increased expression of Rac1 protein with increasing grade (Figure 29). However, significantly elevated expression of a constitutively active splice variant Rac1b (36-38) was detected in ovarian tumors (Figure 30). These findings provide evidence for aberrant expression of Rac1 and Cdc42 in ovarian cancer and suggest that they may represent therapeutic targets for this disease.

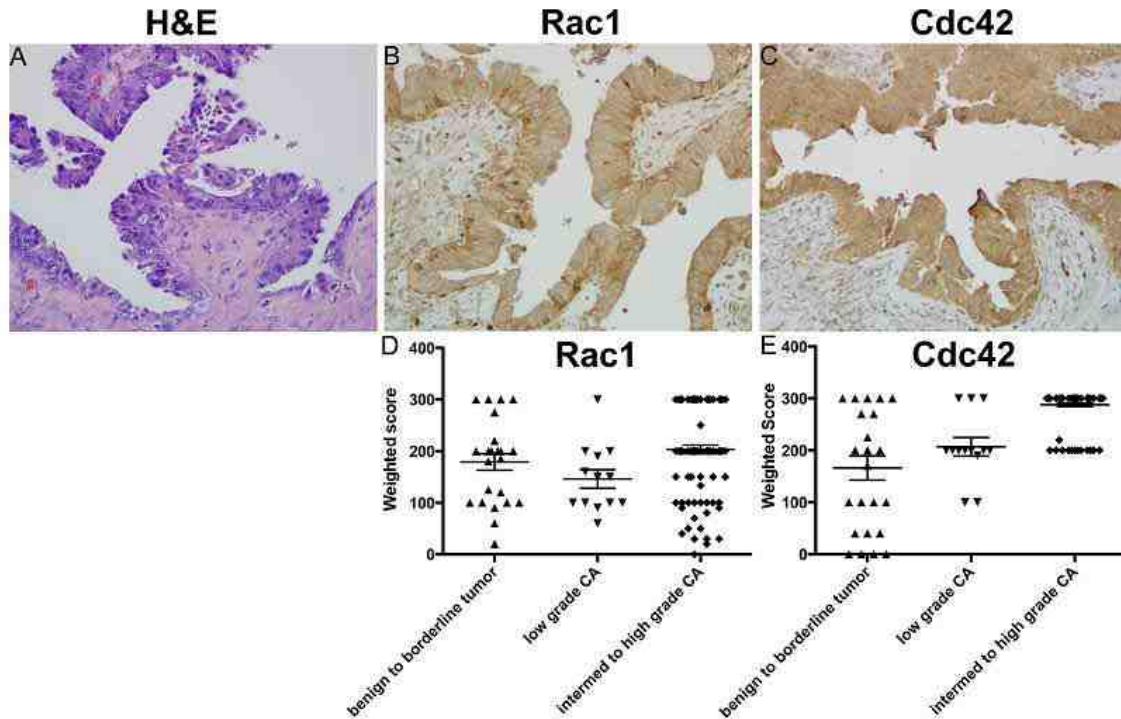


Figure 29. Overexpression of Rac1 and Cdc42 protein in ovarian cancer specimens. (A-C) Representative images of ovarian serous cancer tissue are shown. Clinical characteristics of the samples in the array are provided in Figure 32. Magnification 200X. Scale bar 20 μ m. (A) Hematoxylin/Eosin staining (H&E). (B-C) Samples were stained with antibodies against Rac1 or Cdc42 and avidin/biotin horse radish peroxidase enzyme complex. Controls and tissue samples were developed for identical times. (D-E) Tissue pathology and staining evaluated by board certified pathologist with gynecologic pathology specialization (Lesley Lomo, MD) and statistical analyses by statistician (Ed Bedrick, PhD, University of Colorado Denver, Anschutz Medical Campus). For Rac1 one way non-parametric ANOVA ($p=0.0087$) and Tukey post-test shows normal stroma vs. intermediate to high grade carcinoma ($p<0.05$) with all other comparisons non-

significant. For Cdc42 one way non-parametric ANOVA ($p=0.0001$) and Tukey post-test shows normal stroma and benign to borderline tumor versus intermediate to high-grade carcinoma $p<0.05$ with all other comparisons non-significant. Images provided courtesy of Dr. L. Lomo and Ms. E. Romero (Department of Pathology, University of New Mexico)

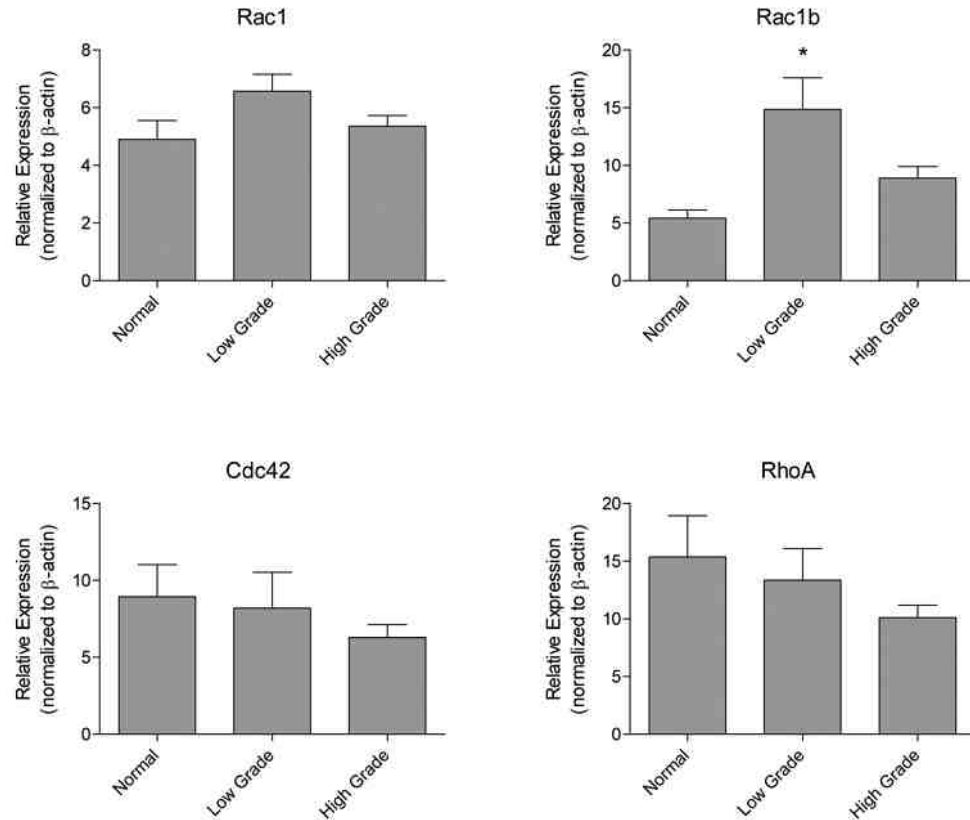


Figure 30. Expression of constitutively active Rac1b mRNA is elevated in ovarian cancer specimens. Tissuescan ovarian cancer cDNA microarrays (Origene) were amplified using primers against Rac1, Rac1b, Cdc42, RhoA, and β -actin as described in Patients and Methods. As per the manufacturer's description, patients with endometriosis, leiomyoma of myometrium, follicular cysts, abscesses, or secretory endometrium, but otherwise healthy ovarian tissue, were considered normal (n=19). Tissues defined as low grade have a FIGO score of 1 (n=19) or 2 (n=32). Tissues considered high grade have a FIGO score of 3 (n=60) or 4 (n=9). The cDNAs of 10 patients were excluded due to a lack of grade information. Clinical characteristics of the samples in the array are provided in Appendix B. Groups were compared to normal using a two-tailed t-

test, and significant increase in Rac1b was detected. * indicates significance is $p < 0.05$. Serous only, analysis by grade is reported in Figure 31. Data provided courtesy of Dr. S.R. Kenney (Department of Pharmaceutical Sciences, University of New Mexico)

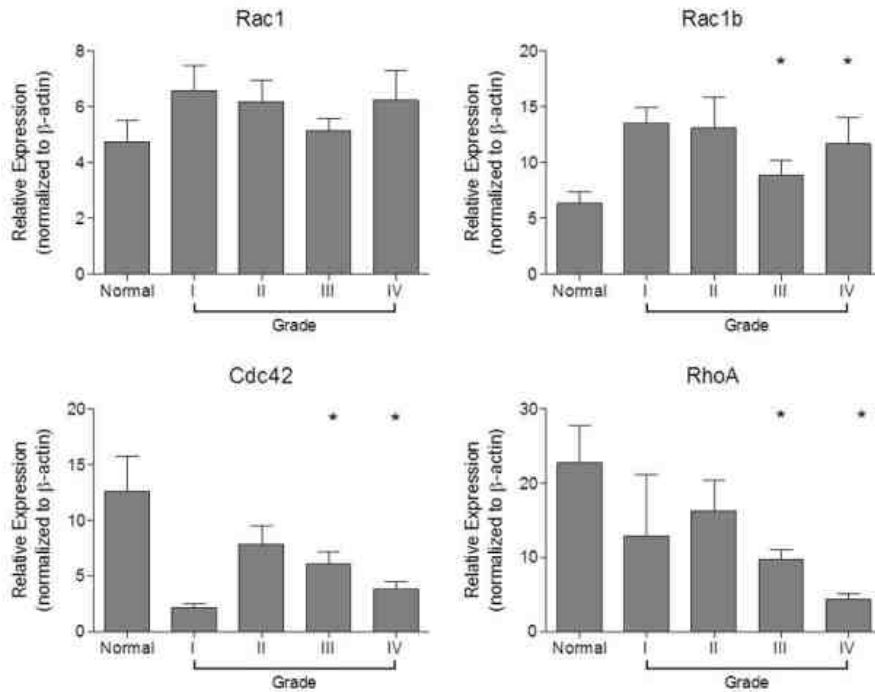


Figure 31. Overexpression of Rac1, Rac1b, Cdc42 and RhoA mRNA is dependent on ovarian cancer grade. This analysis does not include endometrioid tissue. As per the manufacturer description, patients with leiomyoma of myometrium, follicular cysts, abscesses, or secretory endometrium, but otherwise healthy ovarian tissue, were considered normal (n=11). Data from two normal patients were not included due to Grade 3 carcinomas of adjacent tissues. Tissues considered low grade have a FIGO score of 1 (n=19) or 2 (n=32). Tissues considered high grade have a FIGO score of 3 (n=60) or 4 (n=9). The cDNA of 10 patients was removed because they had no grade information. Groups were compared to normal using a two-tailed t-test, * indicates significance is $p \leq 0.05$. Data provided courtesy of Dr. S.R. Kenney (Department of Pharmaceutical Sciences, University of New Mexico)

Study Design and Patient Population

In previous work, R-ketorolac was identified as an inhibitor of Rac1 and Cdc42 at low micromolar concentrations (183, 189). R-ketorolac is inactive against the enzyme targets of S-ketorolac, COX-1 and COX-2 (122, 167, 185), and the inhibitory concentration (IC_{50}) values for inhibition of Rac1 and Cdc42 by S-ketorolac were more than 100-fold greater than R-ketorolac (140). Thus, the racemic (R,S) ketorolac possesses two distinct pharmacologic activities and our findings identify R-ketorolac as a novel inhibitor of Rac1 and Cdc42.

In this “Phase 0” feasibility study, ketorolac was administered for its FDA-approved indication for post-operative pain management. Eligible patients had suspected advanced-stage ovarian, fallopian tube or primary peritoneal cancer with planned optimal cytoreductive efforts. Secondary eligibility was met if the patient had confirmed ovarian cancer, was optimally cytoreduced and had an intraperitoneal port placed for planned peritoneal chemotherapy. The patients had no active postoperative bleeding, did not require therapeutic anticoagulation and had good postoperative organ function. Forty-two patients met primary eligibility, and considering secondary eligibility requirements, twenty patient samples were collected at surgery. Samples of blood and peritoneal fluids after ketorolac administration were obtained from 13 patients. Pathologic analysis of the 20 surgical samples confirmed fifteen patients (75%) had stage III or IV disease. Histologically, 100% had high-grade carcinoma; one was a carcinosarcoma, 16 of 19 were pure serous carcinomas, one was primary peritoneal and one fallopian tube primary, and the rest ovarian primary tumors.

The average age was 60.8 (range 33-81), race and ethnic distribution was 85% Caucasian (29.4% Hispanic), 5% American Indian and 10% Black or African American. Ketorolac dosages administered on the basis of clinical indications were 15 mg (33% of patients) or 30 mg (77% of patients). As illustrated in Figure 32A, blood and peritoneal fluid were obtained at T=0, 1 h, 6 h and 24 h after administration of the recommended dose of ketorolac.

Distribution of R- and S-ketorolac in Peritoneal Fluids

Serum and peritoneal fluid samples were analyzed by HPLC to resolve and quantify R- and S-ketorolac enantiomers in order to determine enantiomeric ratios and distribution over time (Figure 32B, C). Clinical-grade ketorolac tromethamine is a 1:1 mixture of R- and S-enantiomers (Figure 33); however, the racemic distribution favors the R-form in both serum and peritoneal fluids at each time point in keeping with the established shorter half-life of S-ketorolac in human serum based on differences in pharmacokinetic parameters for each enantiomer (122, 167, 185). Ketorolac distributes to the peritoneum within 1h after IV administration, and ketorolac levels in the peritoneal fluids are nearly equivalent to those present in the serum at 6 h and decline dramatically by 24 h in both serum and peritoneal fluids. Our results represent the first evidence of ketorolac distribution to peritoneal fluids.

The IC_{50} values for Rac1 and Cdc42 by R-ketorolac are 0.57 and 1.07 μ M, respectively, whereas the IC_{50} values for S-ketorolac for these targets was >100 μ M (183). The concentrations of R- and S-ketorolac in the peritoneal fluids were

0.98 μM and 0.32 μM , respectively, 6 h after IV ketorolac administration. Thus, R-ketorolac achieved concentrations in the peritoneal fluids at or above the IC_{50} values for Rac1 and Cdc42 and is predicted to inhibit these GTPase targets in cells obtained from this compartment.

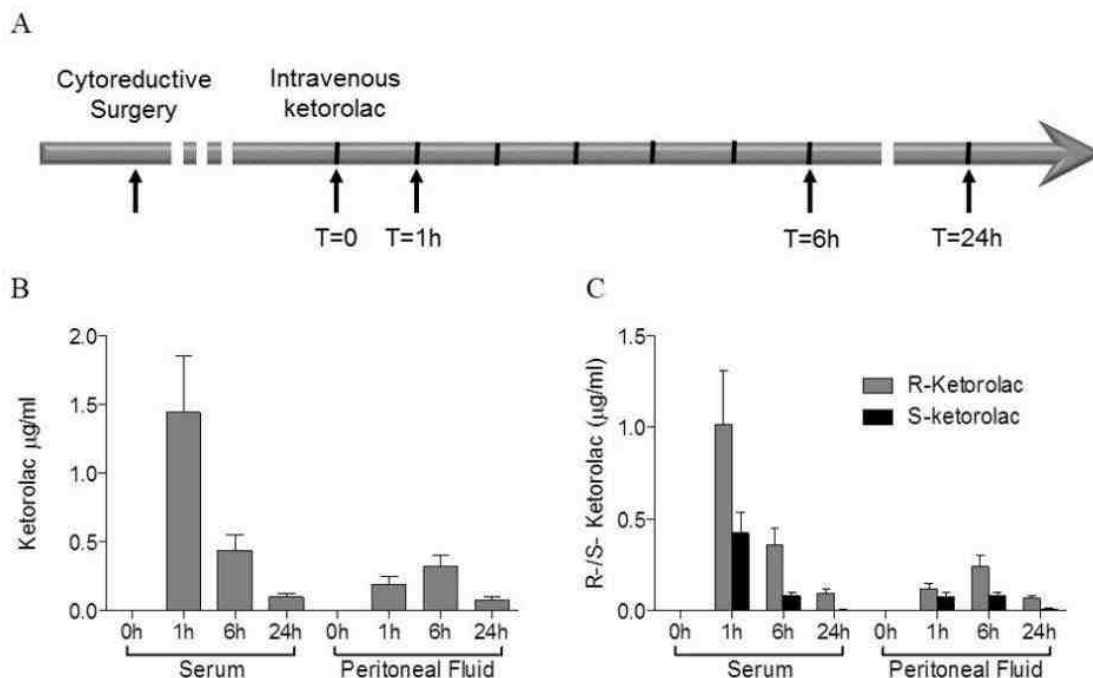


Figure 32. Ketorolac distributes to peritoneal fluids and is enriched in the R-enantiomer. (A) Ascites samples were obtained at cytoreductive surgery and 1 to 3 days after surgery patients received a single dose of either 15 mg or 30 mg of clinical grade racemic ketorolac. Blood and peritoneal fluid from patients were collected before dosing (T=0), and at 1, 6, and 24 h after dosing as depicted by the arrows. (B-C) Ketorolac enantiomers (R and S) were measured in blood and peritoneal fluids using HPLC. (B) Total ketorolac levels in sera and peritoneal fluids. (C) The levels of each ketorolac enantiomer (R or S) at each time point in sera and peritoneal fluids were measured. Concentration conversion to micromolar in serum and peritoneal fluids is provided in Table 5. Administered drug is a 1:1 ratio of R to S (Figure 34), but S-ketorolac is eliminated more rapidly than R-ketorolac leading to a ratio favoring the R-enantiomer in both serum and peritoneal fluids. The *R* value for the standard curve used to calculate

the ketorolac concentrations was 0.9997 and represented a concentration range that spanned established human serum concentrations (0.092 $\mu\text{g/ml}$ to 4.0 $\mu\text{g/ml}$; 3.0 $\mu\text{g/ml}$ = 10 μM). Data (panel B, C) data provided courtesy of Dr. S.R. Kenney (Department of Pharmaceutical Sciences, University of New Mexico)

Analysis of Patient-Derived Cells

Tumor cell enriched fractions were prepared from ascites samples obtained at the time of cytoreductive surgery from ovarian cancer patients and post-surgery immediately prior and 1 h, 6 h, and 24 h post IV ketorolac administration (Figure 33A). Both Rac1 and Cdc42 were highly activated in freshly isolated tumor cells from ascites and the activity level declined within 48 h in culture medium (Figure 34A) suggesting that the ovarian tumor environment fosters Rac1 and Cdc42 GTPase activation. Post-surgery, we observed a statistically significant decrease in Rac1 and Cdc42 activity with time after ketorolac administration (Figure 34B, C). In contrast, RhoA activity was insensitive to ketorolac (Figure 35), further affirming the selectivity of the drug. R-ketorolac predominates in the peritoneal fluids at the S-enantiomer is virtually undetectable at 24 h (Figure 33C) indicating that the R-enantiomer is bioactive and accounts for the observed inhibition of the GTPases in vivo.

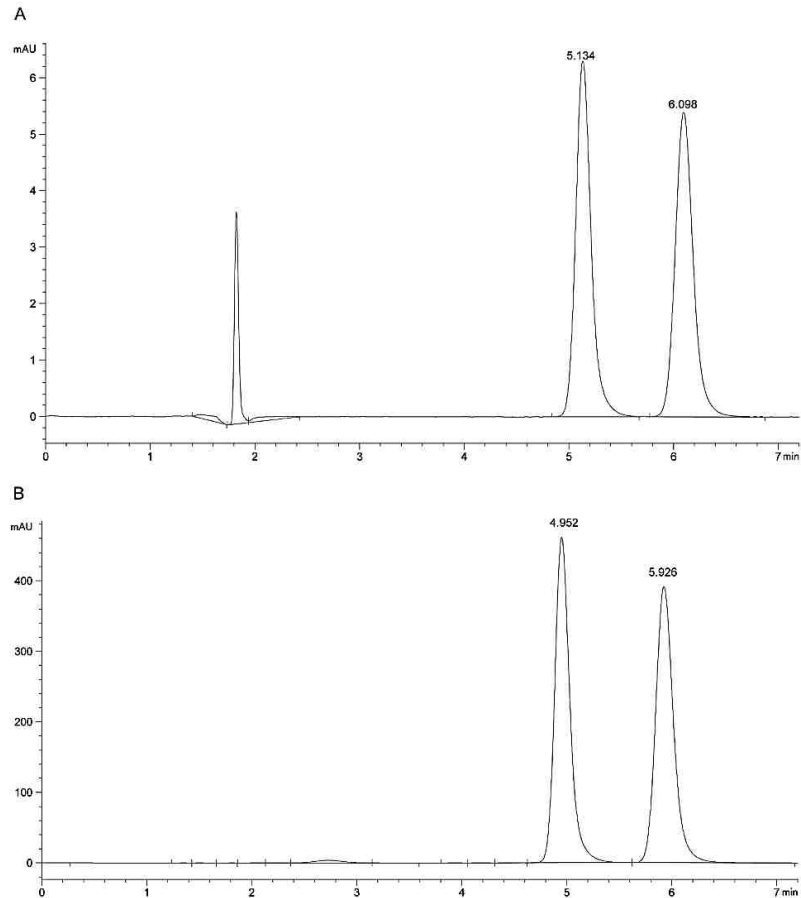


Figure 33. Enantiomer analyses of clinical drug. To confirm that this apparent shift in racemic ratio was not due to either 1) unequal distribution of the racemates in the administered drug or 2) differential extraction of each racemate from serum proteins, we conducted control experiments. (A) Racemic distribution of ketorolac enantiomers of the clinically administered drug was confirmed by HPLC. (B) Clinical grade ketorolac incubated with human serum (shown) and ascites fluid (not shown, but identical results) at 37°C for 1 h and the samples were then processed as for samples obtained from patients. The equal distribution of R- and S-ketorolac in the extracted control sample indicates that the difference in enantiomer composition in patient samples is not due to

differential extraction from serum proteins during sample processing and more likely represents a pharmacokinetic parameter such as preferential binding of S-ketorolac to tissue proteins. Data provided courtesy of Dr. S.R. Kenney (Department of Pharmaceutical Sciences, University of New Mexico)

Table 5. Ketorolac enantiomer concentration in serum or peritoneal fluids.

Sample	[R] μM	[S] μM
Serum 1h	3.97	1.65
Serum 6h	1.44	0.33
Serum 24h	0.40	0.02
Ascites 1h	0.5	0.33
Ascites 6h	0.98	0.32
Ascites 24h	0.27	0.03

Table provided courtesy of Dr. S.R. Kenney (Department of Pharmaceutical Sciences, University of New Mexico)

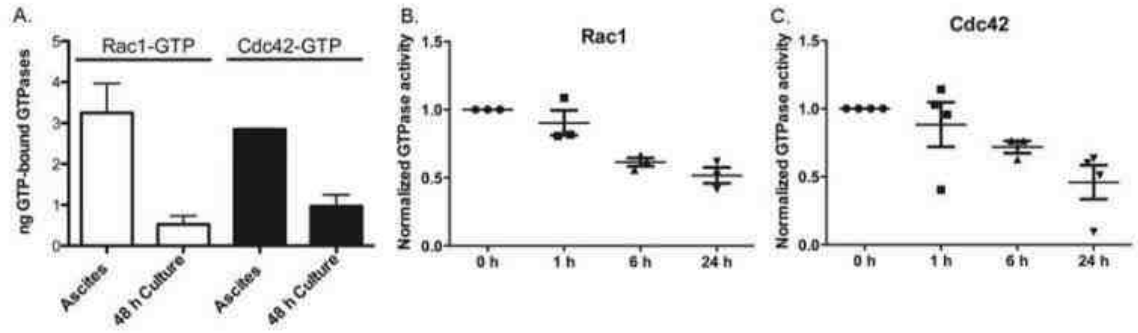


Figure 34. GTPases are activated in patient ascites and inhibited by ketorolac administration *in vivo*. (A) GTPase activity and target inhibition in patient-derived cells. GLISA PAK-effector binding was used to individually detect activated Rac1-GTP or Cdc42-GTP in tumor cells isolated from ovarian cancer patient ascites. Purified GTP-loaded GTPases were used to calculate ng GTP-bound GTPase in the patient sample. Unpaired two-tailed *t* tests showed samples in culture for 48 h were statistically different from fresh ascites samples for both Rac1 and Cdc42 ($p=0.0109$). The levels of active GTPase declined sharply with 48 h in culture, indicating that soluble factors in the ascites serve to upregulate Rac1 and Cdc42 GTPase activities. (B-C) Rac1 GTPase target inhibition following administration of racemic ketorolac to ovarian cancer patients post-surgery. Cells isolated from patient ascites samples post-surgery were assayed for active Rac1 or Cdc42 using a flow based effector-binding assay. Patient diagnoses were all stage III, high grade ovarian serous or papillary serous carcinoma, with one mixed serous endometrioid carcinoma and one suspected primary peritoneal carcinoma (Pt 20, 24, 35, 39, 43). Fluorescence readings were normalized to the 0-h time point drawn immediately before ketorolac administration. For Rac1, one way non-parametric ANOVA ($p=0.0009$)

and Bonferroni multiple comparison test, * indicates $p < 0.05$, ** indicates $p < 0.01$: 0 h versus 6 h (**); 0 h versus 24 h (**); 1 h versus 6 h (*); 1 h versus 24 h (**). Differences between 0 h versus 1 h and 6 h versus 24 h were non-significant. For Cdc42, one way non-parametric ANOVA ($p = 0.0250$) and Bonferroni multiple comparison test, * indicates $p < 0.05$: $p < 0.05$ for 0 h versus 24 h (*) was significant and all others were non-significant. RhoA was not responsive to ketorolac (Figure 35).

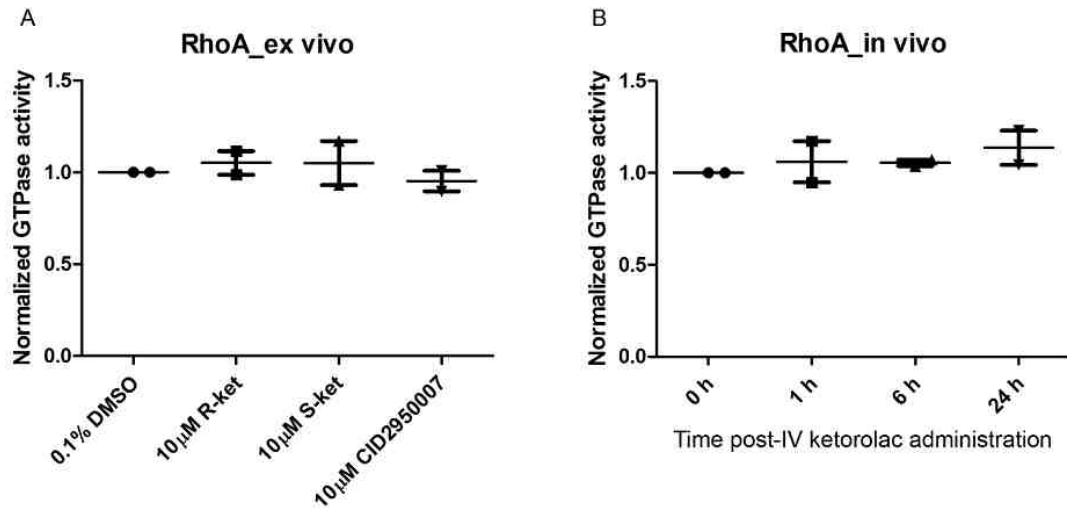


Figure 35. RhoA activity is insensitive to ketorolac treatment. (A-B) RhoA GTPase target inhibition assayed by quantification of active RhoA using a flow based Rhotekin effector binding assay. (A) Patient derived tumor cells purified from ascites fluids at the time of debulking surgery were treated *in vitro* for 1 h with 10 μM R-ketorolac, S-ketorolac or CID2950007– a Cdc42 selective inhibitor (104, 139, 180). Tumor cells incubated with 0.1% DMSO served as a negative control. (B) Results of administration of racemic ketorolac to ovarian cancer patients post-surgery. Cells isolated from patient ascites samples post-surgery were assayed as in (A). Patient diagnoses were stage II-III, high grade ovarian serous or papillary serous carcinoma, with one suspected primary peritoneal carcinoma (Pt 20, 21, 43). Fluorescence readings were normalized to 0.1% DMSO control or the 0 h time point drawn immediately prior to ketorolac administration. One way non-parametric ANOVA and Bonferroni multiple comparison test showed no statistically significant differences between either the *ex vivo* or the *in vivo* samples.

Retrospective Patient Outcomes Review

Peri-operative ketorolac was used in 14% of the 123 women in the study. Younger women (<50 years) were more likely than older women to receive peri-operative ketorolac ($p < 0.05$); all other clinical and treatment characteristics were similar between the two groups. At 60 months of follow-up, 3 of 17 ketorolac-treated patients (18%) and 40 of 92 nontreated patients (43%) had died of ovarian cancer. Stratified log-rank tests for categorical factors such as age group, AJCC stage, completion of chemotherapy as planned, and receipt of neoadjuvant chemotherapy as coded in Table 6, showed a consistent ketorolac survival benefit in each strata (Appendix C-F). The better survival in women treated with ketorolac consistently found in the stratified analysis was also evident in the proportional hazards analysis when we adjusted for age at diagnosis, AJCC stage, completion of chemotherapy as planned, and receipt of neoadjuvant chemotherapy. The adjusted HR for ovarian cancer-specific mortality associated with perioperative ketorolac (yes vs. no) was 0.30 [95% confidence interval (CI), 0.11-0.88, Table 6]. On the basis of the proportional hazards model, an example survival plot is shown in Figure 36 for women who had AJCC stage III cancer, were 50 to 60 years at diagnosis, did not receive neoadjuvant therapy, and completed post-surgery chemotherapy as planned. Other survival plots are shown in Appendix C-F, and although these plots highlight the results for women who completed their post-surgery chemotherapy as planned, all combinations of women defined by stage of disease, age at diagnosis, neoadjuvant therapy, and post-surgery chemotherapy showed a consistently better survival with ketorolac

versus without. These preliminary findings suggest that perioperative ketorolac reduces ovarian cancer-specific mortality.

Table 6. Hazard ratios for ovarian cancer specific mortality for each characteristic adjusted for the other characteristics in the table.

Characteristic	Number	Hazard Ratio (95% Confidence Interval)	p-value**
Peri-operative ketorolac			.011
No	106	1.00 (reference)	
Yes	17	0.30 (0.11 – 0.88)	
AJCC* stage			.050
I	26	1.00 (reference)	
II	11	0.52 (0.11 – 2.47)	
III	57	2.17 (0.97 – 4.86)	
IV	29	1.56 (0.65 – 3.74)	
Age (years)			.045
< 50	36	1.00 (reference)	
50 – 60	55	2.50 (1.17 – 5.35)	
60 +	32	1.85 (0.80 – 4.29)	
Completion of post-surgery chemotherapy as planned			.557
No	78	1.00 (reference)	
Yes	45	1.19 (0.67 – 2.14)	
Neoadjuvant chemotherapy			.050
No	101	1.00 (reference)	
Yes	22	1.94 (1.03 – 3.66)	
*: AJCC = American Joint Committee on Cancer			
**: Likelihood Ratio Test p-value			

Data provided courtesy by Dr. L. Cook (Division of Epidemiology, Biostatistics and Preventive Medicine, Department of Internal Medicine, University of New Mexico School of Medicine).

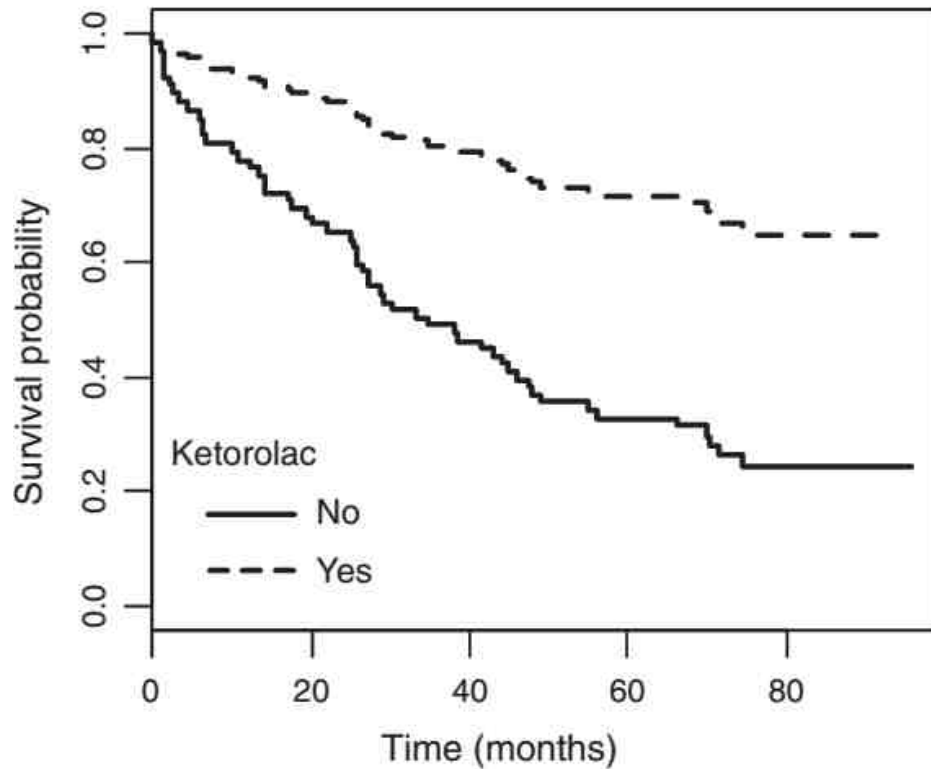


Figure 36. Retrospective survival analyses among ovarian cancer patients with and without peri-operative ketorolac. Cox proportional hazards regression was used to estimate ovarian cancer specific survival probabilities for women who did (dashed line, 17 women) and did not (solid line, 92 women) receive ketorolac among ovarian cancer cases with AJCC Stage III cancer, 50-60 years of age at diagnosis, no neo-adjuvant chemotherapy and completed chemotherapy as planned (overall adjusted Hazard Ratio = 0.30, 95%CI = 0.11 – 0.88, likelihood ratio test p-value = 0.013). Data provided courtesy by Dr. L. Cook (Division of Epidemiology, Biostatistics and Preventive Medicine, Department of Internal Medicine, University of New Mexico School of Medicine).

Conclusion and Discussion

In many human cancers, aberrant Rho-family GTPase activity or downstream signaling pathways are associated with increased aggressiveness and poor patient prognosis (54, 153, 173, 175, 176, 178). The specific mechanisms by which Rho-family GTPases modulate tumor development and progression remain under investigation (54, 68, 107, 153, 175, 176); however, experimental evidence places Rac1 and Cdc42 within the metastatic cascade. Little is known regarding Rac1 and Cdc42 expression in ovarian cancer. We demonstrated elevated expression of Rac1 and Cdc42 in human ovarian cancer specimens and high activity of these GTPases in freshly isolated tumor cells from ascites obtained at surgery (Figure 30 and 34). In a recent study, high Rac1 protein expression in ovarian cancer was associated with early recurrence and poor prognosis (77). Furthermore, partial silencing of Rac1 by shRNA decreased tumor cell proliferation, migration and invasion in culture, and decreased growth of subcutaneous ovarian cancer xenografts *in vivo* (77). We find that R-ketorolac inhibits adhesion and invasion of primary human ovarian tumor cells from patient ascites (183) thereby indicating that pharmacologic inhibition of Rac1 and Cdc42 also blocks these tumor-relevant functions. These observations in conjunction with inhibition of ovarian tumor cell migration by a Cdc42-specific inhibitor (180) indicate the potential value of targeting Rac1 and Cdc42 in ovarian cancer.

The present chapter presents evidence that Rac1 and Cdc42 inhibition can be achieved in ovarian cancer patients following administration of racemic

ketorolac (Toradol®). Ketorolac is a 1:1 racemic mix of the R- and S-enantiomers. The S-form inhibits COX enzymes which confers the drug's anti-inflammatory activities. The COX inhibitory action of S-ketorolac supports its indication for postoperative pain management, but also limits its long term use due to COX-related toxicity (122, 167, 185). R-ketorolac has little activity against COX (122, 167, 185) and therefore is not functional as an NSAID, but is bioactive and inhibits Rac1 and Cdc42 (183). Importantly, the levels of R-ketorolac within the peritoneal fluids were sufficient to inhibit Rac1 and Cdc42 activity in cells obtained from the peritoneal cavity following ketorolac administration. The innovative Phase 0 clinical trial design enabled real-time sampling of fluids and cells from the peritoneal cavity. Direct demonstration of the difference in racemic distribution of ketorolac enantiomers illustrates the value of a study design that allows direct testing of drug and cell activities within peritoneal fluids rather than extrapolation from serum drug levels.

Furthermore, the peritoneal bioactivity of ketorolac is shown to have benefit for ovarian cancer patient outcomes. Perioperative use of ketorolac was found to reduce ovarian cancer specific mortality (Figure 36). There is precedence in the literature that ketorolac usage in the perioperative period is associated with improved cancer outcomes. The first observation was made for breast cancer patients in 2010 (169). In this study, ketorolac use was associated with a decreased risk of breast cancer relapse (HR=0.37, 95%CI=0.0-0.79). Follow-up papers noted that this relapse reduction was most pronounced in the first 24 months post-surgery (53, 184). No change in breast cancer recurrence

was noted in patients who received sufentanil, clonidine, ketamine, or other intraoperative analgesics. Lung cancer patients receiving ketorolac displayed improved overall survival as well (190). The authors hypothesize that the benefit is due to the anti-inflammatory actions of ketorolac, particularly on the extravasation of circulating tumor cells in the transient inflammatory environment stimulated by surgery (172). Ketorolac appears to have more pronounced positive outcomes than other NSAIDs (172), and this may be based on the combined impact of anti-inflammatory activity by the S-enantiomer and R-enantiomer effects on Rac1 and Cdc42 leading to decreased adhesion and implantation of circulating or residual tumor cells. Ketorolac is not cytotoxic to ovarian tumor cells (183), but predicted decreases in establishment or further development of micrometastases due to Rac1 and Cdc42 inhibition would be expected to improve response to subsequent chemotherapy, which cannot be initiated until patients have recovered from cytoreductive surgery. Therefore, administration of ketorolac during a key therapeutic window may offer a particularly efficacious benefit against later relapse.

Collectively, the findings support the potential repositioning of ketorolac as an addition to current ovarian cancer therapy. The work demonstrates that the R-enantiomer of ketorolac acts as a first-in-class drug for inhibition of the cancer-relevant targets Rac1 and Cdc42 (182, 183) and provides the first evidence that these therapeutic targets can be inhibited in humans using an approved drug. There is precedence for pharmacologic activities dictated by R-enantiomers of specific NSAIDs against novel (non-COX) targets (191-193). For example, R-

etodolac and its analogs SDX-301 and SDX-308 display antitumor activity in chronic lymphocytic leukemia and activity against multiple myeloma in cell and animal models (192, 194-197). R-etodolac also significantly suppressed tumors in a colitis-related mouse model colon cancer (191) and retarded tumor development and metastasis in a transgenic mouse model of prostate cancer (193). These examples and others demonstrate that R-enantiomers of NSAIDs can possess unanticipated anticancer activities based on interactions with non-COX targets. Further evidence that targeting Rac1 may provide therapeutic benefit in ovarian cancer was recently reported (198). Zoledronic acid is a nitrogen containing bisphosphonate that inhibits prenylation of small GTPases. Administration of this drug decreased growth of ovarian cancer peritoneal xenografts through inhibition of angiogenesis driven by a Rac1-mediated pathway (198). Collectively, the results suggest that racemic ketorolac may provide a survival benefit to ovarian cancer patients through inhibition of COX enzymes by the S-enantiomer and inhibition of the small GTPases Rac1 and Cdc42 by the R-enantiomer. Additional studies to determine whether clinical benefit can be observed in ovarian cancer patients through perioperative administration of ketorolac in a placebo-controlled clinical trial are in process.

CHAPTER 5

FUTURE PERSPECTIVES

In this thesis work, R-ketorolac is established as a potential anti-tumor drug with previously unrecognized pharmacological property. R-ketorolac is identified as an allosteric inhibitor of Cdc42 and Rac1 using an in vitro nucleotide binding assay. To validate the anti-tumor impact of R-ketorolac, a human patient immortalized ovarian cancer cell line (SKOV3ip) and primary ascites-derived ovarian cancer cells were used to demonstrate that R-ketorolac inhibits the activation of Cdc42 and Rac1 and their downstream PAK signaling axis. As a consequence of the inhibition there is a reduction in ovarian cancer cell adhesion, migration and invasion. In a phase 0 clinical trial, R-ketorolac is found to achieve an effective concentration and persistence in peritoneal fluids for 24 hours. Rac1 and Cdc42 activities in cells retrieved from the peritoneal compartment of post-surgical ovarian cancer patients were substantially reduced in a time-dependent manner following a single IV ketorolac dose for post-operative pain management. A medical record review to compare the ovarian cancer-specific survival of ovarian cancer patients who did or did not receive ketorolac revealed an improved survival with perioperative use of ketorolac. We speculate that ketorolac benefits ovarian cancer patient outcomes through targeted inhibition of Cdc42 and Rac1 GTPases, which in turn decreases adhesion and implantation of circulating or residual tumor cells and/or tumor stem cells.

Docking studies predict R-ketorolac inhibits Cdc42 and Rac1 GTPase activity by excluding magnesium, which is induced by the carboxyl moiety at the chiral center. Follow-on SAR studies support the docking in that trifluoromethyl and 2-thiophene alter ketorolac activity possibly through impact on the carboxyl group at the chiral center. Derivatives modified by trifluoromethyl on the phenyl ring or substitution of the phenyl ring with the heterocyclic, aromatic 3-thiophene selectively switched the activity of ketorolac from inhibition to activation on GTPase activity with increased potencies, indicating that an aromatic ring may increase lipophilic binding to the GTPases, while still accommodating bound nucleotide. To further elucidate the mechanism, SAR analysis will need to be extended by making additional variants of these promising parent compounds. The 3-thiophene is of particular interest because of a potential for increased Rac1 selectivity. The modified analogs with enhanced activity would provide guidance to develop more effective inhibitors. On the other hand, to further verify the magnesium exclusion mechanism of R-ketorolac inhibition against Cdc42 and Rac1, nucleotide binding assays should be performed on GTPase mutants targeting putative amino acid contact points with the docked compound. For example, the methyl group of alanine 59 within Cdc42 or equivalent in Rac1 has been shown to impinge upon magnesium binding within the GEF-GTPase complexes. Introduction of A59G point mutant, which significantly cripples GEF binding and exchange, should be constructed as one way to validate if magnesium exclusion is essential for R-ketorolac activity (199, 200).

Malignant ascites is the accumulation of peritoneal fluid, and is frequently found in high-grade ovarian cancer patients. Ascites is composed of soluble factors such as growth factors, cytokines, and cellular components such as tumor cells, associated stromal cells (mesothelial and fibroblast cells) and inflammatory cells, which provide a pro-inflammatory and tumor-promoting microenvironment (21, 23, 201). Tumor cells in ovarian cancer ascites trigger disease recurrence (202). In the current study, ascites-derived tumor cells are used for the cell-based studies. Compared to immortalized tumor cells, the use of ascites-derived tumor cells represents a more experimentally accurate model to evaluate the impact of ketorolac on ovarian tumor growth and metastasis (18, 21, 23, 201-204). For the initial analyses, the cell adhesion, migration and invasion assays were performed in a 2-D environment, which lack the architectural and cellular complexity of tumors *in vivo*. To mimic the *in vivo* human microenvironment, further study will require testing the impact of ketorolac on ovarian tumor adhesion and invasion in a three-dimensional (3-D) organotypic system or using omental explants (205); the omentum is a preferred seeding site for ovarian tumor metastases *in vivo* (206). In the 3-D organotypic model, primary human ovarian tumor cells or immortalized tumor cell lines are cultured with primary human mesothelial cells isolated from patient omentum, primary human fibroblast and patient-derived ECM which mimic the superficial layer of the peritoneum (204, 207). This *ex vivo* model or omental explants could help establish structural and functional environment of the ovarian tumor tissue for tumor metastasis including adhesion,

migration and invasion, which will provide a more accurate system for drug screening (204, 208).

The retrospective study shows racemic ketorolac has pronounced benefits on patient survival outcomes. The findings that R-ketorolac targets Rac1 and Cdc42, but not RhoA and reduces cell adhesion, migration and invasion of tumor cells suggests that the drug may reduce relapse by making the remaining tumor cells more vulnerable to chemotherapy post-debulking surgery. Accumulating evidence show that cancer stem cells are enriched after first-line chemotherapy for advanced stage ovarian cancer patients, leading to tumor relapse with chemoresistance. The cancer stem cell model could also explain the heterogeneity of phenotypic and functional features in epithelial ovarian cancer, contributing to the poor diagnosis and prognosis (209, 210). Rac1 overexpression is also implicated in quiescence, stemness and cancer cell adhesion to the bone marrow niche (211-213). Therefore, it is also conceivable that through an impact on cancer stem cell Rac1 activity R-ketorolac could increase cell cycling and reduce sequestration of tumor cells or cancer stem cells in a protected niche. Both mechanisms would increase chemotherapy sensitivity and account for the observed improved survival. Thus, targeting of cancer stem cells by ketorolac to suppress proliferation and metastasis would be another explanation for the observed benefits. Further studies of niche adhesion and quiescence in preclinical animal models are needed to evaluate ovarian tumor cell homing to the bone marrow or peritoneal niches. Immortalized ovarian cell lines have been reported to be heterogeneous with highest fractions of stem-like

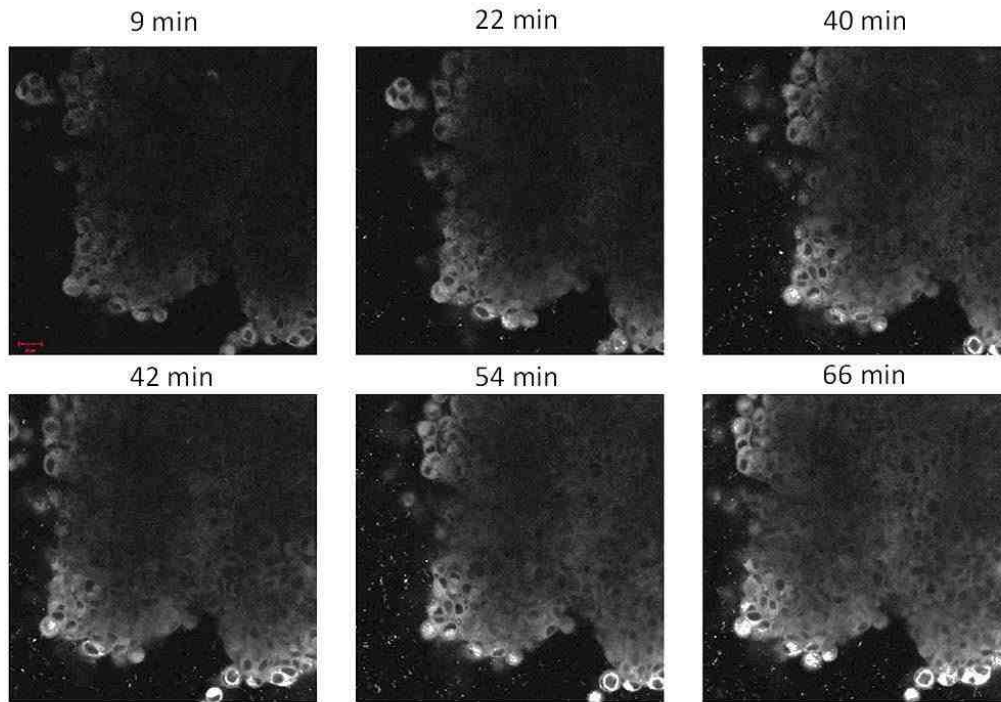
cells detected in the most aggressive lines (214). NSAIDs have been reported to suppress stem cells proliferation, metastasis and differentiation through a COX-dependent (e.g. PGE₂ – NF - κB) or a COX - independent manner (e.g. cell cycle regulators) (215-217). Future work will require investigation of the impact of ketorolac on the proliferation, differentiation and metastasis of ovarian cancer stem cells by using patient-derived ovarian tumor stem cells (e.g. CD133 positive selection) (218, 219). Identifying molecular targets of ketorolac in cancer stem cells and developing ketorolac as an adjuvant anti-tumor therapy could potentially increase tumor sensitivity to chemotherapy, reduce recurrence, and improve ovarian cancer patient outcomes (209, 210).

There are other possibilities for the reduced mortality observed in retrospective analyses of patients receiving post-operative ketorolac as compared to patients who had surgery only or received opioid pain relievers. For example, surgery induced inflammation is known to increase stimulation and proliferation of residual tumor cells. S-ketorolac present in the racemic clinical drug is a powerful anti-inflammatory and has been suggested to provide benefit in breast cancer patients on account of this anti-inflammatory activity (53, 220). However, a purely anti-inflammatory role mediated by COX inhibition by S-ketorolac has been challenged (221). It is also inconsistent with the specificity of ketorolac in reducing tumor relapse in ovarian cancer as demonstrated here, and also reported while the studies were in progress in breast, kidney and other cancers (190, 220). Addressing this question will require further testing in preclinical animal models, e.g. surgery +/- drug administration +/- tumor cells.

To more directly compare if the inhibition of GTPase activity is purely drug-mediated or due to other changes in the post-operative peritoneal cavity, a prospective clinical trial is needed in which patients will be given placebo after surgery and their primary tumor cells will be processed for GTPase activity assays and related measures of GTPase activation. A small placebo trial will further confirm that the observed inhibition of GTPase activity is dependent on ketorolac administration. Through longer term tracking of patients in the trial, GTPase inhibition can be evaluated as a surrogate for time to relapse, progression free survival, and overall survival. Only through continued systematic study can the therapeutic benefits of patient outcomes be specifically attributed to ketorolac administered during perioperative period.

Overall, future studies will focus on 1) identifying critical determinants for Rho GTPase inhibition and developing more effective and selective Cdc42/Rac1 inhibitors; 2) establishing 3-D organotypic models for testing GTPase inhibitors alone or in combination; 3) investigating the impact of ketorolac on stem cells in ovarian cancer and other epithelial cancers; 4) conducting a placebo-controlled clinical trial to confirm the clinical benefit of ketorolac. These studies will offer a rapid translational and clinical study to repurpose FDA-approved drug-ketorolac as an anti-tumor drug for ovarian cancer therapy.

APPENDICES



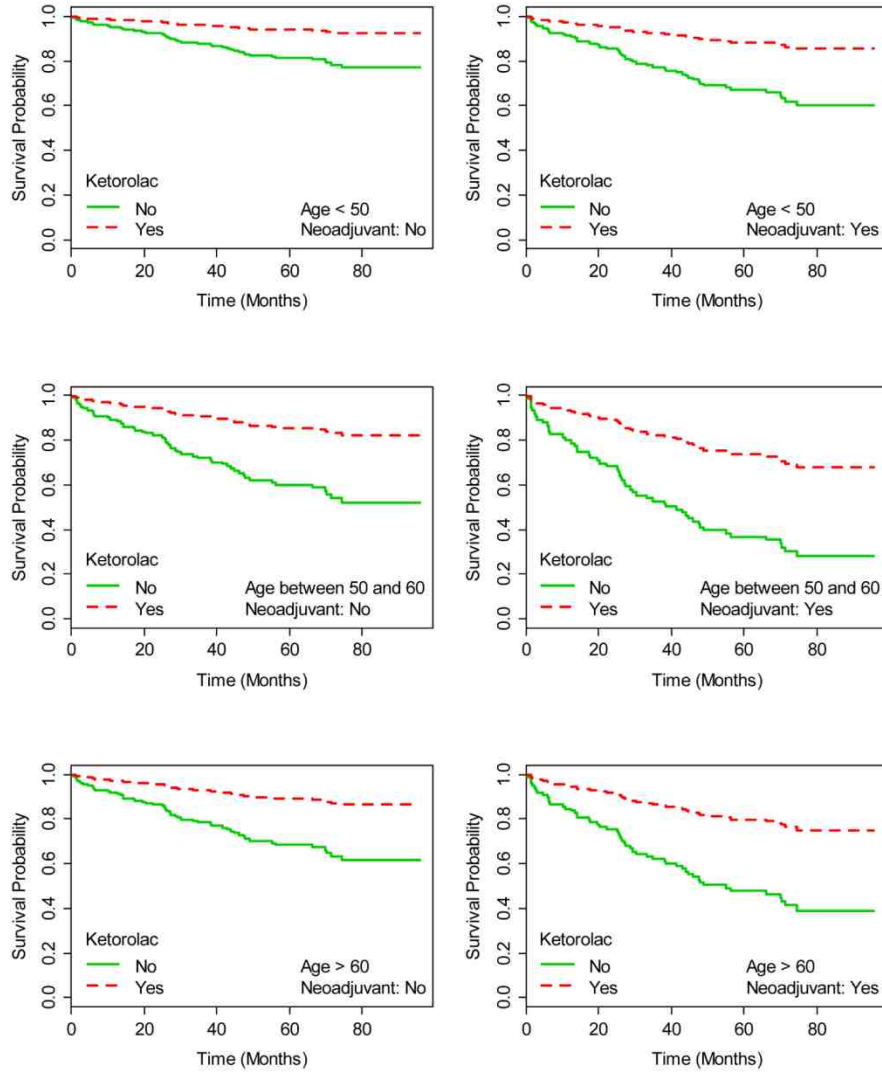
Appendix A. Time lapse imaging of HPY (490) labeled fluorescent compound RS-II-79 penetration into MCA. In the experiment, 2000 multicellular aggregates (SKOV3ip cells) were incubated with 10 μ M RS-II-79. The images were captured at 9, 22, 40, 42, 54 and 66 min by Zeiss Axiovert 200 M inverted confocal microscope. Images provided courtesy of Dr. M. Steinkamp (Department of Pathology, University of New Mexico).

Appendix B. Patient Characteristics for IHC Microarrays OV1005 and OV8010

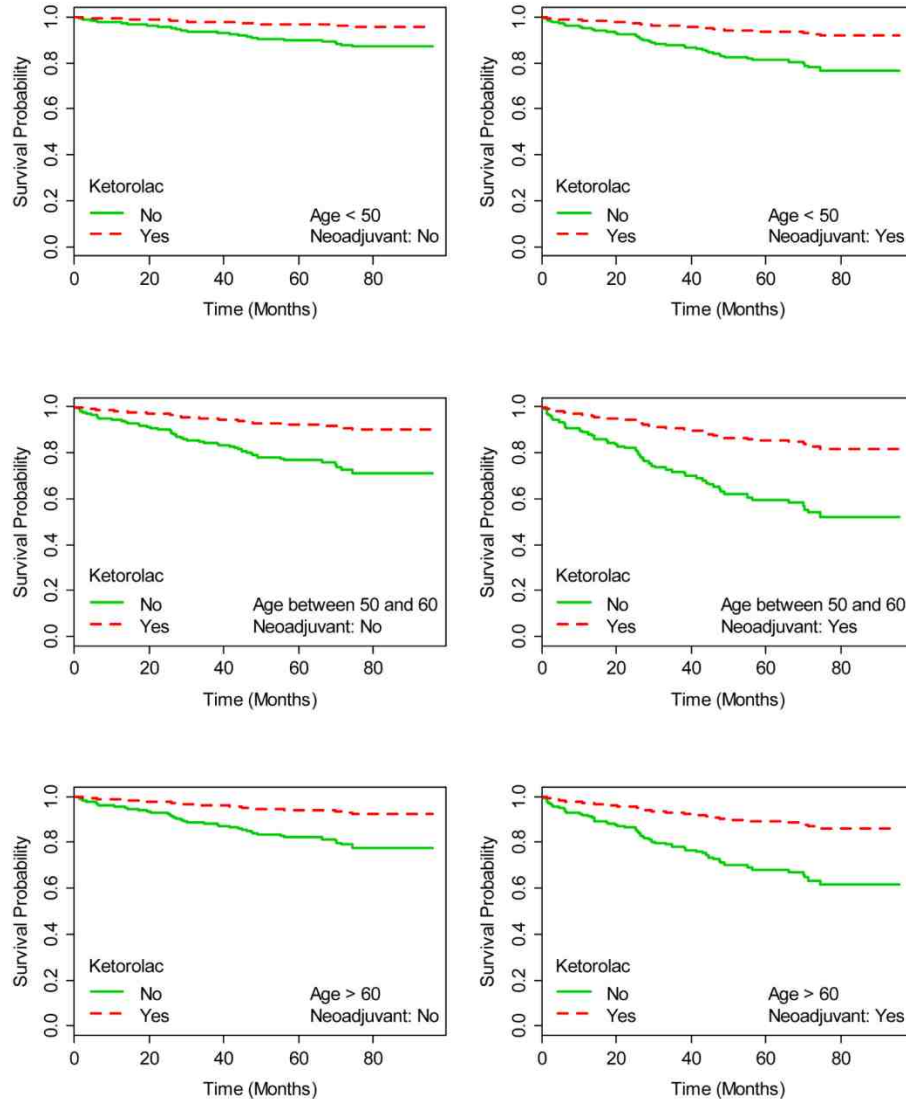
Age [#]	46.6 +/- 13.7 (std. dev)	
Stage I [#]		12
	A	5
	B	5
	C	4
Stage II [#]		21
	A	13
	B	6
	C	3
Stage III [#]		1
	C	31
Stage IV [#]		11
Stage undetermined [#]		51
Normal stroma		20
Benign/borderline		25
Grade - Low* (1 [#])		13
Grade - Intermediate* (1-2, 2 [#])		7
Grade - High* (2, 2-3, 3 [#])		98
<p>*Diagnoses by board certified pathologist with gynecologic pathology specialization were as follows: Clear cell carcinoma (4); endometrioid carcinoma (13); endometrioid neoplasm (5); mucinous carcinoma (4); mucinous neoplasm (9); mucinous cystadenoma (5); normal stroma only-no epithelia (20); papillary serous carcinoma (78); serous neoplasm (5); serous cystadenoma (4); undifferentiated carcinoma (16). There was 77% agreement with [#]BioMax specification sheet, differences were confined to ID of rarer subtypes (endometrioid, clear cell, mucinous, transitional and serous). Samples included in analysis: 163 of 180 total (9% were excluded due to poor staining at edge of slide or no neoplasm in the section).</p>		

Appendix C. Patient Characteristics for cDNA Microarray

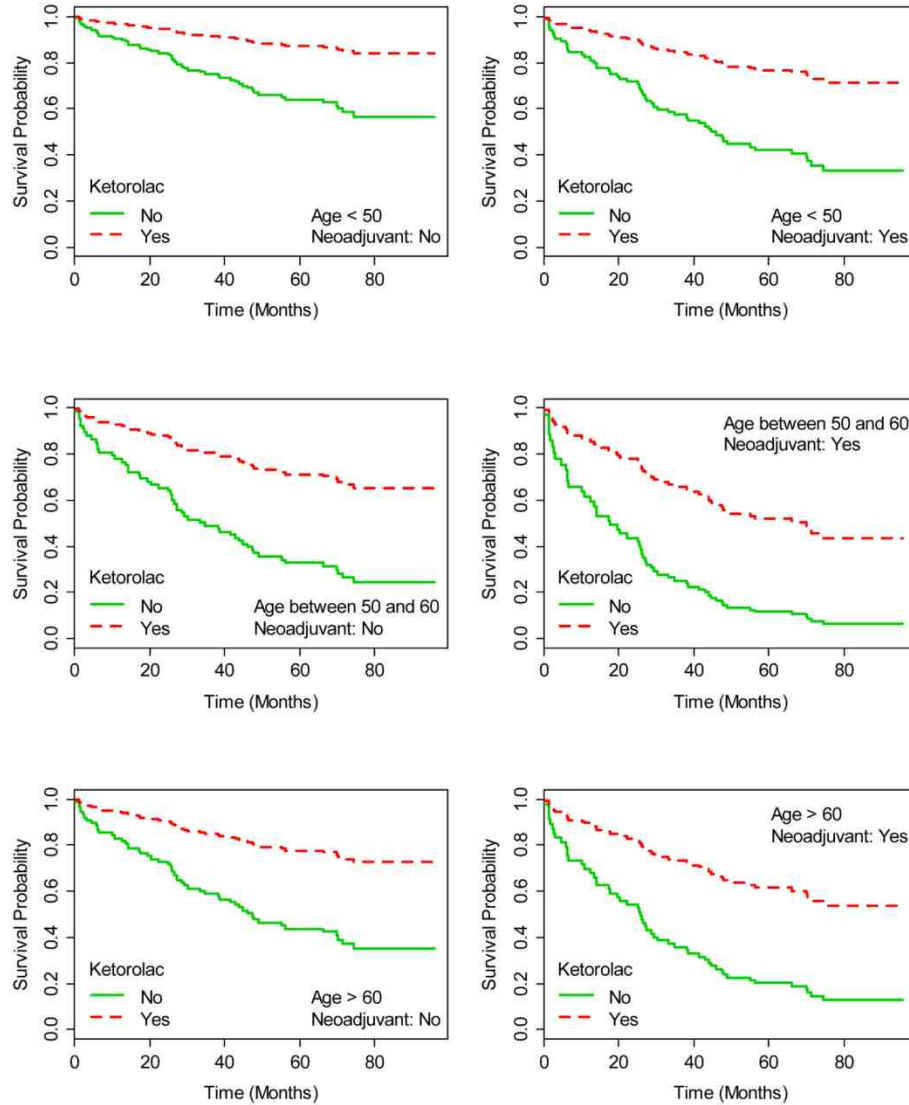
Age	57.26 +/- 14.85 (st. dev)	
Stage I	A	20
	B	8
	C	10
Stage II	A	4
	B	9
	C	4
Stage III	A	15
	B	17
	C	26
Stage IV	A	10
Grade Not Reported		10
Grade I		9
Grade II		32
Grade III		60
Grade IV		9
<p>Diagnoses were as follows: Carcinoma of Ovary (2); Carcinoma of ovary, endometrioid (6); Carcinoma of ovary, papillary serous (8); Carcinoma of ovary, clear cell (1); Adenocarcinoma of ovary, endometrioid (23); Adenocarcinoma of ovary, papillary serous (32); Adenocarcinoma of ovary, serous (28); Adenocarcinoma of ovary, metastatic (2); Adenocarcinoma of ovary, mucinous (4); Adenocarcinoma of ovary, clear cell (5); Tumor of ovary, borderline (2); Tumor of ovary, papillary serous, borderline (2); Tumor of ovary, serous, borderline (5)</p> <p>These microarray plates consisted of 19 normal, 9 Grade I, 32 Grade II, 60 Grade III, 9 Grade IV, and 10 grade not reported patients. Patients with grade not reported were not included in grade analysis.</p>		



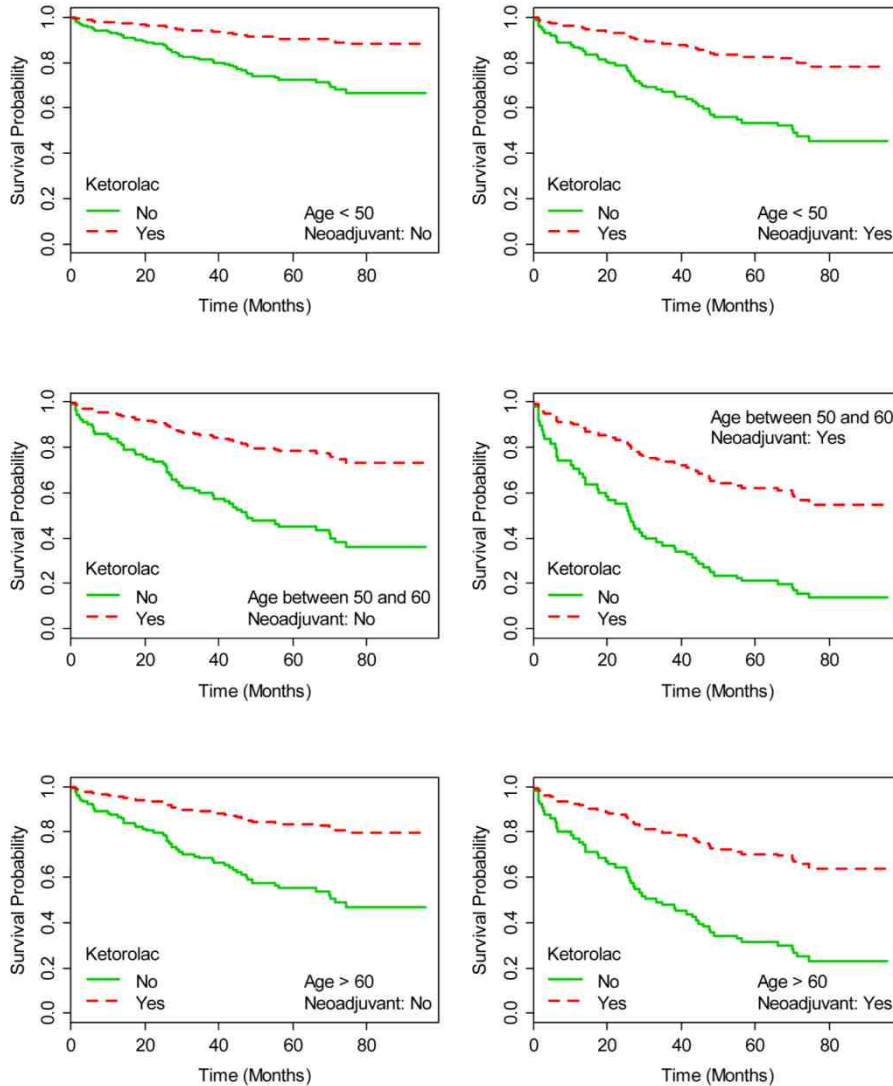
Appendix D. Survival estimates based on Cox-regression for Stage I (AJCC) with completion of chemotherapy. Cox proportional hazards regression was used to estimate ovarian cancer specific survival probabilities for women who did (dashed line) and did not (solid line) receive ketorolac among ovarian cancer cases with AJCC Stage I cancer, sorted by age group and +/- neoadjuvant chemotherapy. Data provided courtesy of Dr. L. Cook (Division of Epidemiology, Biostatistics and Preventive Medicine, Department of Internal Medicine, University of New Mexico School of Medicine).



Appendix E. Survival estimates based on Cox-regression for Stage II (AJCC) with completion of chemotherapy. Cox proportional hazards regression was used to estimate ovarian cancer specific survival probabilities for women who did (dashed line) and did not (solid line) receive ketorolac among ovarian cancer cases with AJCC Stage II cancer, sorted by age group and +/- neoadjuvant chemotherapy. Data provided courtesy of Dr. L. Cook (Division of Epidemiology, Biostatistics and Preventive Medicine, Department of Internal Medicine, University of New Mexico School of Medicine).



Appendix F. Survival estimates based on Cox-regression for Stage III (AJCC) with completion of chemotherapy. Cox proportional hazards regression was used to estimate ovarian cancer specific survival probabilities for women who did (dashed line) and did not (solid line) receive ketorolac among ovarian cancer cases with AJCC Stage III cancer, sorted by age group and +/- neoadjuvant chemotherapy. Data provided courtesy of Dr. L. Cook (Division of Epidemiology, Biostatistics and Preventive Medicine, Department of Internal Medicine, University of New Mexico School of Medicine).



Appendix G. Survival estimates based on Cox-regression for Stage IV (AJCC) with completion of chemotherapy. Cox proportional hazards regression was used to estimate ovarian cancer specific survival probabilities for women who did (dashed line) and did not (solid line) receive ketorolac among ovarian cancer cases with AJCC Stage IV cancer, sorted by age group and +/- neoadjuvant chemotherapy. Data provided courtesy of Dr. L. Cook (Division of Epidemiology, Biostatistics and Preventive Medicine, Department of Internal Medicine, University of New Mexico School of Medicine).

REFERENCES

1. Howlader N NA, Krapcho M, Garshell J, Miller D, Altekruse SF, Kosary CL, Yu M, Ruhl J, Tatalovich Z, Mariotto A, Lewis DR, Chen HS, Feuer EJ, Chronin KA (eds). SEER Cancer Statistics Review, 1975-2011, National Cancer Institute <http://seer.cancer.gov/csr/1975-2011/Dec>. 2014.
2. Soslow RA. Histologic subtypes of ovarian carcinoma: an overview. *International journal of gynecological pathology : official journal of the International Society of Gynecological Pathologists*. 2008 Apr;27(2):161-74. PubMed PMID: 18317227.
3. Bell DA. Origins and molecular pathology of ovarian cancer. *Modern pathology : an official journal of the United States and Canadian Academy of Pathology, Inc*. 2005 Feb;18 Suppl 2:S19-32. PubMed PMID: 15761464.
4. Erickson BK, Conner MG, Landen CN, Jr. The role of the fallopian tube in the origin of ovarian cancer. *American journal of obstetrics and gynecology*. 2013 Nov;209(5):409-14. PubMed PMID: 23583217. Pubmed Central PMCID: 3937451.
5. Dietl J. Revisiting the pathogenesis of ovarian cancer: the central role of the fallopian tube. *Archives of gynecology and obstetrics*. 2014 Feb;289(2):241-6. PubMed PMID: 24100801.
6. Vaughan S, Coward JI, Bast RC, Jr., Berchuck A, Berek JS, Brenton JD, Coukos G, Crum CC, Drapkin R, Etemadmoghadam D, Friedlander M, Gabra H, Kaye SB, Lord CJ, Lengyel E, Levine DA, McNeish IA, Menon U, Mills GB, Nephew KP, Oza AM, Sood AK, Stronach EA, Walczak H, Bowtell DD, Balkwill FR. Rethinking ovarian cancer: recommendations for improving outcomes. *Nature reviews Cancer*. 2011 Oct;11(10):719-25. PubMed PMID: 21941283. Pubmed Central PMCID: 3380637.
7. Nezhat FR, Apostol R, Nezhat C, Pejovic T. New insights in the pathophysiology of ovarian cancer and implications for screening and prevention. *American journal of obstetrics and gynecology*. 2015 Mar 25. PubMed PMID: 25818671.
8. Berns EM, Bowtell DD. The changing view of high-grade serous ovarian cancer. *Cancer research*. 2012 Jun 1;72(11):2701-4. PubMed PMID: 22593197.
9. Zhang Y, Guo B, Bi R. Ovarian cancer: biomarker proteomic diagnosis in progress. *Applied biochemistry and biotechnology*. 2012 Oct;168(4):910-6. PubMed PMID: 22945560.
10. Davidson B, Trope CG. Ovarian cancer: diagnostic, biological and prognostic aspects. *Women's health*. 2014 Sep;10(5):519-33. PubMed PMID: 25335543.

11. Blagden SP. Harnessing Pandemonium: The Clinical Implications of Tumor Heterogeneity in Ovarian Cancer. *Frontiers in oncology*. 2015;5:149. PubMed PMID: 26175968. Pubmed Central PMCID: 4485078.
12. Luvero D, Milani A, Ledermann JA. Treatment options in recurrent ovarian cancer: latest evidence and clinical potential. *Therapeutic advances in medical oncology*. 2014 Sep;6(5):229-39. PubMed PMID: 25342990. Pubmed Central PMCID: 4206613.
13. Hall M, Rustin G. Recurrent ovarian cancer: when and how to treat. *Current oncology reports*. 2011 Dec;13(6):459-71. PubMed PMID: 22045509.
14. McGuire WP. Maintenance therapy for ovarian cancer: of Helsinki and Hippocrates. *Journal of clinical oncology : official journal of the American Society of Clinical Oncology*. 2009 Oct 1;27(28):4633-4. PubMed PMID: 19704055.
15. Coleman MP, Forman D, Bryant H, Butler J, Rachet B, Maringe C, Nur U, Tracey E, Coory M, Hatcher J, McGahan CE, Turner D, Marrett L, Gjerstorff ML, Johannesen TB, Adolfsson J, Lambe M, Lawrence G, Meechan D, Morris EJ, Middleton R, Steward J, Richards MA, Group IMW. Cancer survival in Australia, Canada, Denmark, Norway, Sweden, and the UK, 1995-2007 (the International Cancer Benchmarking Partnership): an analysis of population-based cancer registry data. *Lancet*. 2011 Jan 8;377(9760):127-38. PubMed PMID: 21183212. Pubmed Central PMCID: 3018568.
16. Jayson GC, Kohn EC, Kitchener HC, Ledermann JA. Ovarian cancer. *Lancet*. 2014 Apr 17. PubMed PMID: 24767708.
17. Coleman RL, Monk BJ, Sood AK, Herzog TJ. Latest research and treatment of advanced-stage epithelial ovarian cancer. *Nature reviews Clinical oncology*. 2013 Apr;10(4):211-24. PubMed PMID: 23381004. Pubmed Central PMCID: 3786558.
18. Ahmed N, Stenvers KL. Getting to Know Ovarian Cancer Ascites: Opportunities for Targeted Therapy-Based Translational Research. *Frontiers in oncology*. 2013;3:256. PubMed PMID: 24093089. Pubmed Central PMCID: 3782691.
19. Hudson LG, Zeineldin R, Stack MS. Phenotypic plasticity of neoplastic ovarian epithelium: unique cadherin profiles in tumor progression. *Clinical & experimental metastasis*. 2008;25(6):643-55. PubMed PMID: 18398687. Pubmed Central PMCID: 2836537.
20. Shield K, Ackland ML, Ahmed N, Rice GE. Multicellular spheroids in ovarian cancer metastases: Biology and pathology. *Gynecologic oncology*. 2009 Apr;113(1):143-8. PubMed PMID: 19135710.

21. Thibault B, Castells M, Delord JP, Couderc B. Ovarian cancer microenvironment: implications for cancer dissemination and chemoresistance acquisition. *Cancer metastasis reviews*. 2014 Mar;33(1):17-39. PubMed PMID: 24357056.
22. Naora H. Heterotypic cellular interactions in the ovarian tumor microenvironment: biological significance and therapeutic implications. *Frontiers in oncology*. 2014;4:18. PubMed PMID: 24567915. Pubmed Central PMCID: 3915179.
23. Davidson B, Trope CG, Reich R. The role of the tumor stroma in ovarian cancer. *Frontiers in oncology*. 2014;4:104. PubMed PMID: 24860785. Pubmed Central PMCID: 4026708.
24. Mutsaers SE. The mesothelial cell. *The international journal of biochemistry & cell biology*. 2004 Jan;36(1):9-16. PubMed PMID: 14592528.
25. Mutsaers SE, Wilkosz S. Structure and function of mesothelial cells. *Cancer treatment and research*. 2007;134:1-19. PubMed PMID: 17633044.
26. Zeillemaker AM, Verbrugh HA, Hoyneck van Papendrecht AA, Leguit P. CA 125 secretion by peritoneal mesothelial cells. *Journal of clinical pathology*. 1994 Mar;47(3):263-5. PubMed PMID: 8163699. Pubmed Central PMCID: 501908.
27. Ween MP, Oehler MK, Ricciardelli C. Role of versican, hyaluronan and CD44 in ovarian cancer metastasis. *International journal of molecular sciences*. 2011;12(2):1009-29. PubMed PMID: 21541039. Pubmed Central PMCID: 3083686.
28. Moreno-Bueno G, Peinado H, Molina P, Olmeda D, Cubillo E, Santos V, Palacios J, Portillo F, Cano A. The morphological and molecular features of the epithelial-to-mesenchymal transition. *Nature protocols*. 2009;4(11):1591-613. PubMed PMID: 19834475.
29. Carduner L, Leroy-Dudal J, Picot CR, Gallet O, Carreiras F, Kellouche S. Ascites-induced shift along epithelial-mesenchymal spectrum in ovarian cancer cells: enhancement of their invasive behavior partly dependant on alpha v integrins. *Clinical & experimental metastasis*. 2014 Aug;31(6):675-88. PubMed PMID: 24946950.
30. Shaw D, Clamp A, Jayson GC. Angiogenesis as a target for the treatment of ovarian cancer. *Current opinion in oncology*. 2013 Sep;25(5):558-65. PubMed PMID: 23942301.
31. Nieman KM, Kenny HA, Penicka CV, Ladanyi A, Buell-Gutbrod R, Zillhardt MR, Romero IL, Carey MS, Mills GB, Hotamisligil GS, Yamada SD, Peter ME, Gwin K, Lengyel E. Adipocytes promote ovarian cancer metastasis and provide

energy for rapid tumor growth. *Nature medicine*. 2011;17(11):1498-503. PubMed PMID: 22037646. Pubmed Central PMCID: 4157349.

32. Chen C, Chang YC, Lan MS, Breslin M. Leptin stimulates ovarian cancer cell growth and inhibits apoptosis by increasing cyclin D1 and Mcl-1 expression via the activation of the MEK/ERK1/2 and PI3K/Akt signaling pathways. *International journal of oncology*. 2013 Mar;42(3):1113-9. PubMed PMID: 23354006.

33. Yigit R, Massuger LF, Figdor CG, Torensma R. Ovarian cancer creates a suppressive microenvironment to escape immune elimination. *Gynecologic oncology*. 2010 May;117(2):366-72. PubMed PMID: 20144842.

34. Preston CC, Goode EL, Hartmann LC, Kalli KR, Knutson KL. Immunity and immune suppression in human ovarian cancer. *Immunotherapy*. 2011 Apr;3(4):539-56. PubMed PMID: 21463194. Pubmed Central PMCID: 3147144.

35. Ko SY, Barengo N, Ladanyi A, Lee JS, Marini F, Lengyel E, Naora H. HOXA9 promotes ovarian cancer growth by stimulating cancer-associated fibroblasts. *The Journal of clinical investigation*. 2012 Oct;122(10):3603-17. PubMed PMID: 22945634. Pubmed Central PMCID: 3461910.

36. Raja FA, Chopra N, Ledermann JA. Optimal first-line treatment in ovarian cancer. *Annals of oncology : official journal of the European Society for Medical Oncology / ESMO*. 2012 Sep;23 Suppl 10:x118-27. PubMed PMID: 22987945.

37. Ramirez I, Chon HS, Apte SM. The role of surgery in the management of epithelial ovarian cancer. *Cancer control : journal of the Moffitt Cancer Center*. 2011 Jan;18(1):22-30. PubMed PMID: 21273977.

38. Wakabayashi MT, Lin PS, Hakim AA. The role of cytoreductive/debulking surgery in ovarian cancer. *Journal of the National Comprehensive Cancer Network : JNCCN*. 2008 Sep;6(8):803-10; quiz 11. PubMed PMID: 18926091.

39. Schwartz PE. Cytoreductive surgery in the management of ovarian cancer. *Oncology*. 2008 Aug;22(9):1025-33; discussion 33-8, 41, 45. PubMed PMID: 18777954.

40. Markman M. Current standards of care for chemotherapy of optimally cytoreduced advanced epithelial ovarian cancer. *Gynecologic oncology*. 2013 Oct;131(1):241-5. PubMed PMID: 23726888.

41. Grosso G, Rossetti D, Coccolini F, Bogani G, Ansaloni L, Frigerio L. Intraperitoneal chemotherapy in advanced epithelial ovarian cancer: a survey. *Archives of gynecology and obstetrics*. 2014 Sep;290(3):425-34. PubMed PMID: 24845970.

42. Dedrick RL, Flessner MF. Pharmacokinetic problems in peritoneal drug administration: tissue penetration and surface exposure. *Journal of the National Cancer Institute*. 1997 Apr 2;89(7):480-7. PubMed PMID: 9086004.
43. Horowitz M, Neeman E, Sharon E, Ben-Eliyahu S. Exploiting the critical perioperative period to improve long-term cancer outcomes. *Nature reviews Clinical oncology*. 2015 Apr;12(4):213-26. PubMed PMID: 25601442.
44. Pradeep S, Kim SW, Wu SY, Nishimura M, Chaluvally-Raghavan P, Miyake T, Pecot CV, Kim SJ, Choi HJ, Bischoff FZ, Mayer JA, Huang L, Nick AM, Hall CS, Rodriguez-Aguayo C, Zand B, Dalton HJ, Arumugam T, Lee HJ, Han HD, Cho MS, Rupaimoole R, Mangala LS, Sehgal V, Oh SC, Liu J, Lee JS, Coleman RL, Ram P, Lopez-Berestein G, Fidler IJ, Sood AK. Hematogenous metastasis of ovarian cancer: rethinking mode of spread. *Cancer cell*. 2014 Jul 14;26(1):77-91. PubMed PMID: 25026212. Pubmed Central PMCID: 4100212.
45. Romero-Laorden N, Olmos D, Fehm T, Garcia-Donas J, Diaz-Padilla I. Circulating and disseminated tumor cells in ovarian cancer: a systematic review. *Gynecologic oncology*. 2014 Jun;133(3):632-9. PubMed PMID: 24657303.
46. Fisher B, Gunduz N, Coyle J, Rudock C, Saffer E. Presence of a growth-stimulating factor in serum following primary tumor removal in mice. *Cancer research*. 1989 Apr 15;49(8):1996-2001. PubMed PMID: 2702641.
47. O'Reilly MS, Boehm T, Shing Y, Fukai N, Vasios G, Lane WS, Flynn E, Birkhead JR, Olsen BR, Folkman J. Endostatin: an endogenous inhibitor of angiogenesis and tumor growth. *Cell*. 1997 Jan 24;88(2):277-85. PubMed PMID: 9008168.
48. Abramovitch R, Marikovsky M, Meir G, Neeman M. Stimulation of tumour growth by wound-derived growth factors. *British journal of cancer*. 1999 Mar;79(9-10):1392-8. PubMed PMID: 10188881. Pubmed Central PMCID: 2362730.
49. Gullino PM. Prostaglandins and gangliosides of tumor microenvironment: their role in angiogenesis. *Acta oncologica*. 1995;34(3):439-41. PubMed PMID: 7540024.
50. Kim R, Emi M, Tanabe K, Arihiro K. Tumor-driven evolution of immunosuppressive networks during malignant progression. *Cancer research*. 2006 Jun 1;66(11):5527-36. PubMed PMID: 16740684.
51. Liu MX, Chan DW, Ngan HY. Mechanisms of chemoresistance in human ovarian cancer at a glance. *Gynecologic oncology*. 2012;2(3):1000e104.
52. Steg AD, Katre AA, Bevis KS, Ziebarth A, Dobbin ZC, Shah MM, Alvarez RD, Landen CN. Smoothened antagonists reverse taxane resistance in ovarian

cancer. *Molecular cancer therapeutics*. 2012 Jul;11(7):1587-97. PubMed PMID: 22553355. Pubmed Central PMCID: 3392529.

53. Retsky M, Rogers R, Demicheli R, Hrushesky WJ, Gukas I, Vaidya JS, Baum M, Forget P, Dekock M, Pachmann K. NSAID analgesic ketorolac used perioperatively may suppress early breast cancer relapse: particular relevance to triple negative subgroup. *Breast cancer research and treatment*. 2012 Jul;134(2):881-8. PubMed PMID: 22622810.

54. Hall A. Rho family GTPases. *Biochemical Society transactions*. 2012 Dec 1;40(6):1378-82. PubMed PMID: 23176484.

55. Madaule P, Axel R. A novel ras-related gene family. *Cell*. 1985 May;41(1):31-40. PubMed PMID: 3888408.

56. Jaffe AB, Hall A. Rho GTPases: biochemistry and biology. *Annual review of cell and developmental biology*. 2005;21:247-69. PubMed PMID: 16212495.

57. Etienne-Manneville S, Hall A. Rho GTPases in cell biology. *Nature*. 2002 Dec 12;420(6916):629-35. PubMed PMID: 12478284.

58. Cherfils J, Zeghouf M. Regulation of small GTPases by GEFs, GAPs, and GDIs. *Physiological reviews*. 2013 Jan;93(1):269-309. PubMed PMID: 23303910.

59. Whitehead IP, Zohn IE, Der CJ. Rho GTPase-dependent transformation by G protein-coupled receptors. *Oncogene*. 2001 Mar 26;20(13):1547-55. PubMed PMID: 11313901.

60. Huvencers S, Danen EH. Adhesion signaling - crosstalk between integrins, Src and Rho. *Journal of cell science*. 2009 Apr 15;122(Pt 8):1059-69. PubMed PMID: 19339545.

61. Buchsbaum RJ. Rho activation at a glance. *Journal of cell science*. 2007 Apr 1;120(Pt 7):1149-52. PubMed PMID: 17376960.

62. Hanna S, El-Sibai M. Signaling networks of Rho GTPases in cell motility. *Cellular signalling*. 2013 Oct;25(10):1955-61. PubMed PMID: 23669310.

63. Eswaran J, Soundararajan M, Knapp S. Targeting group II PAKs in cancer and metastasis. *Cancer metastasis reviews*. 2009 Jun;28(1-2):209-17. PubMed PMID: 19160016.

64. Knaus UG, Bokoch GM. The p21Rac/Cdc42-activated kinases (PAKs). *The international journal of biochemistry & cell biology*. 1998 Aug;30(8):857-62. PubMed PMID: 9744077.

65. Kurisu S, Takenawa T. The WASP and WAVE family proteins. *Genome biology*. 2009;10(6):226. PubMed PMID: 19589182. Pubmed Central PMCID: 2718491.
66. Casteel DE, Turner S, Schwappacher R, Rangaswami H, Su-Yuo J, Zhuang S, Boss GR, Pilz RB. Rho isoform-specific interaction with IQGAP1 promotes breast cancer cell proliferation and migration. *The Journal of biological chemistry*. 2012 Nov 2;287(45):38367-78. PubMed PMID: 22992742. Pubmed Central PMCID: 3488105.
67. Wang XY, Gan MX, Li Y, Zhan WH, Han TY, Han XJ, Cheng JQ, Wang JB. Cdc42 induces EGF receptor protein accumulation and promotes EGF receptor nuclear transport and cellular transformation. *FEBS letters*. 2015 Jan 16;589(2):255-62. PubMed PMID: 25497016.
68. Karlsson R, Pedersen ED, Wang Z, Brakebusch C. Rho GTPase function in tumorigenesis. *Biochimica et biophysica acta*. 2009 Dec;1796(2):91-8. PubMed PMID: 19327386.
69. Arias-Romero LE, Villamar-Cruz O, Huang M, Hoeflich KP, Chernoff J. Pak1 kinase links ErbB2 to beta-catenin in transformation of breast epithelial cells. *Cancer research*. 2013 Jun 15;73(12):3671-82. PubMed PMID: 23576562. Pubmed Central PMCID: 3687032.
70. Gao L, Bai L, Nan Q. Activation of Rho GTPase Cdc42 promotes adhesion and invasion in colorectal cancer cells. *Medical science monitor basic research*. 2013;19:201-7. PubMed PMID: 23884297. Pubmed Central PMCID: 3735386.
71. Wertheimer E, Gutierrez-Uzquiza A, Roseblit C, Lopez-Haber C, Sosa MS, Kazanietz MG. Rac signaling in breast cancer: a tale of GEFs and GAPs. *Cellular signalling*. 2012 Feb;24(2):353-62. PubMed PMID: 21893191. Pubmed Central PMCID: 3312797.
72. Ebi H, Costa C, Faber AC, Nishtala M, Kotani H, Juric D, Della Pelle P, Song Y, Yano S, Mino-Kenudson M, Benes CH, Engelman JA. PI3K regulates MEK/ERK signaling in breast cancer via the Rac-GEF, P-Rex1. *Proceedings of the National Academy of Sciences of the United States of America*. 2013 Dec 24;110(52):21124-9. PubMed PMID: 24327733. Pubmed Central PMCID: 3876254.
73. Ma J, Xue Y, Liu W, Yue C, Bi F, Xu J, Zhang J, Li Y, Zhong C, Chen Y. Role of activated rac1/cdc42 in mediating endothelial cell proliferation and tumor angiogenesis in breast cancer. *PloS one*. 2013;8(6):e66275. PubMed PMID: 23750283. Pubmed Central PMCID: 3672132.
74. Friedland JC, Lakins JN, Kazanietz MG, Chernoff J, Boettiger D, Weaver VM. alpha6beta4 integrin activates Rac-dependent p21-activated kinase 1 to

- drive NF-kappaB-dependent resistance to apoptosis in 3D mammary acini. *Journal of cell science*. 2007 Oct 15;120(Pt 20):3700-12. PubMed PMID: 17911169.
75. Olson MF, Ashworth A, Hall A. An essential role for Rho, Rac, and Cdc42 GTPases in cell cycle progression through G1. *Science*. 1995 Sep 1;269(5228):1270-2. PubMed PMID: 7652575.
76. Yang W, Lv S, Liu X, Liu H, Yang W, Hu F. Up-regulation of Tiam1 and Rac1 correlates with poor prognosis in hepatocellular carcinoma. *Japanese journal of clinical oncology*. 2010 Nov;40(11):1053-9. PubMed PMID: 20522449.
77. Leng R, Liao G, Wang H, Kuang J, Tang L. Rac1 expression in epithelial ovarian cancer: effect on cell EMT and clinical outcome. *Medical oncology*. 2015 Feb;32(2):329. PubMed PMID: 25585684.
78. Singh A, Karnoub AE, Palmby TR, Lengyel E, Sondek J, Der CJ. Rac1b, a tumor associated, constitutively active Rac1 splice variant, promotes cellular transformation. *Oncogene*. 2004 Dec 16;23(58):9369-80. PubMed PMID: 15516977.
79. Fiegen D, Haeusler LC, Blumenstein L, Herbrand U, Dvorsky R, Vetter IR, Ahmadian MR. Alternative splicing of Rac1 generates Rac1b, a self-activating GTPase. *The Journal of biological chemistry*. 2004 Feb 6;279(6):4743-9. PubMed PMID: 14625275.
80. Radisky DC, Levy DD, Littlepage LE, Liu H, Nelson CM, Fata JE, Leake D, Godden EL, Albertson DG, Nieto MA, Werb Z, Bissell MJ. Rac1b and reactive oxygen species mediate MMP-3-induced EMT and genomic instability. *Nature*. 2005 Jul 7;436(7047):123-7. PubMed PMID: 16001073. Pubmed Central PMCID: 2784913.
81. Zhou C, Licciulli S, Avila JL, Cho M, Troutman S, Jiang P, Kossenkov AV, Showe LC, Liu Q, Vachani A, Albelda SM, Kissil JL. The Rac1 splice form Rac1b promotes K-ras-induced lung tumorigenesis. *Oncogene*. 2013 Feb 14;32(7):903-9. PubMed PMID: 22430205. Pubmed Central PMCID: 3384754.
82. Schnelzer A, Prechtel D, Knaus U, Dehne K, Gerhard M, Graeff H, Harbeck N, Schmitt M, Lengyel E. Rac1 in human breast cancer: overexpression, mutation analysis, and characterization of a new isoform, Rac1b. *Oncogene*. 2000 Jun 15;19(26):3013-20. PubMed PMID: 10871853.
83. Henriques AF, Barros P, Moyer MP, Matos P, Jordan P. Expression of tumor-related Rac1b antagonizes B-Raf-induced senescence in colorectal cells. *Cancer letters*. 2015 Dec 28;369(2):368-75. PubMed PMID: 26341689.

84. Jordan P, Brazao R, Boavida MG, Gespach C, Chastre E. Cloning of a novel human Rac1b splice variant with increased expression in colorectal tumors. *Oncogene*. 1999 Nov 18;18(48):6835-9. PubMed PMID: 10597294.
85. Alonso-Espinaco V, Cuatrecasas M, Alonso V, Escudero P, Marmol M, Horndler C, Ortego J, Gallego R, Codony-Servat J, Garcia-Albeniz X, Jares P, Castells A, Lozano JJ, Rosell R, Maurel J. RAC1b overexpression correlates with poor prognosis in KRAS/BRAF WT metastatic colorectal cancer patients treated with first-line FOLFOX/XELOX chemotherapy. *European journal of cancer*. 2014 Jul;50(11):1973-81. PubMed PMID: 24833563.
86. Guo Y, Kenney SR, Cook L, Adams S, Rutledge T, Romero E, Oprea TI, Bedrick E, Wiggins CL, Kang H, Lomo L, Muller CY, Wandinger-Ness A, Hudson LG. A novel pharmacologic activity of ketorolac for therapeutic benefit in ovarian cancer patients. *Clinical Cancer Research*. under revision.
87. Ridley AJ. Rho GTPase signalling in cell migration. *Current opinion in cell biology*. 2015 Sep 10;36:103-12. PubMed PMID: 26363959.
88. Huang M, Prendergast GC. RhoB in cancer suppression. *Histology and histopathology*. 2006 Feb;21(2):213-8. PubMed PMID: 16329046.
89. Zhu Y, Zhou J, Xia H, Chen X, Qiu M, Huang J, Liu S, Tang Q, Lang N, Liu Z, Liu M, Zheng Y, Bi F. The Rho GTPase RhoE is a p53-regulated candidate tumor suppressor in cancer cells. *International journal of oncology*. 2014 Mar;44(3):896-904. PubMed PMID: 24399089.
90. Goggs R, Harper MT, Pope RJ, Savage JS, Williams CM, Mundell SJ, Heesom KJ, Bass M, Mellor H, Poole AW. RhoG protein regulates platelet granule secretion and thrombus formation in mice. *The Journal of biological chemistry*. 2013 Nov 22;288(47):34217-29. PubMed PMID: 24106270. Pubmed Central PMCID: 3837162.
91. Leszczynska K, Kaur S, Wilson E, Bicknell R, Heath VL. The role of RhoJ in endothelial cell biology and angiogenesis. *Biochemical Society transactions*. 2011 Dec;39(6):1606-11. PubMed PMID: 22103495.
92. Krauthammer M, Kong Y, Ha BH, Evans P, Bacchiocchi A, McCusker JP, Cheng E, Davis MJ, Goh G, Choi M, Ariyan S, Narayan D, Dutton-Regester K, Capatana A, Holman EC, Bosenberg M, Sznol M, Kluger HM, Brash DE, Stern DF, Materin MA, Lo RS, Mane S, Ma S, Kidd KK, Hayward NK, Lifton RP, Schlessinger J, Boggon TJ, Halaban R. Exome sequencing identifies recurrent somatic RAC1 mutations in melanoma. *Nature genetics*. 2012 Sep;44(9):1006-14. PubMed PMID: 22842228. Pubmed Central PMCID: 3432702.
93. Kawazu M, Ueno T, Kontani K, Ogita Y, Ando M, Fukumura K, Yamato A, Soda M, Takeuchi K, Miki Y, Yamaguchi H, Yasuda T, Naoe T, Yamashita Y, Katada T, Choi YL, Mano H. Transforming mutations of RAC guanosine

triphosphatases in human cancers. Proceedings of the National Academy of Sciences of the United States of America. 2013 Feb 19;110(8):3029-34. PubMed PMID: 23382236. Pubmed Central PMCID: 3581941.

94. Davis MJ, Ha BH, Holman EC, Halaban R, Schlessinger J, Boggon TJ. RAC1P29S is a spontaneously activating cancer-associated GTPase. Proceedings of the National Academy of Sciences of the United States of America. 2013 Jan 15;110(3):912-7. PubMed PMID: 23284172. Pubmed Central PMCID: 3549122.

95. Li A, Machesky LM. Rac1 cycling fast in melanoma with P29S. Pigment cell & melanoma research. 2013 Feb 8. PubMed PMID: 23530970.

96. Alan JK, Lundquist EA. Mutationally activated Rho GTPases in cancer. Small GTPases. 2013 Jul-Sep;4(3):159-63. PubMed PMID: 24088985. Pubmed Central PMCID: 3976972.

97. Adam O, Laufs U. Rac1-Mediated Effects of HMG-CoA Reductase Inhibitors (Statins) in Cardiovascular Disease. Antioxidants & redox signaling. 2013 Sep 19. PubMed PMID: 23919665.

98. Sendur MA, Aksoy S, Yazici O, Ozdemir NY, Zengin N, Altundag K. Statin use may improve clinicopathological characteristics and recurrence risk of invasive breast cancer. Medical oncology. 2014 Feb;31(2):835. PubMed PMID: 24381143.

99. Cardwell CR, Hicks BM, Hughes C, Murray LJ. Statin use after colorectal cancer diagnosis and survival: a population-based cohort study. Journal of clinical oncology : official journal of the American Society of Clinical Oncology. 2014 Oct 1;32(28):3177-83. PubMed PMID: 25092779.

100. Walker EJ, Ko AH, Holly EA, Bracci PM. Statin use and risk of pancreatic cancer: Results from a large, clinic-based case-control study. Cancer. 2015 Apr 15;121(8):1287-94. PubMed PMID: 25649483. Pubmed Central PMCID: 4393339.

101. Berry JG, Hall DE, Kuo DZ, Cohen E, Agrawal R, Feudtner C, Hall M, Kueser J, Kaplan W, Neff J. Hospital utilization and characteristics of patients experiencing recurrent readmissions within children's hospitals. Jama. 2011 Feb 16;305(7):682-90. PubMed PMID: 21325184. Pubmed Central PMCID: 3118568.

102. Habis M, Wroblewski K, Bradaric M, Ismail N, Yamada SD, Litchfield L, Lengyel E, Romero IL. Statin therapy is associated with improved survival in patients with non-serous-papillary epithelial ovarian cancer: a retrospective cohort analysis. PloS one. 2014;9(8):e104521. PubMed PMID: 25118694. Pubmed Central PMCID: 4131884.

103. Pelish HE, Peterson JR, Salvarezza SB, Rodriguez-Boulan E, Chen JL, Stamnes M, Macia E, Feng Y, Shair MD, Kirchhausen T. Secramine inhibits Cdc42-dependent functions in cells and Cdc42 activation in vitro. *Nature chemical biology*. 2006 Jan;2(1):39-46. PubMed PMID: 16408091.
104. Hong L, Kenney SR, Phillips GK, Simpson D, Schroeder CE, Noth J, Romero E, Swanson S, Waller A, Strouse JJ, Carter M, Chigaev A, Ursu O, Oprea T, Hjelle B, Golden JE, Aube J, Hudson LG, Buranda T, Sklar LA, Wandinger-Ness A. Characterization of a Cdc42 protein inhibitor and its use as a molecular probe. *The Journal of biological chemistry*. 2013 Mar 22;288(12):8531-43. PubMed PMID: 23382385. Pubmed Central PMCID: 3605667.
105. Gao Y, Dickerson JB, Guo F, Zheng J, Zheng Y. Rational design and characterization of a Rac GTPase-specific small molecule inhibitor. *Proceedings of the National Academy of Sciences of the United States of America*. 2004 May 18;101(20):7618-23. PubMed PMID: 15128949. Pubmed Central PMCID: 419655.
106. Akbar H, Cancelas J, Williams DA, Zheng J, Zheng Y. Rational design and applications of a Rac GTPase-specific small molecule inhibitor. *Methods in enzymology*. 2006;406:554-65. PubMed PMID: 16472687.
107. Zins K, Lucas T, Reichl P, Abraham D, Aharinejad S. A Rac1/Cdc42 GTPase-Specific Small Molecule Inhibitor Suppresses Growth of Primary Human Prostate Cancer Xenografts and Prolongs Survival in Mice. *PloS one*. 2013;8(9):e74924. PubMed PMID: 24040362. Pubmed Central PMCID: 3770583.
108. Zins K, Gunawardhana S, Lucas T, Abraham D, Aharinejad S. Targeting Cdc42 with the small molecule drug AZA197 suppresses primary colon cancer growth and prolongs survival in a preclinical mouse xenograft model by downregulation of PAK1 activity. *Journal of translational medicine*. 2013;11:295. PubMed PMID: 24279335. Pubmed Central PMCID: 4222769.
109. Montalvo-Ortiz BL, Castillo-Pichardo L, Hernandez E, Humphries-Bickley T, De la Mota-Peynado A, Cubano LA, Vlaar CP, Dharmawardhane S. Characterization of EHop-016, novel small molecule inhibitor of Rac GTPase. *The Journal of biological chemistry*. 2012 Apr 13;287(16):13228-38. PubMed PMID: 22383527. Pubmed Central PMCID: 3339933.
110. Onesto C, Shutes A, Picard V, Schweighoffer F, Der CJ. Characterization of EHT 1864, a novel small molecule inhibitor of Rac family small GTPases. *Methods in enzymology*. 2008;439:111-29. PubMed PMID: 18374160.
111. Duggan KC, Walters MJ, Musee J, Harp JM, Kiefer JR, Oates JA, Marnett LJ. Molecular basis for cyclooxygenase inhibition by the non-steroidal anti-inflammatory drug naproxen. *The Journal of biological chemistry*. 2010 Nov 5;285(45):34950-9. PubMed PMID: 20810665. Pubmed Central PMCID: 2966109.

112. Rothwell PM, Fowkes FG, Belch JF, Ogawa H, Warlow CP, Meade TW. Effect of daily aspirin on long-term risk of death due to cancer: analysis of individual patient data from randomised trials. *Lancet*. 2011 Jan 1;377(9759):31-41. PubMed PMID: 21144578.
113. Waskewich C, Blumenthal RD, Li H, Stein R, Goldenberg DM, Burton J. Celecoxib exhibits the greatest potency amongst cyclooxygenase (COX) inhibitors for growth inhibition of COX-2-negative hematopoietic and epithelial cell lines. *Cancer research*. 2002 Apr 1;62(7):2029-33. PubMed PMID: 11929821.
114. Weber A, Yildirim H, Schror K. Cyclooxygenase-independent inhibition of smooth muscle cell mitogenesis by ibuprofen. *European journal of pharmacology*. 2000 Feb 11;389(1):67-9. PubMed PMID: 10686297.
115. Wechter WJ, Kantoci D, Murray ED, Jr., Quiggle DD, Leipold DD, Gibson KM, McCracken JD. R-flurbiprofen chemoprevention and treatment of intestinal adenomas in the APC(Min)/+ mouse model: implications for prophylaxis and treatment of colon cancer. *Cancer research*. 1997 Oct 1;57(19):4316-24. PubMed PMID: 9331093.
116. Yamamoto Y, Yin MJ, Lin KM, Gaynor RB. Sulindac inhibits activation of the NF-kappaB pathway. *The Journal of biological chemistry*. 1999 Sep 17;274(38):27307-14. PubMed PMID: 10480951.
117. Gurpinar E, Grizzle WE, Piazza GA. NSAIDs inhibit tumorigenesis, but how? *Clinical cancer research : an official journal of the American Association for Cancer Research*. 2014 Mar 1;20(5):1104-13. PubMed PMID: 24311630. Pubmed Central PMCID: 3947450.
118. Gurpinar E, Grizzle WE, Piazza GA. COX-Independent Mechanisms of Cancer Chemoprevention by Anti-Inflammatory Drugs. *Frontiers in oncology*. 2013;3:181. PubMed PMID: 23875171. Pubmed Central PMCID: 3708159.
119. Kwon IK, Schoenlein PV, Delk J, Liu K, Thangaraju M, Dulin NO, Ganapathy V, Berger FG, Browning DD. Expression of cyclic guanosine monophosphate-dependent protein kinase in metastatic colon carcinoma cells blocks tumor angiogenesis. *Cancer*. 2008 Apr 1;112(7):1462-70. PubMed PMID: 18260092.
120. Lee HC, Park IC, Park MJ, An S, Woo SH, Jin HO, Chung HY, Lee SJ, Gwak HS, Hong YJ, Yoo DH, Rhee CH, Hong SI. Sulindac and its metabolites inhibit invasion of glioblastoma cells via down-regulation of Akt/PKB and MMP-2. *Journal of cellular biochemistry*. 2005 Feb 15;94(3):597-610. PubMed PMID: 15546138.
121. Oprea TI, Sklar LA, Agola JO, Guo Y, Siberberg M, Roxby J, Vestling A, Romero E, Surviladze Z, Murry-Krezan C, Waller A, Ursau O, Hudson L,

Wandinger-Ness A. Novel activities of select NSAID R-enantiomers against Rac1 and Cdc42 GTPases. PloS one. 2015;in press.

122. Handley DA, Cervoni P, McCray JE, McCullough JR. Preclinical enantioselective pharmacology of (R)- and (S)- ketorolac. Journal of clinical pharmacology. 1998 Feb;38(2 Suppl):25S-35S. PubMed PMID: 9549656.

123. Dorfman RI. Chemistry and pharmacology of naproxen. Arzneimittel-Forschung. 1975 Feb;25(2A):278-81. PubMed PMID: 1173774.

124. Segre EJ. Naproxen sodium (Anaprox): pharmacology, pharmacokinetics and drug interactions. The Journal of reproductive medicine. 1980 Oct;25(4 Suppl):222-5. PubMed PMID: 7001021.

125. Sadok A, Marshall CJ. Rho GTPases: masters of cell migration. Small GTPases. 2014;5:e29710. PubMed PMID: 24978113. Pubmed Central PMCID: 4107589.

126. Leve F, Morgado-Diaz JA. Rho GTPase signaling in the development of colorectal cancer. Journal of cellular biochemistry. 2012 Aug;113(8):2549-59. PubMed PMID: 22467564.

127. Grise F, Bidaud A, Moreau V. Rho GTPases in hepatocellular carcinoma. Biochimica et biophysica acta. 2009 Apr;1795(2):137-51. PubMed PMID: 19162129.

128. Vetter IR, Wittinghofer A. The guanine nucleotide-binding switch in three dimensions. Science. 2001 Nov 9;294(5545):1299-304. PubMed PMID: 11701921.

129. Yang J, Zhang Z, Roe SM, Marshall CJ, Barford D. Activation of Rho GTPases by DOCK exchange factors is mediated by a nucleotide sensor. Science. 2009 Sep 11;325(5946):1398-402. PubMed PMID: 19745154.

130. Kulkarni K, Yang J, Zhang Z, Barford D. Multiple factors confer specific Cdc42 and Rac protein activation by dedicator of cytokinesis (DOCK) nucleotide exchange factors. The Journal of biological chemistry. 2011 Jul 15;286(28):25341-51. PubMed PMID: 21613211. Pubmed Central PMCID: 3137105.

131. Leonard DA, Lin R, Cerione RA, Manor D. Biochemical studies of the mechanism of action of the Cdc42-GTPase-activating protein. The Journal of biological chemistry. 1998 Jun 26;273(26):16210-5. PubMed PMID: 9632678.

132. Richnau N, Aspenstrom P. Rich, a rho GTPase-activating protein domain-containing protein involved in signaling by Cdc42 and Rac1. The Journal of biological chemistry. 2001 Sep 14;276(37):35060-70. PubMed PMID: 11431473.

133. Schwartz SL, Tessema M, Buranda T, Pylypenko O, Rak A, Simons PC, Surviladze Z, Sklar LA, Wandinger-Ness A. Flow cytometry for real-time measurement of guanine nucleotide binding and exchange by Ras-like GTPases. *Analytical biochemistry*. 2008 Oct 15;381(2):258-66. PubMed PMID: 18638444. Pubmed Central PMCID: 2633595.
134. Agola JO, Hong L, Surviladze Z, Ursu O, Waller A, Strouse JJ, Simpson DS, Schroeder CE, Oprea TI, Golden JE, Aube J, Buranda T, Sklar LA, Wandinger-Ness A. A competitive nucleotide binding inhibitor: in vitro characterization of Rab7 GTPase inhibition. *ACS chemical biology*. 2012 Jun 15;7(6):1095-108. PubMed PMID: 22486388. Pubmed Central PMCID: 3440014.
135. Buranda T, Basuray S, Swanson S, Agola J, Bondu V, Wandinger-Ness A. Rapid parallel flow cytometry assays of active GTPases using effector beads. *Analytical biochemistry*. 2013 Nov 15;442(2):149-57. PubMed PMID: 23928044.
136. Hapuarachchige S, Montano G, Ramesh C, Rodriguez D, Henson LH, Williams CC, Kadavakkollu S, Johnson DL, Shuster CB, Arterburn JB. Design and synthesis of a new class of membrane-permeable triazaborolopyridinium fluorescent probes. *Journal of the American Chemical Society*. 2011 May 4;133(17):6780-90. PubMed PMID: 21473622. Pubmed Central PMCID: 3244355.
137. Surviladze Z, Ursu O, Miscioscia F, Curpan R, Halip L, Bologna C, Oprea T, Waller A, Strouse J, Salas V, Wu Y, Edwards B, Wandinger-Ness A, Sklar L. Three small molecule pan activator families of Ras-related GTPases. *Probe Reports from the NIH Molecular Libraries Program*. Bethesda (MD)2010.
138. Surviladze Z, Waller A, Strouse JJ, Bologna C, Ursu O, Salas V, Parkinson JF, Phillips GK, Romero E, Wandinger-Ness A, Sklar LA, Schroeder C, Simpson D, Noth J, Wang J, Golden J, Aube J. A Potent and Selective Inhibitor of Cdc42 GTPase. *Probe Reports from the NIH Molecular Libraries Program*. Bethesda (MD)2010.
139. Hong L, Guo Y, BasuRay S, Agola JO, Romero E, Simpson DS, Schroeder CE, Simons P, Waller A, Garcia M, Carter M, Ursu O, Gouveia K, Golden JE, Aube J, Wandinger-Ness A, Sklar LA. A Pan-GTPase Inhibitor as a Molecular Probe. *PLoS one*. 2015;10(8):e0134317. PubMed PMID: 26247207. Pubmed Central PMCID: 4527730.
140. Oprea TI, Sklar LA, Agola JO, Guo Y, Siberberg M, Roxby J, Vestling A, Romero E, Surviladze Z, Waller A, Ursa O, Wandinger-Ness A, Hudson LG. Novel activities of select NSAID R-enantiomers against Rac1 and Cdc42 GTPases. under revision.
141. Blum R, Cox AD, Kloog Y. Inhibitors of chronically active ras: potential for treatment of human malignancies. *Recent patents on anti-cancer drug discovery*. 2008 Jan;3(1):31-47. PubMed PMID: 18289122.

142. Sun D, Xu D, Zhang B. Rac signaling in tumorigenesis and as target for anticancer drug development. *Drug resistance updates : reviews and commentaries in antimicrobial and anticancer chemotherapy*. 2006 Dec;9(6):274-87. PubMed PMID: 17234445.
143. Wiemer AJ, Wiemer DF, Hohl RJ. Geranylgeranyl diphosphate synthase: an emerging therapeutic target. *Clinical pharmacology and therapeutics*. 2011 Dec;90(6):804-12. PubMed PMID: 22048229.
144. Rane C, Minden A. P21 activated kinases: Structure, regulation, and functions. *Small GTPases*. 2014 Mar 21;5(1). PubMed PMID: 24658305.
145. Zhao ZS, Manser E. PAK family kinases: Physiological roles and regulation. *Cellular logistics*. 2012 Apr 1;2(2):59-68. PubMed PMID: 23162738. Pubmed Central PMCID: 3490964.
146. Pickup MW, Mouw JK, Weaver VM. The extracellular matrix modulates the hallmarks of cancer. *EMBO reports*. 2014 Dec;15(12):1243-53. PubMed PMID: 25381661. Pubmed Central PMCID: 4264927.
147. Mattila PK, Lappalainen P. Filopodia: molecular architecture and cellular functions. *Nature reviews Molecular cell biology*. 2008 Jun;9(6):446-54. PubMed PMID: 18464790.
148. Parri M, Chiarugi P. Rac and Rho GTPases in cancer cell motility control. *Cell communication and signaling : CCS*. 2010;8:23. PubMed PMID: 20822528. Pubmed Central PMCID: 2941746.
149. Lawson CD, Burridge K. The on-off relationship of Rho and Rac during integrin-mediated adhesion and cell migration. *Small GTPases*. 2014;5:e27958. PubMed PMID: 24607953. Pubmed Central PMCID: 4114617.
150. Evers EE, Zondag GC, Malliri A, Price LS, ten Klooster JP, van der Kammen RA, Collard JG. Rho family proteins in cell adhesion and cell migration. *European journal of cancer*. 2000 Jun;36(10):1269-74. PubMed PMID: 10882865.
151. Noritake J, Watanabe T, Sato K, Wang S, Kaibuchi K. IQGAP1: a key regulator of adhesion and migration. *Journal of cell science*. 2005 May 15;118(Pt 10):2085-92. PubMed PMID: 15890984.
152. Baker NM, Yee Chow H, Chernoff J, Der CJ. Molecular pathways: targeting RAC-p21-activated serine-threonine kinase signaling in RAS-driven cancers. *Clinical cancer research : an official journal of the American Association for Cancer Research*. 2014 Sep 15;20(18):4740-6. PubMed PMID: 25225063. Pubmed Central PMCID: 4166583.

153. Heasman SJ, Ridley AJ. Mammalian Rho GTPases: new insights into their functions from in vivo studies. *Nature reviews Molecular cell biology*. 2008 Sep;9(9):690-701. PubMed PMID: 18719708.
154. Ridley AJ. Rho GTPases and cell migration. *Journal of cell science*. 2001 Aug;114(Pt 15):2713-22. PubMed PMID: 11683406.
155. Courtneidge SA. Cell migration and invasion in human disease: the Tks adaptor proteins. *Biochemical Society transactions*. 2012 Feb;40(1):129-32. PubMed PMID: 22260678. Pubmed Central PMCID: 3425387.
156. Price LS, Collard JG. Regulation of the cytoskeleton by Rho-family GTPases: implications for tumour cell invasion. *Seminars in cancer biology*. 2001 Apr;11(2):167-73. PubMed PMID: 11322835.
157. Jacob A, Jing J, Lee J, Schedin P, Gilbert SM, Peden AA, Junutula JR, Prekeris R. Rab40b regulates trafficking of MMP2 and MMP9 during invadopodia formation and invasion of breast cancer cells. *Journal of cell science*. 2013 Oct 15;126(Pt 20):4647-58. PubMed PMID: 23902685. Pubmed Central PMCID: 3795337.
158. C M. A Pilot Trial to Study the Availability and Effect of Post-OP IV Ketorolac on Ovarian, Fallopian Tube or Primary Peritoneal Cancer, Cells Retrieved From the Peritoneal Cavity: New Mexico Cancer Care Alliance; [cited 2015 May 18]. Available from: <https://clinicaltrials.gov/ct2/show/NCT01670799?term=ketorolac+and+ovarian+cancer&rank=1>.
159. Shepherd TG, Theriault BL, Campbell EJ, Nachtigal MW. Primary culture of ovarian surface epithelial cells and ascites-derived ovarian cancer cells from patients. *Nature protocols*. 2006;1(6):2643-9. PubMed PMID: 17406520.
160. Humphries MJ. Cell adhesion assays. *Molecular biotechnology*. 2001 May;18(1):57-61. PubMed PMID: 11439699.
161. Bellone S, Siegel ER, Cocco E, Cargnelutti M, Silasi DA, Azodi M, Schwartz PE, Rutherford TJ, Pecorelli S, Santin AD. Overexpression of epithelial cell adhesion molecule in primary, metastatic, and recurrent/chemotherapy-resistant epithelial ovarian cancer: implications for epithelial cell adhesion molecule-specific immunotherapy. *International journal of gynecological cancer : official journal of the International Gynecological Cancer Society*. 2009 Jul;19(5):860-6. PubMed PMID: 19574774.
162. Taylor DD, Gercel-Taylor C, Parker LP. Patient-derived tumor-reactive antibodies as diagnostic markers for ovarian cancer. *Gynecologic oncology*. 2009 Oct;115(1):112-20. PubMed PMID: 19647308. Pubmed Central PMCID: 2760307.

163. Dummler B, Ohshiro K, Kumar R, Field J. Pak protein kinases and their role in cancer. *Cancer metastasis reviews*. 2009 Jun;28(1-2):51-63. PubMed PMID: 19165420. Pubmed Central PMCID: 3923596.
164. Bokoch GM, Reilly AM, Daniels RH, King CC, Olivera A, Spiegel S, Knaus UG. A GTPase-independent mechanism of p21-activated kinase activation. Regulation by sphingosine and other biologically active lipids. *The Journal of biological chemistry*. 1998 Apr 3;273(14):8137-44. PubMed PMID: 9525917.
165. Diaz-Munoz MD, Osma-Garcia IC, Iniguez MA, Fresno M. Cyclooxygenase-2 deficiency in macrophages leads to defective p110gamma PI3K signaling and impairs cell adhesion and migration. *Journal of immunology*. 2013 Jul 1;191(1):395-406. PubMed PMID: 23733875.
166. Arjonen A, Kaukonen R, Ivaska J. Filopodia and adhesion in cancer cell motility. *Cell adhesion & migration*. 2011 Sep-Oct;5(5):421-30. PubMed PMID: 21975551. Pubmed Central PMCID: 3218609.
167. Jett MF, Ramesha CS, Brown CD, Chiu S, Emmett C, Voronin T, Sun T, O'Yang C, Hunter JC, Eglen RM, Johnson RM. Characterization of the analgesic and anti-inflammatory activities of ketorolac and its enantiomers in the rat. *The Journal of pharmacology and experimental therapeutics*. 1999 Mar;288(3):1288-97. PubMed PMID: 10027870.
168. Reyners AK, de Munck L, Erdkamp FL, Smit WM, Hoekman K, Lalisang RI, de Graaf H, Wymenga AN, Polee M, Hollema H, van Vugt MA, Schaapveld M, Willemse PH, DoCaCel Study G. A randomized phase II study investigating the addition of the specific COX-2 inhibitor celecoxib to docetaxel plus carboplatin as first-line chemotherapy for stage IC to IV epithelial ovarian cancer, Fallopian tube or primary peritoneal carcinomas: the DoCaCel study. *Annals of oncology : official journal of the European Society for Medical Oncology / ESMO*. 2012 Nov;23(11):2896-902. PubMed PMID: 22689176.
169. Forget P, Vandenhende J, Berliere M, Machiels JP, Nussbaum B, Legrand C, De Kock M. Do intraoperative analgesics influence breast cancer recurrence after mastectomy? A retrospective analysis. *Anesthesia and analgesia*. 2010 Jun 1;110(6):1630-5. PubMed PMID: 20435950.
170. Patil R, Laguerre A, Wielens J, Headey SJ, Williams ML, Hughes ML, Mohanty B, Porter CJ, Scanlon MJ. Characterization of two distinct modes of drug binding to human intestinal fatty acid binding protein. *ACS chemical biology*. 2014 Nov 21;9(11):2526-34. PubMed PMID: 25144524.
171. Dormond O, Foletti A, Paroz C, Ruegg C. NSAIDs inhibit alpha V beta 3 integrin-mediated and Cdc42/Rac-dependent endothelial-cell spreading, migration and angiogenesis. *Nature medicine*. 2001 Sep;7(9):1041-7. PubMed PMID: 11533708.

172. Forget P, Berliere M, van Maanen A, Duhoux FP, Machiels JP, Coulie PG, Bouche G, De Kock M, Ketorolac in Breast Cancer trial g. Perioperative ketorolac in high risk breast cancer patients. Rationale, feasibility and methodology of a prospective randomized placebo-controlled trial. Medical hypotheses. 2013 Oct;81(4):707-12. PubMed PMID: 23937996.
173. Bid HK, Roberts RD, Manchanda PK, Houghton PJ. RAC1: an emerging therapeutic option for targeting cancer angiogenesis and metastasis. Molecular cancer therapeutics. 2013 Oct;12(10):1925-34. PubMed PMID: 24072884. Pubmed Central PMCID: 3823055.
174. Jemal A, Siegel R, Xu J, Ward E. Cancer statistics, 2010. CA Cancer J Clin. 2010 Sep-Oct;60(5):277-300. PubMed PMID: 20610543.
175. Stengel K, Zheng Y. Cdc42 in oncogenic transformation, invasion, and tumorigenesis. Cellular signalling. 2011 Sep;23(9):1415-23. PubMed PMID: 21515363. Pubmed Central PMCID: 3115433.
176. Mack NA, Whalley HJ, Castillo-Lluva S, Malliri A. The diverse roles of Rac signaling in tumorigenesis. Cell cycle. 2011 May 15;10(10):1571-81. PubMed PMID: 21478669. Pubmed Central PMCID: 3127158.
177. Vega FM, Ridley AJ. Rho GTPases in cancer cell biology. FEBS letters. 2008 Jun 18;582(14):2093-101. PubMed PMID: 18460342.
178. Mardilovich K, Olson MF, Baugh M. Targeting Rho GTPase signaling for cancer therapy. Future oncology. 2012 Feb;8(2):165-77. PubMed PMID: 22335581.
179. Friesland A, Zhao Y, Chen YH, Wang L, Zhou H, Lu Q. Small molecule targeting Cdc42-intersectin interaction disrupts Golgi organization and suppresses cell motility. Proceedings of the National Academy of Sciences of the United States of America. 2013 Jan 22;110(4):1261-6. PubMed PMID: 23284167. Pubmed Central PMCID: 3557054.
180. Surviladze Z, Waller A, Wu Y, Romero E, Edwards BS, Wandinger-Ness A, Sklar LA. Identification of a small GTPase inhibitor using a high-throughput flow cytometry bead-based multiplex assay. Journal of biomolecular screening. 2010 Jan;15(1):10-20. PubMed PMID: 20008126. Pubmed Central PMCID: 3433230.
181. Surviladze Z, Young SM, Sklar LA. High-throughput flow cytometry bead-based multiplex assay for identification of Rho GTPase inhibitors. Methods in molecular biology. 2012;827:253-70. PubMed PMID: 22144280. Pubmed Central PMCID: 4467469.
182. Oprea TI, Bauman JE, Bologa CG, Buranda T, Chigaev A, Edwards BS, Jarvik JW, Gresham HD, Haynes MK, Hjelle B, Hromas R, Hudson L, Mackenzie DA, Muller CY, Reed JC, Simons PC, Smagley Y, Strouse J, Surviladze Z,

Thompson T, Ursu O, Waller A, Wandinger-Ness A, Winter SS, Wu Y, Young SM, Larson RS, Willman C, Sklar LA. Drug Repurposing from an Academic Perspective. *Drug discovery today Therapeutic strategies*. 2011 Winter;8(3-4):61-9. PubMed PMID: 22368688. Pubmed Central PMCID: 3285382.

183. Guo Y, Kenney SR, Jr., Muller CY, Adams S, Rutledge T, Romero E, Murray-Krezan C, Prekeris R, Sklar LA, Hudson LG, Wandinger-Ness A. R-ketorolac Targets Cdc42 and Rac1 and Alters Ovarian Cancer Cell Behaviors Critical for Invasion and Metastasis. *Molecular cancer therapeutics*. 2015 Jul 23. PubMed PMID: 26206334.

184. Forget P, Bentin C, Machiels JP, Berliere M, Coulie PG, De Kock M. Intraoperative use of ketorolac or diclofenac is associated with improved disease-free survival and overall survival in conservative breast cancer surgery. *British journal of anaesthesia*. 2014 Jul;113 Suppl 1:i82-7. PubMed PMID: 24464611.

185. Mroszczak E, Combs D, Chaplin M, Tsina I, Tarnowski T, Rocha C, Tam Y, Boyd A, Young J, Depass L. Chiral kinetics and dynamics of ketorolac. *Journal of clinical pharmacology*. 1996 Jun;36(6):521-39. PubMed PMID: 8809637.

186. Phenomenex. Phenomenex Chiral Column Protocols-online. APP ID: 20367.

187. Vakily M, Corrigan B, Jamali F. The problem of racemization in the stereospecific assay and pharmacokinetic evaluation of ketorolac in human and rats. *Pharmaceutical research*. 1995 Nov;12(11):1652-7. PubMed PMID: 8592665.

188. Bast RC, Jr., Hennessy B, Mills GB. The biology of ovarian cancer: new opportunities for translation. *Nature reviews Cancer*. 2009 Jun;9(6):415-28. PubMed PMID: 19461667. Pubmed Central PMCID: 2814299.

189. Kenney SR, Roxby J, Romero E, Ursa O, Oprea T, Sklar L. Enantiomer specific inhibition of Rac1 and Cdc42 in ovarian cancer. *Molec Biol Cell*. 2012;22:abstr 1363.

190. Forget P, Machiels JP, Coulie PG, Berliere M, Poncelet AJ, Tombal B, Stainier A, Legrand C, Canon JL, Kremer Y, De Kock M. Neutrophil:lymphocyte ratio and intraoperative use of ketorolac or diclofenac are prognostic factors in different cohorts of patients undergoing breast, lung, and kidney cancer surgery. *Annals of surgical oncology*. 2013 Dec;20 Suppl 3:S650-60. PubMed PMID: 23884751.

191. Inoue T, Murano M, Yoda Y, Kuramoto T, Kakimoto K, Ishida K, Kawakami K, Abe Y, Morita E, Murano N, Tokioka S, Maemura K, Umegaki E, Higuchi K. R-etodolac induces E-cadherin and suppresses colitis-related mouse colon tumorigenesis. *Oncology reports*. 2010 Dec;24(6):1487-92. PubMed PMID: 21042743.

192. Yasui H, Hideshima T, Hamasaki M, Roccaro AM, Shiraishi N, Kumar S, Tassone P, Ishitsuka K, Raje N, Tai YT, Podar K, Chauhan D, Leoni LM, Kanekal S, Elliott G, Munshi NC, Anderson KC. SDX-101, the R-enantiomer of etodolac, induces cytotoxicity, overcomes drug resistance, and enhances the activity of dexamethasone in multiple myeloma. *Blood*. 2005 Jul 15;106(2):706-12. PubMed PMID: 15802527. Pubmed Central PMCID: 1895170.
193. Kolluri SK, Corr M, James SY, Bernasconi M, Lu D, Liu W, Cottam HB, Leoni LM, Carson DA, Zhang XK. The R-enantiomer of the nonsteroidal antiinflammatory drug etodolac binds retinoid X receptor and induces tumor-selective apoptosis. *Proceedings of the National Academy of Sciences of the United States of America*. 2005 Feb 15;102(7):2525-30. PubMed PMID: 15699354. Pubmed Central PMCID: 548323.
194. Feng R, Lentzsch S. Treatment of multiple myeloma with SDX-308. *Drug news & perspectives*. 2007 Sep;20(7):431-5. PubMed PMID: 17992265.
195. Lindhagen E, Nissle S, Leoni L, Elliott G, Chao Q, Larsson R, Aleskog A. R-etodolac (SDX-101) and the related indole-pyran analogues SDX-308 and SDX-309 potentiate the antileukemic activity of standard cytotoxic agents in primary chronic lymphocytic leukaemia cells. *Cancer chemotherapy and pharmacology*. 2007 Sep;60(4):545-53. PubMed PMID: 17186240.
196. Robak P, Smolewski P, Robak T. The role of non-steroidal anti-inflammatory drugs in the risk of development and treatment of hematologic malignancies. *Leukemia & lymphoma*. 2008 Aug;49(8):1452-62. PubMed PMID: 18608871.
197. Yasui H, Hideshima T, Ikeda H, Ocio EM, Kiziltepe T, Vallet S, Okawa Y, Neri P, Sukhdeo K, Podar K, Chauhan D, Richardson PG, Raje N, Carrasco DR, Anderson KC. Novel etodolac analog SDX-308 (CEP-18082) induces cytotoxicity in multiple myeloma cells associated with inhibition of beta-catenin/TCF pathway. *Leukemia*. 2007 Mar;21(3):535-40. PubMed PMID: 17268521.
198. Gonzalez-Villasana V, Fuentes-Mattei E, Ivan C, Dalton HJ, Rodriguez-Aguayo C, Fernandez-de Thomas RJ, Aslan B, Del CMP, Velazquez-Torres G, Previs RA, Pradeep S, Kahraman N, Wang H, Kanlikilicer P, Ozpolat B, Calin G, Sood AK, Lopez-Berestein G. Rac1/Pak1/p38/MMP-2 Axis Regulates Angiogenesis in Ovarian Cancer. *Clinical cancer research : an official journal of the American Association for Cancer Research*. 2015 Jan 16. PubMed PMID: 25595279.
199. Kintscher C, Groemping Y. Characterisation of the nucleotide exchange factor ITSN1L: evidence for a kinetic discrimination of GEF-stimulated nucleotide release from Cdc42. *Journal of molecular biology*. 2009 Mar 27;387(2):270-83. PubMed PMID: 19356586.

200. Zhang B, Zhang Y, Wang Z, Zheng Y. The role of Mg²⁺ cofactor in the guanine nucleotide exchange and GTP hydrolysis reactions of Rho family GTP-binding proteins. *The Journal of biological chemistry*. 2000 Aug 18;275(33):25299-307. PubMed PMID: 10843989.
201. Musrap N, Diamandis EP. Revisiting the complexity of the ovarian cancer microenvironment--clinical implications for treatment strategies. *Molecular cancer research : MCR*. 2012 Oct;10(10):1254-64. PubMed PMID: 22896662.
202. Smolle E, Taucher V, Haybaeck J. Malignant ascites in ovarian cancer and the role of targeted therapeutics. *Anticancer research*. 2014 Apr;34(4):1553-61. PubMed PMID: 24692682.
203. Latifi A, Luwor RB, Bilandzic M, Nazaretian S, Stenvers K, Pyman J, Zhu H, Thompson EW, Quinn MA, Findlay JK, Ahmed N. Isolation and characterization of tumor cells from the ascites of ovarian cancer patients: molecular phenotype of chemoresistant ovarian tumors. *PloS one*. 2012;7(10):e46858. PubMed PMID: 23056490. Pubmed Central PMCID: 3466197.
204. Lengyel E, Burdette JE, Kenny HA, Matei D, Pilrose J, Haluska P, Nephew KP, Hales DB, Stack MS. Epithelial ovarian cancer experimental models. *Oncogene*. 2014 Jul 10;33(28):3619-33. PubMed PMID: 23934194. Pubmed Central PMCID: 3990646.
205. Chu Y, Tang H, Guo Y, Guo J, Huang B, Fang F, Cai J, Wang Z. Adipose-derived mesenchymal stem cells promote cell proliferation and invasion of epithelial ovarian cancer. *Experimental cell research*. 2015 Sep 10;337(1):16-27. PubMed PMID: 26209607.
206. Yeung TL, Leung CS, Yip KP, Au Yeung CL, Wong ST, Mok SC. Cellular and molecular processes in ovarian cancer metastasis. A Review in the Theme: Cell and Molecular Processes in Cancer Metastasis. *American journal of physiology Cell physiology*. 2015 Oct 1;309(7):C444-56. PubMed PMID: 26224579. Pubmed Central PMCID: 4593771.
207. White EA, Kenny HA, Lengyel E. Three-dimensional modeling of ovarian cancer. *Advanced drug delivery reviews*. 2014 Dec 15;79-80:184-92. PubMed PMID: 25034878. Pubmed Central PMCID: 4426864.
208. Cunnea P, Stronach EA. Modeling platinum sensitive and resistant high-grade serous ovarian cancer: development and applications of experimental systems. *Frontiers in oncology*. 2014;4:81. PubMed PMID: 24860781. Pubmed Central PMCID: 4029026.
209. Tomao F, Papa A, Rossi L, Strudel M, Vici P, Lo Russo G, Tomao S. Emerging role of cancer stem cells in the biology and treatment of ovarian cancer: basic knowledge and therapeutic possibilities for an innovative approach. *Journal*

of experimental & clinical cancer research : CR. 2013;32:48. PubMed PMID: 23902592. Pubmed Central PMCID: 3734167.

210. Chen X, Zhang J, Zhang Z, Li H, Cheng W, Liu J. Cancer stem cells, epithelial-mesenchymal transition, and drug resistance in high-grade ovarian serous carcinoma. *Human pathology*. 2013 Nov;44(11):2373-84. PubMed PMID: 23850493. Pubmed Central PMCID: 3797876.

211. Wang JY, Yu P, Chen S, Xing H, Chen Y, Wang M, Tang K, Tian Z, Rao Q, Wang J. Activation of Rac1 GTPase promotes leukemia cell chemotherapy resistance, quiescence and niche interaction. *Molecular oncology*. 2013 Oct;7(5):907-16. PubMed PMID: 23726395.

212. Akunuru S, Palumbo J, Zhai QJ, Zheng Y. Rac1 targeting suppresses human non-small cell lung adenocarcinoma cancer stem cell activity. *PloS one*. 2011;6(2):e16951. PubMed PMID: 21347385. Pubmed Central PMCID: 3036726.

213. Yoon CH, Hyun KH, Kim RK, Lee H, Lim EJ, Chung HY, An S, Park MJ, Suh Y, Kim MJ, Lee SJ. The small GTPase Rac1 is involved in the maintenance of stemness and malignancies in glioma stem-like cells. *FEBS letters*. 2011 Jul 21;585(14):2331-8. PubMed PMID: 21704033.

214. Zucha MA, Wu AT, Lee WH, Wang LS, Lin WW, Yuan CC, Yeh CT. Bruton's tyrosine kinase (Btk) inhibitor ibrutinib suppresses stem-like traits in ovarian cancer. *Oncotarget*. 2015 May 30;6(15):13255-68. PubMed PMID: 26036311. Pubmed Central PMCID: 4537012.

215. Wang D, Fu L, Sun H, Guo L, DuBois RN. Prostaglandin E Promotes Colorectal Cancer Stem Cell Expansion and Metastasis in Mice. *Gastroenterology*. 2015 Aug 7. PubMed PMID: 26261008.

216. Chang JK, Li CJ, Wu SC, Yeh CH, Chen CH, Fu YC, Wang GJ, Ho ML. Effects of anti-inflammatory drugs on proliferation, cytotoxicity and osteogenesis in bone marrow mesenchymal stem cells. *Biochemical pharmacology*. 2007 Nov 1;74(9):1371-82. PubMed PMID: 17714695.

217. Qiu W, Wang X, Leibowitz B, Liu H, Barker N, Okada H, Oue N, Yasui W, Clevers H, Schoen RE, Yu J, Zhang L. Chemoprevention by nonsteroidal anti-inflammatory drugs eliminates oncogenic intestinal stem cells via SMAC-dependent apoptosis. *Proceedings of the National Academy of Sciences of the United States of America*. 2010 Nov 16;107(46):20027-32. PubMed PMID: 21041628. Pubmed Central PMCID: 2993406.

218. He QZ, Luo XZ, Wang K, Zhou Q, Ao H, Yang Y, Li SX, Li Y, Zhu HT, Duan T. Isolation and characterization of cancer stem cells from high-grade serous ovarian carcinomas. *Cellular physiology and biochemistry : international journal of experimental cellular physiology, biochemistry, and pharmacology*. 2014;33(1):173-84. PubMed PMID: 24504111.

219. Cole JM, Joseph S, Sudhahar CG, Cowden Dahl KD. Enrichment for chemoresistant ovarian cancer stem cells from human cell lines. *Journal of visualized experiments : JoVE*. 2014 (91):51891. PubMed PMID: 25285606.
220. Retsky M, Demicheli R, Hrushesky WJ, Forget P, De Kock M, Gukas I, Rogers RA, Baum M, Sukhatme V, Vaidya JS. Reduction of breast cancer relapses with perioperative non-steroidal anti-inflammatory drugs: new findings and a review. *Current medicinal chemistry*. 2013;20(33):4163-76. PubMed PMID: 23992307. Pubmed Central PMCID: 3831877.
221. Bailard NS, Flores RA. Could opioid sparing, rather than a direct non-steroidal anti-inflammatory drug effect, be responsible for improved survival after conservative breast surgery? *British journal of anaesthesia*. 2015 Mar;114(3):527. PubMed PMID: 25694564.